

**Development of preclinical imaging to refine studies of
dysfunctional blood flow in the brain**

Thesis submitted for the degree of
Doctor of Philosophy
at the University of Leicester

by

Andrew Crofts BSc (Hons), MRes
Department of Neuroscience, Psychology and Behaviour
University of Leicester
March 2020

Abstract: Development of preclinical imaging to refine studies of dysfunctional blood flow in the brain.

Andrew Crofts

The brain has the highest energy demand of any organ in the body, but despite this, has very little energy reserves. Because of this, the brain rapidly redirects blood flow, in response to changes in demand, through the process of neurovascular coupling. In the healthy brain, a 5% increase in oxygen demand is met by a 50% increase in blood flow, providing sufficient energy for normal activity. However, with age, or in pathological conditions such as hypertension or ischaemic stroke, this coupling is disrupted, which is thought to contribute to cognitive impairment in these conditions. To understand the processes behind this, non-invasive imaging of animal models would be beneficial.

Functional magnetic resonance imaging (fMRI) is a non-invasive imaging modality which uses changes in oxyhaemoglobin and deoxyhaemoglobin to image changes in brain activity (the Blood Oxygen Level Dependent, or BOLD, signal). Its use in longitudinal preclinical studies is currently limited by factors including appropriate anaesthesia, as current anaesthetic agents can be harmful or impair the vascular response detected.

This PhD aims to address the limitations of preclinical fMRI through development of a novel anaesthesia protocol, and use of additional MRI sequences to supplement BOLD fMRI, including functional magnetic resonance spectroscopy (fMRS) and perfusion MRI using arterial spin labelling (ASL). When these methods were applied to a rodent model of healthy ageing, fMRI using forepaw stimulation showed a decrease in the size of the activated region in the somatosensory cortex with age, coupled with a decrease in glutamate turnover, while cerebral blood flow remained the same. This suggests that the change in BOLD signal observed in ageing is a consequence of a reduction in neuronal metabolism, rather than impairment of neurovascular coupling. When applied to a rodent model of hypertension, the opposite was observed, in which an increase in resting CBF was observed as hypertension progressed, followed by a decrease in the size of the BOLD signal, with no significant change in glutamate turnover, suggesting the changes in BOLD signal are vascular in origin. Due to the high variability in lesion volume, stroke experiments were inconclusive.

This thesis shows that propofol is a suitable anaesthetic agent for longitudinal fMRI, and that other less common MRI modalities combined with BOLD fMRI can provide new insights into long term changes in neurovascular function.

Credit author statement

Andrew Crofts: conceptualization, methodology, data curation, writing – original draft.

Melissa Trotman-Lucas: methodology, supervision, animal MCAO surgery.

Justyna Janus: methodology, supervision.

Michael Kelly: conceptualization, funding acquisition, supervision, methodology, writing-review and editing

Claire Gibson: conceptualization, funding acquisition, supervision, methodology, writing-review and editing

Tracy Farr: resting state fMRI data analysis

Gerard Hall: resting state fMRI data analysis

Publications list

Crofts A, Kelly ME, and Gibson CL. Imaging functional recovery following ischemic stroke: Clinical and preclinical fMRI studies. *J Neuroimaging* 2020; 30: 5-14

Review paper including sections of chapter 1 on anaesthetic and chapters 1 and 4 on ischaemic stroke.

Crofts A, Trotman-Lucas M, Janus J, Kelly ME and Gibson CL. A longitudinal, multi-parametric functional MRI study to determine age-related changes in the rodent brain. *Neuroimage* 2020. doi: 10.1016/j.neuroimage.2020.116976 Online ahead of print.

Research paper containing fMRI, fMRS and ASL results from the ageing study presented in chapter 3.

Crofts A, Trotman-Lucas M, Janus J, Kelly ME and Gibson CL. Longitudinal multi-modal fMRI to investigate neurovascular changes in Spontaneously Hypertensive Rats. *J Neuroimaging* 2020. DOI: 10.1111/jon.12753. In Press.

Research paper containing results of the hypertension study presented in chapter 5.

Acknowledgements

Firstly, I would like to thank the Medical Research Council, for providing funding through their IMPACT doctoral training partnership for this PhD project.

I would like to thank my supervisors, Professor Claire Gibson and Dr. Michael Kelly, for all their support and guidance over the last three years. Both of you trusted me to develop my own ideas that were probably completely different from where you saw the project going, and thanks to everything you taught me, some of them worked. I could not have asked for better supervisors. I would also like to thank Dr. Doug Barrett for stepping in as co-supervisor late in the day when circumstances changed so I could get through my final year.

I would also like to thank Justyna Janus and Melissa Trotman-Lucas for their help with the animal and MRI work, none of which would have been possible without their expertise. Also thanks to Tracy Farr and Gerard Hall for their help with data analysis.

Thanks also to the technical staff in the PRF, for all their hard work caring for the animals, and to my fellow students in the Gibson group, NPB, and my DTP cohort for their help.

Finally, I would like to thank my family and friends for being so patient and supportive for the last three years.

Contents

Chapter 1: Introduction. P8

- 1.1. Functional neuroimaging. P8
- 1.2. Current challenges in fMRI research. P13
- 1.3. Mechanisms of neurovascular coupling. P16
- 1.4. Neurovascular coupling in ageing and disease. P18
- 1.5. Hypertension. P24
- 1.6. Cerebral stroke. P26
- 1.7. PhD aims. P29

Chapter 2: Development of imaging and anaesthetic protocols. P32

- 2.1. Introduction. P32
- 2.2. Methods. P36
- 2.3. Discussion. P45

Chapter 3: Longitudinal functional MRI for animal studies of neurovascular coupling in healthy ageing. P47

- 3.1. Introduction. P47
- 3.2. Methods. P50
- 3.3. Results. P54
- 3.4. Discussion. P61

Chapter 4: Longitudinal functional MRI of recovery following experimental stroke in rats. P66

- 4.1. Introduction. P66
- 4.2. Methods. P73
- 4.3. Results. P77
- 4.4. Discussion. P84

Chapter 5: Longitudinal functional MRI imaging changes in the BOLD response of Spontaneously Hypertensive Rats. P91

5.1. Introduction. P91

5.2. Methods. P94

5.3. Results. P97

5.4. Discussion. P102

Chapter 6: Discussion and Conclusions. P106

6.1. Development, validation and applications of methods – Anaesthetic protocol. P106

6.2. Development, validation and applications of methods – MRI protocol. P107

6.3. Limitations of the current studies. P110

6.4. Future directions. P111

References. P114

Figures and Tables

Table 1.1 – Mediators of vasodilation and vasoconstriction, P18

Figure 1.1 – Anatomy of the Circle of Willis, P21

Table 2.1 – Spatial SNR of EPI sequences in a water phantom, P39

Table 2.2 – Temporal SNR of EPI sequences in a water phantom, P40

Figure 2.1 – Processing steps to prepare an EPI image for analysis, P41

Figure 2.2 – Steps required to locate the region of interest with scout scans, P44

Figure 3.1 – Weight progression in ageing rats, P55

Figure 3.2 – Example BOLD fMRI images in ageing rats, P55

Figure 3.3 – Effect of age on BOLD signal, P56

Figure 3.4 – Effect of age on time-to-peak of BOLD signal, P57

Figure 3.5 – Effect of age on glutamate turnover, P58

Figure 3.6 – Effect of age on NAA and Inositol levels, P58

Figure 3.7 – Heirarchy matrix showing functional connectivity in rats, P59

Table 3.1 – Changes in functional connectivity with age, P60

Figure 3.8 – Effect of age on cerebral blood flow, P60

Table 4.1 – Summary of methods/outcomes of fMRI studies of experimental stroke in rats, P67

Figure 4.1 – Rat weights prior to and following MCAO, P77

Figure 4.2 – Neurological score of rats post-MCAO, P78

Figure 4.3 – Progression of stroke lesions following MCAO, P79

Figure 4.4 – Change in BOLD signal following experimental stroke, P81

Figure 4.5 – Difference in BOLD signal by lesion volume following experimental stroke, P81

Table 4.2 – Time taken for each rat to exhibit a BOLD response in S1FL following MCAO, P82

Figure 4.6 – Glutamate turnover following MCAO, P83

Figure 4.7 – NAA levels following MCAO, P83

Figure 4.8 – Cerebral blood flow change following MCAO, P84

Figure 5.1 – Change in blood pressure over time in SHRs, P98

Figure 5.2 – Example BOLD fMRI images in SHRs, P99

Figure 5.3 – Effect of age on BOLD signal in SHRs, P100

Figure 5.4 – Effect of age on glutamate turnover in SHRs, P101

Figure 5.5 – Effect of age on NAA levels in SHRs, P101

Figure 5.6 – Effect of age on cerebral blood flow in SHRs, P102

Chapter 1: Introduction

In the past few decades, it has become apparent that neurovascular dysfunction is also a major factor in the progression of age-related neurodegenerative diseases (Girouard and Iadecola, 2006). Neurovascular changes are present to a lesser extent in healthy, aged humans (D'Esposito *et al.*, 1999). Comparisons using fMRI and cognitive tests in humans have identified differences in the blood oxygen level dependent (BOLD) signal in young vs old adults (Fabiani *et al.*, 2014; West *et al.*, 2019), as well as differences in neuronal metabolism (Boumezbeur *et al.*, 2010), cerebral blood flow (CBF, Tarumi and Zhang, 2018) and cognitive ability (Zahr *et al.*, 2013). Functional MRI has also been used to show changes in task-related BOLD activity in studies comparing healthy aged subjects with subjects displaying mild cognitive impairment (Machulda *et al.*, 2009). However, in rodents, fMRI has not previously been used to study changes in healthy ageing. Ischaemic stroke, in which a vessel in the brain becomes occluded, also causes severe impairment to neurovascular coupling, as well as neuronal death, followed by reorganisation during recovery (Feydy *et al.*, 2002). How recovery progresses has been characterised in humans using fMRI, however rodent models show high variability in functional imaging studies (Dijkhuizen *et al.*, 2001; 2003; Weber *et al.*, 2008; Lake *et al.*, 2017a; b), and so studying recovery in a controlled model, and development of therapeutics, is difficult. Hypertension, known to cause cognitive impairment (Kitagawa *et al.*, 2009) and as a risk factor for stroke, Alzheimer's disease and vascular dementia (Iadecola and Gottesman, 2019), has also been shown to affect task-related BOLD signal (Coulson *et al.*, 2015) and CBF (Jennings *et al.*, 1998) in humans. However, this has also not been previously studied in a preclinical model. This thesis will use a multi-parametric MRI protocol to investigate changes to the BOLD signal, cerebral blood flow (CBF) and neuronal metabolism in healthy ageing, ischaemic stroke and hypertension. This section will discuss the mechanisms behind neurovascular coupling, and how these are affected by normal ageing, ischaemic stroke and hypertension.

1.1 Functional neuroimaging

1.1.1 PET, SPECT, Optical Image Spectroscopy and Near Infrared Spectroscopy

The study of changes in brain activity in humans is made possible by a number of non-invasive functional imaging methods. These methods are also beneficial in pre-clinical studies, as minimally invasive techniques are beneficial for animal welfare, as well as having a lesser impact on the measured outcome. Common methods between clinical and pre-clinical studies is also beneficial for translatability of research, as the differences between an animal model

and a human subject can be better characterised if methods are kept the same between the two. Before discussing functional MRI (fMRI), this section will briefly summarise the advantages and disadvantages of other functional imaging methods used in pre-clinical and clinical research.

Positron emission tomography (PET) imaging allows for a wide variety of tissue types and metabolic processes to be imaged using radiolabelled tracers. Use of PET was particularly common in neuroimaging research before use of fMRI became widespread (Chollet *et al.*, 1990; Weiller *et al.*, 1992; Dieber *et al.*, 1997; Kuge *et al.*, 1997), and still remains in use due to its application in imaging receptor and enzyme kinetics, metabolism of substrates such as glucose and oxygen, and blood flow (Cherry, 2001; Carey *et al.*, 2006). In preclinical research, PET has been applied to the study of neurological diseases including stroke, Alzheimer's, and multiple sclerosis (Janssen *et al.*, 2016). MR can be applied to studying metabolism, through use of MR spectroscopy for a 1D spectrum of metabolites, or MRS imaging for 2D and 3D metabolite imaging (Rosen and Lenkinski, 2007). However, PET has the advantage of being highly specific to the chosen metabolite, with greater spatial and temporal resolution, and a broader range of metabolites and processes that can be detected. The main disadvantage of PET is the requirement for a radioactive tracer, which emits gamma rays, and thus there are practical limitations around production and storage of tracers as well as radiation safety limits on how frequently imaging can be performed (Tremoleda *et al.*, 2012).

Single-photon emission computed tomography (SPECT) is based on a similar principle to PET. SPECT tracers emit single gamma photons, which are recorded by detectors rotating around the animal, allowing a 3D image to be reconstructed (Tremoleda *et al.*, 2012). SPECT has many of the same advantages as PET, with a wide variety of tracers available for metabolic imaging, and applications in preclinical models of stroke, Alzheimer's, Parkinson's, and other neurological diseases (Khalil *et al.*, 2011). SPECT tracers have a longer half-life than PET tracers, and are cheaper to produce, making SPECT more practical for applications that do not require the high sensitivity of PET. This also allows SPECT to be used for imaging over hours or even days (Rahmim and Zaidi, 2008). However, the disadvantage of SPECT is a reduced sensitivity and temporal resolution compared to PET, and so PET is more common for functional imaging (Khalil *et al.*, 2011).

For functional imaging in the cortex, near-infrared spectroscopy (NIRS) and optical image spectroscopy (OIS) can be used as an alternative to fMRI, or in conjunction with fMRI. These methods detect the same changes in cerebral blood flow that are detected by fMRI (Kennerly

et al., 2005). Like fMRI, these methods do not use ionising radiation, and one advantage over fMRI is not using a magnetic field, making them compatible with patients or animals that have metallic or electronic implants. Both also have the advantage of not using large machinery, allowing a wider variety of tasks or stimuli to be presented to the subject. For example, NIRS has been used to image healthy subjects during activities including table tennis, playing the piano and playing the violin (Balardin *et al.*, 2017), while OIS can be used in awake animals (Martin *et al.*, 2002). The main disadvantage is the limited depth which can be imaged, due to use of the visible and infrared spectra, and so light scattering by the tissue prevents subcortical regions from being imaged (Patil *et al.*, 2011). Additionally, OIS does not translate to human studies, due to the requirement for surgery to give the animal a cranial window (Kennerly *et al.*, 2005). Laser Doppler Flowmetry (LDS), which uses a similar principle as OIS, does not require a cranial window, however the output is a time series over a given region, rather than a functional image (Cuccione *et al.*, 2017). However, where the location of the region of interest is known, and of suitable depth, these methods do provide a suitable alternative to fMRI where fMRI would be impractical due to cost, anaesthesia, or use of metallic or electronic implants.

1.1.2. Functional MRI

Functional MRI, a non-invasive imaging method, is commonly used in preclinical and clinical studies to detect changes in brain activity. Functional MRI relies on the magnetic properties of oxyhaemoglobin and deoxyhaemoglobin to detect localised changes in blood flow caused by neuronal activity (the blood oxygen level dependent, or BOLD, response, Ogawa *et al.*, 1992). When neurons are active, blood flow to the region increases to meet the increased demand for oxygen through neurovascular coupling (Kim and Ogawa, 2012). This allows activity in response to a task or stimulus to be localised and quantified, using the BOLD response as a proxy for neuronal activity. As fMRI doesn't use ionising radiation, chemical tracers or require invasive surgery/implants, it is an ideal method for clinical studies into progressive neurovascular pathologies such as stroke.

Functional MRI images can be taken in a number of ways. The most common fMRI method is measuring the Blood Oxygenation Level Dependent (BOLD) response. BOLD fMRI detects changes in diamagnetic oxyhaemoglobin and paramagnetic deoxyhaemoglobin levels, typically by acquiring T_2 -star (T_2^*)-weighted images. T_2^* -weighting measures differences in tissue contrast due to the transverse relaxation of protons following the radiofrequency (RF) excitation pulse. Random atomic interactions and magnetic field inhomogeneity cause

dephasing of protons' spins as the signal decays, this dephasing can be detected to provide contrast between tissues (Chavhan *et al.*, 2009). In BOLD-fMRI, deoxyhaemoglobin provides the contrast, as the blood vessels and surrounding tissues are paramagnetic, resulting in local magnetic field inhomogeneities that can be detected by the MRI scanner (Nair, 2005). These changes provide a proxy for neuronal activity, through the mechanism of functional hyperaemia. The structure of the local vasculature is a confounding factor, depending on the relation of draining veins, venules and capillaries to the brain region, and changes to the imaging method can compensate for this. A second confounding factor detected in some studies is the 'initial dip', in which neuronal activity and CBF are thought to be briefly uncoupled, causing a short negative BOLD response as oxidative metabolism increases without a corresponding increase in blood flow (Ances, 2003). This initial dip has also been used in some studies as a method of improving spatial resolution, as it was found that only the region with the maximal response to a stimulus exhibited an initial dip, while neighbouring regions exhibited an increased BOLD response without an initial dip, thus providing improved localisation of activity in some contexts (Malonek and Grinvald, 1996; Thompson *et al.*, 2003).

Another fMRI technique, arterial spin labelling (ASL), has the advantage of fewer factors contributing to the signal, potentially making it easier to interpret signal changes during activation. ASL uses RF pulses to magnetically align the water molecules in a given volume of blood as it flows through the carotid artery, in continuous ASL, or in the imaging slice, in pulsed ASL. This allows water in flowing blood to function as an endogenous tracer, allowing for detection of changes in blood flow when a post-labelling image is acquired at the imaging region (Williams *et al.*, 1992). This detection of CBF is thought to be better localised to the site of activation than BOLD, and has fewer confounding factors. Neither the metabolic rate of oxygen consumption, nor the oxygen extraction fraction contributes to the signal and information on perfusion of a brain region can be easily extracted. Also, magnetic effects that can degrade the BOLD signal do not affect the ASL signal (Petcharunpaisan *et al.*, 2010). Instabilities in the image intensity can be accounted for better than BOLD by combining control images with labelled images. This is an advantage in longitudinal studies, allowing for more accurate tracking of changes over time. The main confounding factors are the intrinsically low SNR, and the change in exchange rate of water molecules between the capillaries and extracellular space during activation (Detre and Wang, 2002).

1.1.3. Resting-state fMRI

BOLD fMRI can also be used to investigate functional connectivity between brain regions in the absence of a task, known as resting-state fMRI (Biswal *et al.*, 1995). Baseline brain activity when not actively performing a task or responding to sensory input causes slow, repetitive increases and decreases in blood flow, or low-frequency fluctuations (Lowe *et al.*, 2000). Resting-state fMRI measures the frequency and amplitude of these fluctuations, and through independent component analysis, functionally independent regions can be visualised. Correlations between these components and the amplitude of low-frequency fluctuations can then be used to identify brain networks, for example the sensorimotor network, visual network, or the default mode network (Cordes *et al.*, 2000; Lowe *et al.*, 2000; De Luca *et al.*, 2006; Fox and Raichle, 2007), and the strength of these networks is thought to underlie the brain's ability to integrate information from several inputs and give rise to cognitive processes (Gordon *et al.*, 2018).

1.1.4. Magnetic Resonance Spectroscopy

MR spectroscopy can also provide valuable insights into brain function, through quantifying metabolite and neurotransmitter levels. In MRS a single voxel is scanned and several averages are compiled to give a spectrum, in which each peak represents metabolites that resonate at different frequencies with the magnetic field, depending on the proton content (Rosen and Lenkinski, 2007). In the brain, these metabolites include N-Acetyl Aspartate (NAA), Lactate, Creatine, Choline, Glutamine/Glutamate and Glycine, and at lower field strengths, the presence or absence of these signals is dependent on echo time (Zhu and Barker, 2011). At higher field strengths, increased sensitivity and larger chemical shift dispersion means more metabolites can be reliably detected with less reliance on echo time, with the disadvantage that field inhomogeneity can cause increased noise (Xin *et al.*, 2016). Quantification of NAA, Lactate, Creatine and Choline can reveal information on age-related changes in the brain (Pfefferbaum *et al.*, 1999, Boumezbeur *et al.*, 2009), and the progression of pathologies such as stroke or Alzheimer's disease (Graham *et al.*, 1992; Schuff *et al.*, 1998), and research at higher field strengths has provided new insights into changes in glutamate, glutamine, glycine and myo-inositol on these conditions. While the low signal strength means that several averages are required to build adequate signal-to-noise ratio (SNR), as technology advances there has been interest in applying MR Spectroscopy to functional studies to investigate changes in glutamate turnover and lactate production in response to stimuli or tasks, which may provide novel insights into brain function and complement BOLD fMRI studies.

1.2. Current challenges in fMRI research

For preclinical fMRI to become more widespread, and fMRI research to better translate to human studies, there are still several challenges to overcome. The non-invasive nature of MRI is beneficial in terms of animal welfare and for longitudinal studies. Many studies using MRI for structural measurements use a longitudinal study design, however in functional MRI this is more difficult. A longitudinal experimental design is important in the study of healthy ageing, progressive diseases, such as Alzheimer's disease, or recovery following injury such as stroke. From an ethical perspective, use of longitudinal experiments reduces animal numbers, and requires the use of minimally invasive protocols to refine studies and cause less suffering to individual animals. From a scientific perspective, use of separate groups at each time point increases inter-subject variability, due to the increased number of animals. It is also then not possible to determine the progression of disease or aging, as animals are compared to a separate control group, whereas in longitudinal studies, a baseline for each animal can be obtained, and individual animals can be tracked over time. In order to perform longitudinal studies, the methods used must give a strong BOLD signal, and not cause additional harm to the animal.

1.2.1. Anaesthetics

A major confounding factor in preclinical fMRI is the requirement to anaesthetise animals for scanning. While all anaesthetic agents will cause differences in brain and vascular activity from the awake state, different anaesthetics affect fMRI acquisition in different ways. Choice of anaesthetic agent is important to longitudinal preclinical fMRI studies, to minimise the impact on the BOLD signal, neuronal responses and functional connectivity. Urethane and alpha-chloralose are the two most commonly used injectable anaesthetics for fMRI, and while they both allow for robust BOLD responses, their carcinogenic effects prevent their use for longitudinal experiments (Tremoleda *et al.*, 2012). For longitudinal fMRI, some studies use a continuous infusion of medetomidine (Weber *et al.*, 2006). However, medetomidine does introduce some confounding factors, as it produces a variable depth of anaesthesia, and large changes in heart rate over time (Pawela *et al.*, 2009). Additionally, in functional connectivity studies, animals show impaired connectivity compared to the awake state or other anaesthetics, with all regions showing a reduction in correlation coefficients, and the thalamo-cortical pathway showing complete loss of activity (Paasonen *et al.*, 2018). Low doses of isoflurane have also been used in some fMRI studies (Van Meer *et al.*, 2010). However, even low doses can affect the BOLD signal, which compromises the accuracy of results, particularly

in longitudinal studies, as a reduction in signal amplifies the effects of physiological noise and inter-animal variation (Masamoto *et al.*, 2009). Halothane also has similar effects on stimulus-based BOLD signal, and is also considered unsuitable for use in fMRI studies (Austin *et al.*, 2005). There is evidence to suggest that isoflurane may be suitable for resting-state fMRI studies, depending on the dose rate and regions being investigated. Cortical functional connectivity is well preserved under isoflurane (Passonen *et al.*, 2018). However, fluctuations in subcortical regions are impaired in a dose-dependent manner, requiring less than 1% isoflurane for any subcortical or thalamocortical networks to be identified (Liu *et al.*, 2013; Hamilton *et al.*, 2017).

Propofol, while less commonly used than medetomidine, isoflurane or urethane, has been suggested as a good candidate for preclinical fMRI studies (Paasonen *et al.*, 2018; Lahti *et al.*, 1999; Kelly *et al.*, 2010; Griffin *et al.*, 2010). It has been shown that cerebral autoregulation and cerebrovascular reactivity are maintained under propofol while they are lost under isoflurane (Strebel *et al.*, 1995; Cenic *et al.*, 2000), and signal intensity under propofol is approximately three times greater than under medetomidine, with haemodynamic response function (HRF) closer to that of the awake state (Schlegel *et al.*, 2015). Functional connectivity responses, cerebral autoregulation, cerebrovascular reactivity under propofol are also closer to that of the awake state (Griffin *et al.*, 2010; Paasonen *et al.*, 2018). However, to date, use of propofol in disease models such as ischaemic stroke is limited to a few studies observing changes in global CBF in response to hypercapnia (Lake *et al.*, 2017a; b).

While for practical reasons anaesthetising animals for MRI studies has been the norm, protocols have been developed for scanning awake animals (Martin *et al.*, 2013; Aksenov *et al.*, 2015). The benefit of this is clear, rendering animals unconscious affects brain and vascular activity, so functional responses in an anaesthetised animal are different to those in an awake animal. Similarly, if comparing human and animal studies, using anaesthesia introduces a new confounding factor, as humans are usually awake when undergoing scanning. When studies have compared awake and anaesthetised animals, regardless of anaesthetic used, a greater signal change and activated area were found in the awake condition, with propofol giving the next largest BOLD signal change (Aksenov *et al.*, 2015; Lahti *et al.*, 1999; Peeters *et al.*, 2001). Different anaesthetic protocols also alter network activation (Paasonen *et al.*, 2018) and can have a variety of adverse effects on blood pressure, breathing, oxygen saturation and temperature, depending on choice of agent and dose (Tremoleda *et al.*, 2012). Anaesthetising animals does mean movement is minimised, thus preventing loss of image quality and signal artefacts. It also prevents stress from the sound of the MRI scanner, reflexive movement in response to stimulation, and discomfort from attachment of electrodes or physiological

monitoring equipment. However, there are several problems in implementing an awake imaging protocol in longitudinal and disease studies. Awake rodents have not, to date, been reported in functional imaging in other age-related neurological disease models. Thus, it is unclear if, or how disease may affect acclimatisation to the scanner and the extensive pre-training required. Training of rats for awake imaging is time consuming, with studies performing training sessions daily for at least two weeks (Martin *et al.*, 2013; Stenroos *et al.*, 2018) and any condition which may have damaging effects on memory, spatial awareness, motor control, and stress levels will have a detrimental effect on the habituation state of the animals (Wang *et al.*, 2009)

1.2.2. fMRI methodological challenges

Another drawback of fMRI, both in preclinical and clinical settings, is that the BOLD signal is not a true measure of neuronal activity, CBF, or neurovascular coupling. The BOLD signal is comprised of the increase in deoxyhaemoglobin from oxygen metabolism in the active region, and the disproportionately large increase in oxyhaemoglobin in the active region and surrounding areas (Ogawa *et al.*, 1992). Thus, without data on cerebral metabolic rate of oxygen (CMRO₂), the BOLD signal can only be quantified in arbitrary units. This also means that several factors can influence both the magnitude of the signal and the size of the active region, including neuronal activity, neuronal metabolism, changes in signalling pathways, vascular reactivity, and resting CBF. Because of this, changes in the BOLD signal may not truly represent changes in brain activity. The advantage of BOLD fMRI is high spatial and temporal resolution, however more specific imaging methods may complement the BOLD signal and aid in understanding changes in the underlying neuronal and vascular processes.

Neuronal metabolism is one more direct method of measuring neuronal activity, and can be done in conjunction with measuring the BOLD signal. As discussed previously, PET imaging can be used to image cerebral oxygen and glucose metabolism (Cherry, 2001), and concurrent PET/fMRI studies have been used to investigate the haemodynamic response and postsynaptic receptor activity concurrently (Wey *et al.*, 2014; Sander *et al.*, 2016). However, the drawbacks of PET imaging mean this method is not suitable for longitudinal studies.

An alternative method of quantifying neuronal metabolism is through MR spectroscopy (MRS). MRS can detect a range of metabolites in a given voxel, and of particular interest for functional studies are glutamate and lactate. Glutamate, the most common neurotransmitter in the brain, increases with neuronal activity as stored glutamate is released and more glutamate is produced. Some studies have shown that this change can be detected using MRS to take spectra

during stimulus blocks in the same manner as fMRI (Gussew *et al.*, 2010). Lactate may also be quantifiable this way. Lactate, produced during anaerobic respiration, is thought to be “shuttled” from astrocytes to neurons in order to maximise the energy efficiency of neurons, and lactate production is thought to increase during stimulation (Deitmer *et al.*, 2019). Through use of functional MRS in conjunction with fMRI, it may be possible to use these metabolic changes as a non-invasive method of quantifying neuronal activity (Pritchard *et al.*, 1991).

Some studies have shown that it may be possible to use MRI to image synaptic activity directly. When post-synaptic sodium and calcium channels open to depolarise the post-synaptic membrane, extracellular water flows into the cell by osmosis. This alters the proportion of extracellular vs intracellular water, the signal detected by diffusion-weighted MRI (dMRI, Le Bihan *et al.*, 2006)). The relatively unconstrained diffusion of extracellular water, compared to the limited diffusion of intracellular water, can be used to give very high resolution structural images, and when used in diffusion tensor imaging, can image white matter tracts and build maps of structural connectivity (Moseley, 2002). Using a short repetition time, and a stimulus or task as used in BOLD fMRI, changes in water diffusion with activity can be imaged. These changes occur in the same region as changes in the BOLD signal under the same condition, but over a much smaller area and with a shorter time-to-peak, supporting the hypothesis that these changes in signal are neuron driven rather than blood driven (Nunes *et al.*, 2019). However, due to technical challenges such as lower SNR, and the safety of the rapid pattern of gradient switching required, means that this technique is not yet widely used.

Through a combination of an improved anaesthetic protocol and multiparametric fMRI protocols, animal use can be reduced, and studies can be refined to use less invasive methodology, while still giving data on both neurological and vascular aspects of neurovascular coupling in ageing and disease.

1.3. Mechanisms of Neurovascular Coupling

Of all the organs in the body, the brain uses the most energy, accounting for 20% of oxygen consumption, while only taking 2% of body mass. Despite this high energy demand, the brain has no ability to store energy, and thus is reliant on an uninterrupted blood supply and the ability to control blood flow to meet changing demand. Neural activation is met by a rapid increase of blood flow to the local area, providing the increased oxygen and glucose needed to maintain this activity and facilitating the rapid removal of waste products (Girouard and Iadecola, 2006). The mechanism behind this localised control of blood flow is referred to as neurovascular coupling. On a larger scale, the brain continuously responds to fluctuations in

arterial pressure from normal activity in order to maintain a stable level of cerebral blood flow (CBF), known as cerebrovascular autoregulation (Armstead, 2016). On an even larger scale, blood flow from the periphery can be redistributed to increase cerebral perfusion (Leishout *et al.*, 2003).

The system of vascular components, glia and neurons controlling local changes in blood flow is termed the Neurovascular unit. The neurovascular unit is defined by interactions between neuronal terminals, glia, the various components of arteriolar or capillary walls, extracellular matrix and basement membrane. Through signalling between neuronal terminals and vessel walls, particularly through endothelial cells, myocytes, pericytes and glia, as well as response to compounds in the blood, local changes in blood flow are controlled to increase or decrease perfusion where necessary (Girouard and Iadecola, 2006). In particular, the process of functional hyperemia is controlled through interactions within the neurovascular unit, to increase oxygen and glucose delivery during neuronal activity (Stanimirovic and Friedman, 2012).

The process of functional hyperemia is detected by functional MRI, as well as other functional imaging methods such as positron emission tomography (PET), near-infrared spectroscopy and optical image spectroscopy (Ogawa *et al.*, 1992; Raichle, 1998; Kennerly *et al.*, 2005). Increased neuronal activity causes an increase in oxygen and glucose metabolism, and a rapid, local increase in blood flow to meet this demand (Ogawa *et al.*, 1992). During neuronal activation, CBF has been found to increase by as much as 50%, while CMRO₂ only increases by 5% (Fox and Raichle, 1986). This causes an overall increase in local oxyhaemoglobin concentration, and a change in local magnetic susceptibility due to the diamagnetic properties of oxyhaemoglobin, compared to the paramagnetic deoxyhaemoglobin, which is detected as the blood oxygen level dependent (BOLD) signal (Ogawa *et al.*, 1992). Through analysing the energy consumption behind individual components of neuronal activity, it was found that the most energy demanding processes are restoration of ion homeostasis following action potentials and postsynaptic potentials (47% and 34% of neuronal energy demand, respectively), followed by maintaining resting potential (13%), glutamate recycling and presynaptic calcium currents making approximately 3% each of energy demand, with vesicle recycling using the least energy (1%), suggesting that it is postsynaptic activity that drives functional hyperaemia (Attwell and Laughlin, 2001). Several signalling mechanisms contribute to functional hyperaemia, including direct signalling from neurons to smooth muscles and pericytes, connecting interneurons, and astrocyte-mediated signalling, the mechanisms behind which are summarised in table 1.1. Metabolic changes and dysfunction in these

signalling mechanisms may contribute to the impairment of neurovascular coupling with age and disease (Stanimirovic and Friedman, 2012).

Pathway	Molecular mediator(s)	Effect	Ref
Astrocyte	MGluRs	Arachidonic acid release, smooth muscle dilation	Carmignoto and Gomez-Gonzala, 2010
Astrocyte	K ⁺ flow	K ⁺ uptake and release by astrocytes activates smooth muscle receptors, causes dilation	Filosa <i>et al.</i> , 2006
Cholinergic neurons	Muscarinic M3/ M5 receptors	Acetylcholine binding activates nitric oxide synthase in the capillary endothelium, capillaries dilate.	Elhusseiny and Hamel, 2000
Cholinergic neurons	Muscarinic M1 receptors	Acetylcholine binding stimulates vascular smooth muscle dilation in cerebral arteries.	Dauphin <i>et al.</i> , 1991
Serotonergic neurons	5HT receptors	Serotonin binding stimulates smooth muscle constriction in arterioles.	Cohen <i>et al.</i> , 1996
GABA-ergic interneurons	Neuropeptide Y	Stimulates smooth muscle constriction in cerebral arteries	Tuor <i>et al.</i> , 1990

Table 1.1: Mediators of vasodilation and vasoconstriction

There has been some debate surrounding which vessels generate the hyperaemic response. The initial response is thought to begin in the local capillary bed, triggered by nitric oxide and

cyclooxygenase 1 and 2 signalling (Berwick *et al.*, 2005; Chen *et al.* 2011), though there was resistance to this idea for some time due to the lack of smooth muscle on capillaries (Sheth *et al.*, 2005; Vanzetta *et al.*, 2005). This initial response is mediated by pericytes (Chen *et al.*, 2011), which express actin filaments similar to muscle cells giving them contractile properties (Alarcon-Martinez *et al.*, 2018). Signalling then propagates upstream through gap junction signalling to arterioles and arteries, providing increased blood flow to the larger region. This, combined with the weighting from deoxygenated blood as capillaries drain, may explain the discrepancy between the size of the group of active neurons and size of the BOLD response seen on fMRI (Chen *et al.*, 2011). Inhibitory mechanisms activate when neuronal activity returns to resting levels (Boorman *et al.*, 2010), triggering vasoconstriction to return local CBF to baseline levels.

This variety of mechanisms underlying neurovascular coupling allows for a highly adaptable system, allowing the neurovascular unit to respond to support short term and long term changes in neuronal activity, at the capillary level and at the arteriole level. However, with ageing, these mechanisms become less active and neurovascular coupling becomes less efficient. Similarly, a variety of neurological and vascular diseases, including Alzheimer's Disease, Parkinson's Disease, stroke, atherosclerosis, and atrial fibrillation can disrupt neurovascular coupling (Girouard and Iadecola, 2006).

1.4. Neurovascular Coupling in Ageing and Disease

A reduction in cognitive function is a well-documented effect of ageing (Christensen, 2001; Bishop *et al.*, 2010). Particular aspects of cognitive function that are impaired with age are cognitive speed, relating to performance on perception and motor tasks, and short term declarative memory, measured by recall tasks, while cognitive functions such as vocabulary and procedural memory are less affected (Christensen, 2001). Changes in neurovascular coupling are thought to be a major contributing factor to this, which can include reduction of cerebral blood flow (Kannurpatti *et al.*, 2010), reduction of cerebral metabolism (Cichocka and Beres, 2018), or changes in the activity of the signalling pathways discussed above. There is a degree of variability between different studies in which factors are affected by ageing, and this section will address these differences.

Signalling in the neurovascular unit can become dysfunctional with ageing in a number of ways. One example is the cholinergic signalling system. Studies in rodents and humans have shown a reduced sensitivity to nicotine in the vasculature with age, while muscarinic acetylcholine receptors and acetylcholine release remain unaffected (Nordberg *et al.*, 1994;

Uchida *et al.*, 2000). Nitric oxide (NO) signalling is also altered in the ageing brain. Nitric oxide is produced by the nitric oxide synthase pathway, in neurons and endothelial cells, each with their own isoform of nitric oxide synthase (NOS), with each pathway showing different changes in neurovascular coupling (Dormanns *et al.*, 2016). While neuronal NO release is not impaired, vascular responsiveness to NO is reduced by as much as 40% (Ledo *et al.*, 2017; Laurencio *et al.*, 2018). Astrocyte structure, expression of aquaporin water channels, and K⁺ and Ca²⁺ signalling are also disrupted in ageing. When aquaporin channels are lost, impaired osmosis causes shrinking and retraction of astrocytic end-feet, and disruption of potassium and calcium currents (Duncombe *et al.*, 2017). These signalling changes underlie a systemic change in cerebral perfusion. Resting CBF is thought to be reduced in age (Tarumi and Zhang, 2018), and the linear coupling between increased activity and increased CBF is impaired (Fabiani *et al.*, 2014). In addition to dysfunctional signalling mechanisms, structural changes also contribute to this effect. This includes changes in the structure of the vessels themselves and in the anatomy of the vascular network in the brain.

To briefly summarise the anatomy of the arteries providing blood supply to the brain, anterior and posterior cerebral circulation are provided by two groups of arteries, the internal carotid and the vertebral arteries, respectively. Communicating arteries in the Circle of Willis (Fig. 1.1. Vrselja *et al.*, 2014) provide connection between the two and distribute blood laterally (Lee, 1995; Dickey *et al.*, 1996; Hartkamp *et al.*, 1999). Other, smaller collaterals are also present between the terminals of the three major arteries, as well as connecting arterioles and collaterals elsewhere in the system (Lee, 1995). Under normal conditions, blood from the internal carotid and vertebral arteries do not mix, however the Circle of Willis allows for blood supply from one to compensate for reduced flow in the other. The internal carotid supplies arteries targeting the frontal lobe, anterior hypothalamus, hippocampus and amygdala (including the middle cerebral artery (MCA), which will be discussed in detail later. The vertebral arteries supply regions including the occipital lobe, thalamus and posterior hypothalamus. These arteries enter at the base of the skull before branching out across the surface of the cortex, in the subarachnoid space. The arteries enter the brain perpendicular to the cortex, before branching out into the network of arterioles and capillaries (Lee *et al.*, 1995). It is important to note that, in humans, there is a high variability in the Circle of Willis anatomy and the branching arteries. It is estimated that approximately 50% of the population has at least one absent or under developed artery in the Circle of Willis (Vrselja *et al.*, 2014), and while mathematical models suggest this should have no detrimental effect on brain perfusion in healthy individuals, if an artery is occluded then this reduced collateral flow can

impair reperfusion and exacerbate injury (Alastruey *et al.*, 2007). The number of collateral connections is approximately 4-5 times higher in rats, however rats are thought to show less variability than humans (Coyle and Jokelainen, 1982; Lee, 1995)

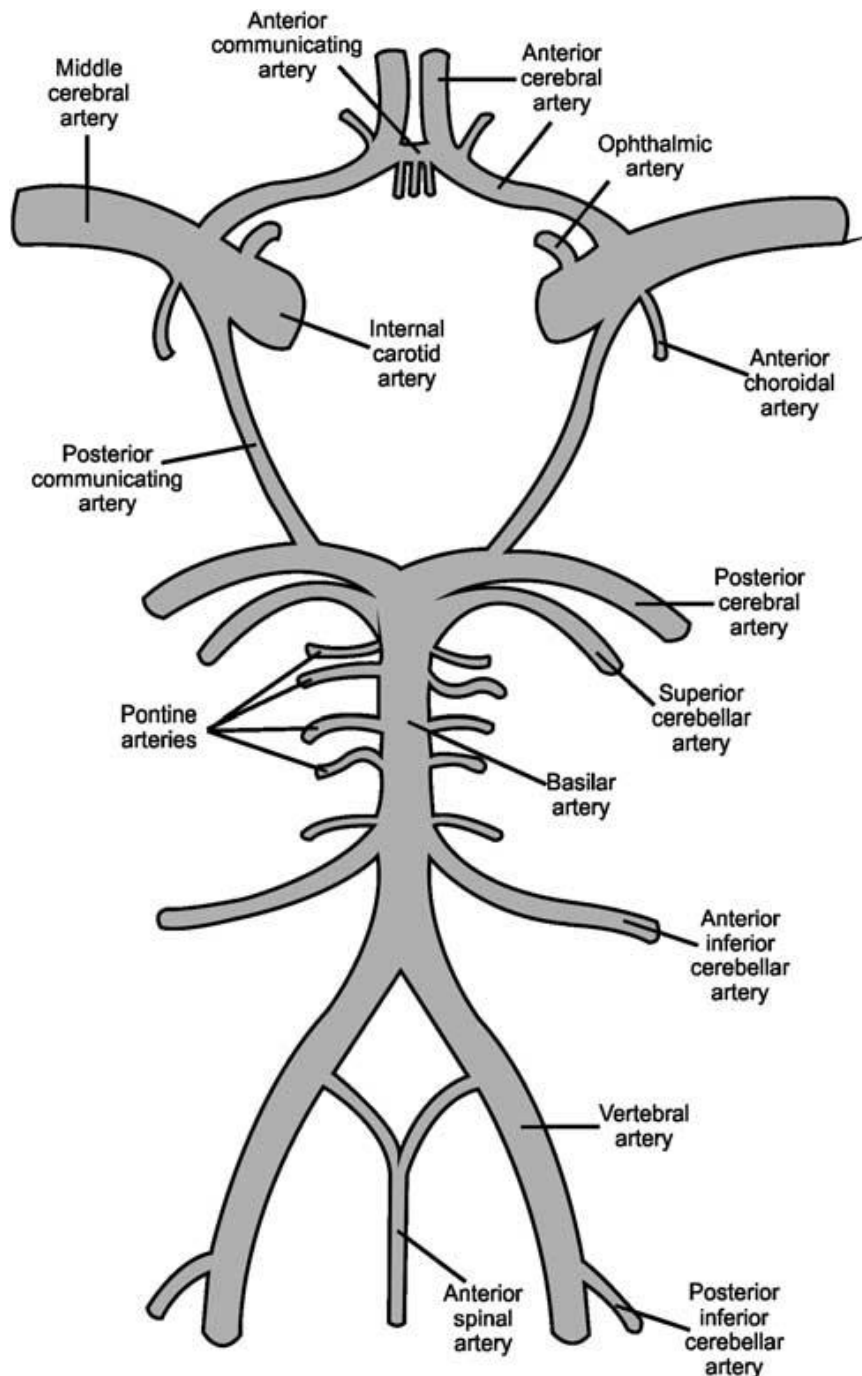


Fig. 1.1: Anatomy of the Circle of Willis and the main collateral arteries (Vrselja *et al.*, 2014)

Of the three main cerebral arteries, the MCA has the greatest blood flow velocity, between 20-30 cm/sec greater than the anterior cerebral artery. The posterior has the lowest blood flow velocity, lower than the anterior by approximately 10 cm/sec. The blood flow velocities

of these arteries have all been shown to decrease by approximately 20% between the ages of 20 and 70 (Vriens *et al.*, 1989; Krejza *et al.*, 1999). Animal studies into the mechanism behind this decrease found a combination of two factors, a more sensitive vasoconstrictor response and a smaller vasodilator response. Application of the vasodilator adenosine causes a reduced vasodilatory response in older animals compared to younger animals (Jiang *et al.*, 1992), while application of intravascular serotonin produced a larger vasoconstrictive response in the aged group (Hajdu *et al.*, 1993), suggesting an overall decrease in lumen volume, causing a reduction in flow. These findings, and the studies into signalling in the neurovascular unit discussed above, show that reduced CBF with ageing is a systemic phenomenon, occurring at the arterial level and at the capillary level.

The ultrastructure of the capillary network is also greatly affected by ageing. Several structural factors affect the function of the capillary network and are altered with ageing, including microvascular density, vessel tortuosity, collagen deposits and basement membrane thickness. The basement membrane (BM) is a continuous protein sheet that envelops the vasculature, serving as a scaffold for vessel formation, and forms an integral part of the blood brain barrier (BBB). The main components, collagen and laminin sheets, are selectively permeable to certain signalling molecules, such as vascular endothelial growth factor (VEGF), which are required for endothelial function (Stanimirovic and Friedman, 2012). However, collagen deposition increases with age, leading to a slow thickening of the basement membrane (Farkas and Luiten, 2001), and the BM thickness can more than double from this. This reduces blood-brain barrier (BBB) permeability to glucose and amino acids (Mooradian *et al.*, 1991, Samuels *et al.*, 1983), contributing to the age-related uncoupling of neuronal activity, metabolism and blood flow. Several other age-related pathologies, such as hypertension and atherosclerosis, are known to exacerbate this effect (Farkas *et al.*, 2000). This process also occurs in veins and venules, known as venous collagenosis, particularly affecting white matter regions. Narrowing of the lumen of these veins leads to a reduction in CBF, and can cause ischaemia (Brown *et al.*, 2002). These changes can also disrupt blood brain barrier function, and impair neurovascular coupling through disrupting glucose and amino acid transport and toxin removal (Vorbrodt *et al.*, 1999; Toornvliet *et al.*, 2006). The BBB also becomes more permeable to several blood-borne molecules that then leak into the brain, including albumin (Vorbrodt *et al.*, 1995), IgG (Pelegri *et al.*, 2007) and TNF- α (Banks *et al.*, 2000). Together these factors can cause damage to neurons, astrocytes and endothelial cells through disruption of respiration, oxidative stress and inflammation (Dringen, 2005; Chan-Ling *et al.*, 2007).

Vascular stiffening is another consequence of the thickening of vessel walls. This is accompanied by a decrease in total CBF, with an increased pulsatility of CBF, as vessels do not expand in response to left ventricular ejection pressure, and arterial wave reflection increases, increasing CBF pulse pressure while reducing diastolic CBF, causing neuronal and microvascular damage, neurovascular uncoupling, cognitive decline, and age related pathologies such as white matter hyperintensities (Cooper *et al.*, 2006; Tarumi *et al.*, 2014; Zarinkoob *et al.*, 2016). Arteriolar tortuosity also contributes to this, particularly in arterioles supplying deep white matter. As new blood vessels grow over time through angiogenesis, this causes vessels to extend and loop tighter, particularly in cavities where neuronal loss has occurred. This causes changes in cerebrovascular autoregulation to compensate for increased vessel length, and thus a requirement for higher pressure, which has further effects on arteriolar stiffness and neurovascular uncoupling (Heffernan *et al.*, 2018).

In addition to vascular structure, vascular density also changes with age and has a large impact on neurovascular coupling. In healthy brains, the density of the capillary network differs between gray matter and white matter, different cortical layers, or functional region correlating with glucose utilisation (Hudetz, 1997). Several studies found a reduction in capillary density with age in rats, with reduced capillary numbers, reduced capillary length and increased intercapillary distance (Hinds and McNelly, 1982, Casey and Feldman, 1985, Buchweitz-Milton and Weiss, 1987, Jucker *et al.*, 1990, Shao *et al.*, 2010). Many human studies also show reduced capillary density with age (Bell and Ball, 1981, Bell and Ball, 1990, Abernethy *et al.*, 1993). These studies show differences in capillary loss between brain regions, with studies showing loss in the frontal cortex, hippocampus and paraventricular nucleus, but not the supraoptic nucleus, putamen, or temporal cortex (Abernethy *et al.*, 1993). This vessel loss is thought in part to be down to reduced angiogenesis. Vascular remodelling in young brains is one aspect of neuronal plasticity, with vessel growth and loss accompanying formation and loss of neuronal connections. Angiogenesis and an increase in vascular density is also a response to hypoxia in the healthy brain (Boero *et al.*, 1999). However, these mechanisms become less functional with ageing, and thus one mechanism behind disruption of neurovascular coupling is a failure of angiogenesis during plasticity or after hypoxia (Rivard *et al.*, 1999).

These neurovascular changes are associated with cognitive impairment, from the mild reduction in cognitive function associated with normal ageing, which becomes more prominent with vascular pathologies such as hypertension and atherosclerosis, to severe impairment in patients with Vascular Dementia and Alzheimer's disease.

1.5. Hypertension

Hypertension is a common chronic condition, with a prevalence of 30% in British adults (Joffres *et al.*, 2013), defined as increased blood pressure above 140/90 mmHg (Messerli *et al.*, 2007). While manageable, its effects on neurovascular coupling make it a risk factor for cognitive decline. Over time, hypertension alters the structure of the cerebral microvasculature and disrupts vascular responsiveness, changes which are associated with cognitive decline and are common across patients with hypertension, Alzheimer's disease and Parkinson's disease (Farkas *et al.*, 2000). These changes include pericyte degeneration, basement membrane thickening and vessel fibrosis, leading to capillary and arteriole stiffening (Farkas *et al.*, 2000), and vessel stiffening in the brain and in major arteries has been linked to decline in memory and cognitive processing (Cooper *et al.*, 2006; Waldenstein *et al.*, 2008; Kitagawa *et al.*, 2009). Neurovascular coupling is also impaired in chronic hypertension. For example, in a rat model of sustained hypertension, disruption of functional hyperaemia develops over 10 weeks after onset of hypertension, and was not reversible with treatment with anti-hypertensive drugs (Calcinaghi *et al.*, 2013). Task-based fMRI in humans has also shown impaired BOLD signal change in hypertension (Coulson *et al.*, 2015). Understanding the changes in neurovascular coupling caused by sustained hypertension is of great importance, to identify and treat neurovascular problems in hypertensive patients. Hypertension is also the greatest risk factor for stroke mortality (Dahlof *et al.*, 2007), with a 1mmHg increase in systolic blood pressure in hypertensive patients increasing the risk of death by 2% (Palmer *et al.*, 1992).

During hypertension, the arterial walls respond in two ways during hypertension: eutrophic and hypertrophic remodelling. In eutrophic remodelling, smooth muscle cells become reorganised and reduce the size of the lumen without any change in mass or size (Baumbach and Hajdu, 1993; Bakker *et al.*, 2002). In hypertrophic remodelling, the smooth muscle cells grow thicker, restricting the size of the lumen (Baumbach and Hajdu, 1993; Farkas *et al.*, 2000). This reduces the resting blood flow, distensibility and maximum dilatatory capacity of the vessel, particularly in the large cerebral arteries due to the high level of collagen in the walls (Heagerty *et al.*, 1993; Baumbach and Hajdu, 1993). This mechanism may confer some advantages in the short term, with increased wall thickness alleviating the potential for stress caused by the increase in pressure, and reducing blood flow further downstream, attenuating the damaging effects of increased pressure on the microvasculature (Baumbach and Heistad, 1989; Fridez *et al.*, 2001). However, over time arterial and arteriolar stiffening reduces

functional hyperaemia, and the reduction in lumen size does reduce CBF in the long term (Ficzere *et al.*, 1997; Jefferson *et al.*, 2018). Progression of hypertrophy and remodelling is determined by Angiotensin type II, and treatment of spontaneously hypertensive rats with angiotensin converting enzyme inhibitors prevented remodelling when treatment was started at three months of age (Chillon and Baumbach, 1999). The timing of such treatment is important, as rats treated at 20 weeks did not show a reversal in neurovascular changes (Calcinaghi *et al.*, 2013), so blocking Angiotensin II prevents remodelling rather than reverses it. Vessel distensibility also undergoes adaptation to hypertension that is beneficial in the short term but harmful long term. During the onset of hypertension, matrix metalloproteinases are activated and promote an increase in vessel distensibility, through breakdown of collagen and synthesis of other extracellular matrix proteins which promote flexibility of vessel walls. However, over time and sustained hypertension, this mechanism becomes less effective and matrix protein turnover combined with loss of elastin instead promotes more rigid vessels (Hajdu *et al.*, 1990; Flamant *et al.*, 2007). The vascular endothelium is also affected, with response to vasodilators becoming impaired, due to a reduced sensitivity to bradykinin and disruption of the NOS pathways (Didion and Faraci, 2003). Because of this, bradykinin or ACh induced dilation is disrupted, but dilation from neuronal or astrocytic release of NO remains intact.

These changes in neurovascular coupling correlate with alterations in brain structure and deficits in cognitive function. Subcortical or periventricular white matter hyperintensities (WMH) were found to occur in a quarter of hypertensive patients in one study using MRI (de Leeuw *et al.*, 2002), which is thought to be caused by transient falls in CBF during periods of reduced blood pressure and/or the longer term changes in CBF caused by remodelling. Hypertension is also known to cause cognitive deficits, particularly in working memory and executive function (Harrington *et al.*, 2000). MRI scans found that these cognitive deficits correlated with white matter hyperintensities localised to the prefrontal cortex and the underlying white matter, a region which is also particularly vulnerable to the effects of normal ageing. Notably, this study found the same cognitive deficits and structural changes in patients on medication to control their blood pressure (Raz *et al.*, 2003), consistent with studies showing that remodelling of arteries and arterioles is irreversible (Calcinaghi *et al.*, 2013), so neurovascular coupling can still be impaired in patients with controlled hypertension.

Hypertension can also promote formation of atherosclerotic plaques in small vessels, or fibrinoid necrosis in penetrating arteries and arterioles, two pathologies which can cause

arterial occlusions and ischaemia. In atherosclerosis, Low density lipoprotein (LDL) is deposited in the subendothelial space in artery walls. When LDLs are oxidised, it causes endothelial cells to express adhesion molecules, causing leukocytes to bind and enter the subendothelial space. The lesion causes swelling of the artery wall, increasing vascular resistance of that section of artery. The inflammatory response of the leukocytes and the reactive oxygen species produced contribute to oxidising further LDL deposits, and degrade the extracellular matrix. Signalling between leukocytes also causes increased expression of procoagulant tissue factors. Eventually, the lamina of the artery wall ruptures and the release of the coagulant factor from the lesion causes vessel occlusion (Libby, 2002). Hypertension both increases the risk of atherosclerosis, and causes it to spread further into the small vessels of the cerebrovascular bed, causing an increase in plaques in 200-800µm microvessels (Lammie, 2002). The changes in microvascular endothelial cells discussed above can all contribute to the process of plaque development, particularly the reduction in endothelium-derived NO. NO, as well as acting as a vasodilator, is anti-inflammatory and inhibits expression of vascular cell adhesion molecule 1 (VCAM-1), the main adhesion molecule driving the binding of leukocytes (Caterina *et al.*, 1995). Together with the production of ROS by Angiotensin II (Kazama *et al.*, 2004), which contributes to the oxidation of LDLs, this can greatly increase the risk of plaque formation. Increased wall stress from hypertension can also promote the production of proteoglycans, which also promote lipoprotein deposition (Lee *et al.*, 2001). Hypertension can also lead to fibrinoid necrosis in smaller arterioles, between 40-300µm diameter. This is caused by plasma proteins, mostly fibrin, becoming incorporated into the vessel wall, distorting the wall structure and narrowing the lumen and causing damage to smooth muscle cells (Rosenblum, 2008). This can cause the wall to rupture, leading to thrombosis, or the narrowed lumen can cause a drop in flow and localised hypotension. These lesions are not related to inflammation, and are thought to be caused by the increased stress on the vessel wall caused by high pressure (Lammie, 2002). Atherosclerotic and fibrinoid lesions are also two major mechanisms that can lead to an ischaemic event in hypertensive patients.

1.6. Cerebral Stroke

Cerebral stroke is one of the most common causes of death or disability, with approximately 795,000 people suffering from a stroke in the UK between 2001-2010, accounting for over 300,00 deaths in that time (Seminog *et al.*, 2019). 87% of strokes are ischaemic, in which

blood flow to a section of the brain is cut off, and 13% are haemorrhagic, in which blood leaks into the brain tissue. This section will focus on ischaemic stroke.

Ischaemic stroke has several causes, which were divided into 5 subtypes for one clinical study, the Trial of Org 10172 for Acute Stroke Treatment, becoming known as the TOAST classification system (Adams *et al.*, 1993, Adams and Biller, 2015), listing the subtypes as larger-artery atherosclerosis, cardioembolism, small artery occlusion (lacunar), other determined etiology, covering known but rare causes such as nonatherosclerotic vasculopathy or hypercoagulable disorders, and unknown etiology. Occlusions can be classified as either thrombotic, in which a clot forms within the cerebral arteries or small vessels, or embolic, in which a clot forms in the heart, aorta or carotid artery and is carried into smaller vessels in the cerebral vasculature (Olsen *et al.*, 1985). In addition to these subtypes, ischaemic stroke can also be caused by hypoperfusion, either through systemic hypotension or by occlusion of the carotid or vertebral artery, classified as a haemodynamic stroke (Klijn and Kappelle, 2010). An ischaemic stroke can also be preceded by a transient ischaemic attack (TIA), defined as stroke symptoms that last less than 24 hours (Lloyd-Jones *et al.*, 2009).

Although the factor that triggers an ischaemic event is variable, the progression in the initial phase is similar. If CBF falls to 20ml/100g tissue/min, neuronal tissue compensates through increased oxygen extraction, and cells remain intact and functional. Below this, neuronal function is impaired, but tissue remains viable above 12 ml/100g/min, and if reperfused, cells will fully recover. However, if CBF falls below this threshold, hypoxia and metabolite shortage occurs, respiration ceases, Na/K ATPase fails, and loss of membrane function causes an uncontrolled influx of water into the cell, causing cytotoxic oedema and irreversible damage (Baron 2001). Occlusion of a vessel causes two distinct areas of damage, which vary in size depending on the vasculature around the occlusion. In the core, CBF drops below the threshold for irreversible damage, and cell death occurs quickly. Surrounding this is an area of acute ischaemic tissue known as the penumbra that, due to nearby arterioles still providing some blood supply, is damaged but still salvageable if perfusion is restored (Kloska *et al.*, 2010). However, reperfusion does also carry risk of causing further injury (Lin *et al.*, 2016). When perfusion is re-established, this causes formation of compounds such as peroxynitrite, which are triggers of necrosis and apoptosis, as well as production of pro-inflammatory mediators (Eltzschig and Eckle, 2011; Nour *et al.*, 2013).

Several cellular processes underlie tissue damage and death following an ischaemic event, and each of these processes can influence or be influenced by others, with the final outcome being

determined by how these events interact. Together these processes are known as the ischaemic cascade (Zivin, 1998). The first process of the cascade is bioenergetic failure, due to the loss of oxygen and glucose supply. Neurons rely on oxidative phosphorylation for respiration, and in normal conditions metabolise lactate produced by anaerobic glycolysis in astrocytes. When oxygen supply is lost after ischaemia, lactate rapidly builds up in the ischaemic tissue, as astrocytes continue metabolising stored glucose and exporting lactate. This lactate can spread from the infarcted tissue to exert further damage on the surrounding regions (Brouns *et al.*, 2008). The inability of neurons to produce ATP after hypoxia disrupts all active cellular processes. Most importantly, active transport of ions and neurotransmitters is lost, causing membrane depolarisation, loss of electrochemical gradients, and breakdown in ion and water homeostasis, glutamate build up and calcium excitotoxicity (Katsura *et al.*, 1994). This process of hypoxia and excitotoxicity, combined with oxidative damage triggered by the influence of calcium on the NOS pathway (Endres *et al.*, 1998; Love, 1999; Broughton *et al.*, 2009) rapidly cause cell death in the core, and excessive neurotransmitter release and ion imbalance can trigger cortical spreading depolarisation, triggering these same processes in hypoperfused tissue in the penumbra (Strong *et al.*, 2000).

In the penumbra, preservation or loss of neurovascular coupling is a major factor determining stroke progression. As the penumbral tissue is still being partially perfused, cells are still viable and protective mechanisms against oxidative stress, excitotoxicity and oedema are still partly functional (Stanimirovic and Friedman, 2012). When spreading depolarisation is triggered by a transient insult, and the tissue is otherwise healthy, the increase in neurotransmitter activity and depolarisation causes hyperaemia, in the same manner as normal neuronal activity but with a greater effect (100% increase in blood flow) due to the increased levels of glutamate, NO, arachidonic acid and other vasodilators, as well as the longer time course compared to normal activity (Lauritzen *et al.*, 1992). However, in stroke, neurovascular coupling breaks down and further arterial constriction causes spreading ischaemia, as cell signalling mechanisms are disrupted by oxidative damage. As ischaemia spreads, neurons in the penumbra begin to suffer hypoxia, and neuroprotective mechanisms against excitotoxicity and oxidative damage fail, causing further cell death. As distance from the core increases, the vascular response changes from monophasic ischaemia to biphasic ischaemia and hyperaemia, becoming monophasic hyperaemia at the furthest distance from the core (Woitzik *et al.*, 2013). The extent of these regions depends on the extent of collateral perfusion throughout the penumbra, and this is a determinant of the severity of infarct expansion (Beretta *et al.*, 2015). In regions of biphasic ischaemia and hyperaemia, the ischaemic response is normally

transient and does not cause lasting damage, thus the tissue most at risk is the peri-infarct region exhibiting a sustained ischaemic response. Here, the infarct expands in a stepwise manner until the point where perfusion is sufficient to counteract the effect of spreading depolarisation. Upon reaching healthier tissue, the waves of depolarisation instead cause transient depression of activity rather than pathological loss of neuronal function, and CBF increases allowing for sufficient metabolic activity to counteract the effects of depolarisation (Takeda *et al.*, 2011). A main determinant of this recovery is sodium/potassium pump function. If neurons are producing enough ATP to enable Na/K pump activity, ionic gradients can be restored, and hyperaemia is triggered. Loss of Na/K pump function, through metabolic deficit or inhibition, causes oedema, cell death, and prolongs spreading ischaemia as vasodilatory potassium and nitric oxide signalling is lost (Major *et al.* 2017). Metabolically, the distinction between tissue that recovers and tissue that becomes necrotic can be defined by the release of inorganic phosphate, as stored high energy phosphates such as P-Creatine are broken down in hypoxic tissue to generate ATP. If levels of high-energy phosphate remain reduced, and inorganic phosphate accumulates, ATP cannot be recycled and energy dependent processes fail (Selman *et al.*, 2004).

The changes discussed above in signalling and microstructure cause major changes in neurovascular coupling, neuronal activity, brain structure and vascular structure in aging, hypertension and stroke. Understanding the progressive changes in aging, hypertension and stroke is an important goal for developing therapies, identifying risk factors, and improving quality of life. In aging and hypertension, understanding the mechanisms behind mild cognitive impairments, and whether changes originate in neuronal or vascular activity, could aid the development of preventative strategies. Understanding how neurovascular coupling adapts and brain activity is restored following stroke could aid in the development of therapeutics to improve quality of life post-stroke, and aid in rehabilitation in patients. Through use of functional imaging, these changes in activity can be assessed, and progressive changes in neuronal activity and neurovascular coupling with aging, hypertension, and during recovery following ischaemic stroke can be understood.

1.7. PhD Aims

This PhD focuses on developing imaging methods and a suitable minimally invasive anaesthesia protocol, which can be applied to longitudinal studies of different animal models in order to improve the understanding of neurovascular coupling in aging, ischaemic stroke and hypertension. MR provides a non-invasive tool for structural and functional imaging of the

brain, and for quantifying metabolite turnover. These tools are now commonly used in clinical studies, and have led to an increased understanding of the neurovascular mechanisms of ageing, hypertension and stroke. Preclinical studies using MRI are less common, due to confounding factors involved in using animal models. This has led to a limited number of studies investigating the progression of recovery following stroke, and no fMRI studies on the progression of ageing or hypertension in rodents. Through addressing the confounding factors in the animal model, and applying a multi-parametric MRI protocol including structural, functional and resting-state imaging and spectroscopy, this PhD aims to develop a method for longitudinal functional MRI in rats, and apply this to rodent models of ageing, stroke and hypertension. Using these models, as well as providing new insights into these conditions and methods that can be transferred to other age-related diseases, may facilitate translatability between preclinical and clinical studies, and benefit research into treatment of age-related disease. The specific objectives of this thesis are:

- To refine rodent anaesthesia and monitoring protocols to facilitate longitudinal fMRI studies with minimal impact on animal welfare.
- To implement suitable MRI sequences for functional imaging of the haemodynamic response, neuronal metabolism, and cerebral blood flow.
- To utilise these methods in the study of ageing, ischaemic stroke, and hypertension.

This thesis is divided into the following chapters:

- Method development – validation of anaesthesia protocol and MRI sequences.
- Healthy ageing – to determine what changes occur in the stimulus-evoked BOLD signal activity, stimulus-evoked neurotransmitter activity, resting state networks and resting cerebral blood flow in the rodent brain with age.
- Ischaemic stroke – to determine what changes occur in the stimulus-evoked BOLD signal activity, stimulus-evoked neurotransmitter activity, resting state networks and resting cerebral blood flow in the rodent brain during recovery following ischaemic stroke.
- Hypertension – to determine what changes occur in the stimulus-evoked BOLD signal activity, stimulus-evoked neurotransmitter activity, resting state networks and resting cerebral blood flow in the rodent brain as hypertension progresses.
- Conclusions – to discuss how the findings of each of these studies build on previous work in the fields of ageing, stroke and hypertension, further work that can be carried

out in this field, and how the methods used here can be applied to rodent models of other neurological diseases.

Chapter 2: Development of imaging and anaesthetic protocols

2.1. Introduction

In order to investigate changes in neurovascular coupling over an animal's lifetime, and to investigate the underlying neuronal and vascular changes contributing to this, a suitable anaesthesia protocol must be implemented. Aspects of brain structure and function that are of interest in this study must be identified and appropriate MRI sequences must be chosen or developed. An anaesthetic protocol must take into account depth and duration of anaesthesia, impact on BOLD signal, short-term and long-term health risks to the animal. Ensuring animal welfare during scanning requires improvements on standard physiological monitoring of respiration and temperature. To ensure animal health long-term, housing procedures must be implemented that focus on animal welfare.

To develop an appropriate MRI protocol, the outcome measures that describe important aspects of neurovascular coupling must be identified. BOLD fMRI relies on the difference in magnetic susceptibility between oxyhaemoglobin and deoxyhaemoglobin, and the signal is a combination of changes in local cerebral blood flow, cerebral blood volume and the cerebral metabolic rate of oxygen (Ogawa *et al.*, 1992). Neurovascular uncoupling due to age or disease can disrupt the BOLD signal (D'esposito *et al.*, 1999), reducing the ability to accurately infer neuronal activity (Burke and Burhle, 2006). To account for this, methods to detect changes in neurons, for example detecting metabolic changes and neurotransmitter turnover, must be combined with CBF-weighted MRI to understand the two components of neurovascular coupling.

This chapter focuses on the development of anaesthetic, physiological monitoring and MRI protocols that will have minimal impact on animal welfare, while still allowing for reliable multi-parametric MRI data to be collected.

2.1.1. Animal Welfare

To study healthy ageing, animal housing must be improved in order to ensure animals remain physiologically healthy for the duration of the study. Animals housed in standard cages are at risk of becoming obese with age, which has detrimental effects on the cardiovascular system and neurovascular coupling, and increases the risk of mortality from obesity-related conditions (Martin *et al.*, 2010). This is undesirable from both an ethical and scientific viewpoint, as this mortality risk goes against provisions for a humane end point to the study. Furthermore, if

animals become obese it will be impossible to separate changes related to poor health and changes due to normal ageing.

To ensure animals remain healthy, they require adequate exercise, environmental enrichment and social interaction to mimic healthy ageing in a more natural environment (Makowska and Weary, 2016). Regular time in a large playpen, with all cages in a study being mixed during this time, may achieve this within the practical constraints of animal unit regulations, available space and staff. Recommendations from the NC3Rs include multiple floors and surfaces suitable for climbing, water baths, buried or submerged food for foraging, and items of different textures to gnaw on. Integrating multiple cages into the same playpen will also be beneficial as increased social interaction may reduce stress.

In these studies, all animals received daily access to a playpen for between one and five hours, and were returned to their home cage afterwards. While a future study comparing enrichment vs no enrichment would be beneficial both to the case for improved animal housing and welfare, and to understanding the impact of exercise on neurovascular function, for this study the enriched environment was solely for the purpose of improved animal welfare and not data collection.

2.1.2. Anaesthesia in functional MRI

Several studies have focused on developing an appropriate anaesthetic protocol for fMRI. Urethane and alpha-chloralose are the two most commonly used injectable anaesthetics for fMRI, and while they both allow for robust BOLD responses, their carcinogenic effects prevent their use for longitudinal experiments (Tremoleda *et al.*, 2012). For longitudinal fMRI, some studies use a continuous infusion of medetomidine. Previous rat fMRI studies have revealed BOLD responses to forepaw stimulation, with two sessions under medetomidine or alpha-chloralose, revealing clear, reproducible changes with no significant difference between signal intensity under medetomidine or alpha-chloralose (Weber *et al.*, 2006). However, medetomidine has been found to introduce some confounding factors, as it produces a variable depth of anaesthesia (Pawela *et al.*, 2009) It has been shown that long term anaesthesia with medetomidine causes an increase in heart rate over time, and an increase in dose rate is generally required to maintain anaesthesia (Pawela *et al.*, 2009). Medetomidine can also cause hypoxia, and when the method was first described, oxygen had to be increased to 30% part way through scans in order to maintain adequate blood oxygen levels (Weber *et al.*, 2006) The use of a low dose of medetomidine combined with another sedative, such as ketamine, has been

recommended instead of medetomidine alone in scientific and veterinary settings (Tremoleda *et al.*, 2012; Sinclair, 2003) Additionally, in functional connectivity studies performed under medetomidine, animals have shown impaired connectivity compared to the awake state or other anaesthetics, with all regions showing a reduction in correlation coefficients, and the thalamo-cortical pathway showing complete loss of activity (Paasonen *et al.*, 2018).

In terms of inhalational anaesthetics, some recent fMRI studies report using low doses of isoflurane anaesthesia (Van Meer *et al.*, 2010). However, isoflurane has known vasodilation and neural suppression effects, and even low doses can affect the BOLD signal, which compromises the accuracy of results, particularly in longitudinal studies, as a reduction in signal amplifies the effects of physiological noise and inter-animal variation (Masamoto *et al.*, 2009). Long term changes may also be lost, for example where hyperactivation may be observed in the awake animal, isoflurane will reduce the maximum signal change that can be observed, masking this effect (Aksenov *et al.*, 2015). The effect of isoflurane on the BOLD signal is quite complex, with dose dependent effects on several different factors contributing to the signal, for example, isoflurane reduces local cerebral glucose utilisation (LGCU) by 40-60%, while increasing resting CBF by 25-60% measured using radiolabelling methods (Lenz *et al.*, 1998). However, BOLD signal intensity does not change linearly with dose, instead signal intensity peaks between 2%-2.5% isoflurane and drops as the dose is either reduced to 1.5% or increased to 3%, which is thought to reflect the different effects of isoflurane on arteries and microvasculature. BOLD responses are the same in the arteries and microvasculature at 1.5% and 3% isoflurane, but at 2-2.5% the arterial BOLD signal is larger (Tsurugizawa *et al.*, 2016). Even 0.5% isoflurane showed a significant drop in evoked BOLD signal, with one study comparing awake animals with animals under 0.5% isoflurane showing a 50% decrease in BOLD signal under 0.5% isoflurane, while local field potential and multi-unit activity signals only decreased by 10% (Aksenov *et al.*, 2015). Halothane also has similar effects on stimulus-based BOLD signal, and is therefore considered unsuitable for use in fMRI studies (Austin *et al.*, 2005) There is evidence to suggest that isoflurane may be suitable for resting-state fMRI studies, depending on the dose rate and regions being investigated. Cortical functional connectivity is well preserved under isoflurane (Paasonen *et al.*, 2018). However, at doses higher than 1% isofurane, subcortical and thalamocortical networks cannot be identified. (Liu *et al.*, 2013; Hamilton *et al.*, 2017).

Propofol, while less commonly used than medetomidine, isoflurane or urethane, has been suggested as a good candidate for preclinical fMRI studies (Paasonen *et al.*, 2018; Lahti *et al.*, 1999; Kelly *et al.*, 2010; Griffin *et al.*, 2010). Propofol is an i.v. anaesthetic that acts to increase

GABA receptor activity, inducing anaesthesia by causing an increase in synaptic inhibition. It has a rapid onset and recovery, causes minimal disturbance to vascular reactivity or heart rate, is not thought to have any direct action on the vasculature, does not accumulate and has no long term detrimental effects. Like other injectable anaesthetics, propofol does cause some reduction in CBF, however unlike isoflurane, a clear BOLD response is still detectable, showing a 1-6% change in BOLD signal at a field strength of 2T, compared to 6-26% in conscious rats (Lahti *et al.*, 1999). Increased field strength does increase signal intensity, as experiments with α -chloralose show 3% signal change at 2T, 11% at 4.7T and 17% at 7T, so for our experiments at 9.4T we can expect a greater signal change under propofol than found at 2T. Studies at 7T with propofol using both arterial spin labelling and BOLD fMRI showed that animals under propofol anaesthesia have greater cerebral blood volume than animals under medetomidine, another candidate for anaesthesia in longitudinal studies, and a greater increase in CBV following forepaw stimulation (Kelly *et al.*, 2010). Further studies showed high reproducibility between sessions for all quantifiable perfusion parameters (CBV, mean transit time, capillary transit time). The authors also noted that the vasoconstriction caused by propofol combined with the greater vascular reactivity compared to other anaesthetics could enhance the signal to noise ratio of the hyperaemic response as the baseline blood flow is reduced (Griffin *et al.*, 2010).

Studies of hypercapnia show that cerebral autoregulation and cerebrovascular reactivity are maintained under propofol while they are lost under isoflurane (Strebel *et al.*, 1995; Cenic *et al.*, 2000). A study comparing isoflurane, medetomidine, propofol and urethane showed signal intensity under propofol to be three times greater than under medetomidine, and a haemodynamic response function (HRF) closer to that of the awake state (Schlegel *et al.*, 2015). Studies using ASL have also shown that propofol gives a clear CBF response, and comparison between studies by the same group using propofol and medetomidine show a greater baseline CBF and stimulus induced CBF response under propofol than medetomidine (Kelly *et al.*, 2010; Griffin *et al.*, 2010). As functional connectivity responses, cerebral autoregulation, cerebrovascular reactivity and the HRF under propofol are shown to be close to that of the awake state, propofol appears to be an ideal choice of anaesthetic protocol for fMRI. However, to date, use of propofol in disease models such as ischemic stroke is limited to a few studies observing changes in global CBF in response to hypercapnia (Lake *et al.*, 2017a; b).

For these reasons, propofol was selected as the anaesthetic agent for this study, as it is expected to have the least impact on the BOLD signal while still ensuring stable anaesthesia with minimal impact on animal welfare.

2.2. Methods

2.2.1. Anaesthetic protocol

Before the first MRI time point, bench tests were performed to ensure safety of the anaesthesia protocol and that the dose rate was correct, under supervision from the named veterinary surgeon. Animals were initially anaesthetised with 3% isoflurane in 100% oxygen, and maintained on isoflurane while the tail vein was cannulated. Once the cannula was in place, animals were given a bolus of 7.5mg/kg propofol over one minute, as described by Griffin *et al* (2010). Isoflurane was reduced to 1%, and respiration was monitored over this time. The initial bolus caused respiration to decrease by ~50%. After 3 minutes, a continuous infusion of 45mg/kg/hr was given using a syringe driver. After confirming that this did not cause further respiratory depression, isoflurane was gradually reduced to 0.5%, then to 0. At 45mg/kg/hr, rats' breathing rate increased, and rats displayed a response to toe pinch, so isoflurane was switched on, cannula removed and animals were recovered. The procedure was repeated with a 10% (49.5mg/kg/hr) and 20% (54mg/kg/hr) increase in dose rate of propofol, and 54mg/kg/hr was shown to give stable anaesthesia without impairing breathing rate in the Wistar Han strain. Animals were monitored for the duration using a respiration pillow (Small Animal Instruments Inc. Stony Brook, NY, United States) placed under the chest, rectal temperature probe (Small Animal Instruments Inc. Stony Brook, NY, United States) and pulse oximeter (Starr Life Sciences, Oakmont, PA, United States) attached to the hind paw, to give data on breathing and heart rate, oxygen saturation and temperature.

Once dose rate had been confirmed, the protocol for MRI scans was as follows:

- Animal anaesthetised with 3% isoflurane in oxygen.
- Under isoflurane, tail vein cannulated.
- Animal transferred to MRI cradle, pulse oximeter, respiration pillow and temperature probe connected, isoflurane reduced to 2%.
- 9mg/kg bolus of propofol given over 1 minute with syringe driver, isoflurane reduced to 1%.
- Copper electrodes inserted subcutaneously into forepaw.

- 3 minutes after end of bolus, 54mg/kg/hr infusion of propofol began.
- Animal placed into scanner, isoflurane off.
- After shimming, prior to functional experiments, animal switched to breathing room air provided at 2-3L/min using an air pump (Clarke Wiz-Air, Clarke Tools, Dunstable, UK).
- Animal returned to 100% oxygen after functional experiments.
- At end of scan, animal is removed from scanner and placed in a recovery cage.

While the low dose rate was not expected to impair respiration and animals were breathing freely, precautions were taken to ensure safety of this method as it is not yet commonly used in fMRI, and has not previously been used in ageing animals. Oxygen saturation was monitored throughout, and animals were only switched onto room air for fMRI, functional MRS and resting-state fMRI scans, and were kept on 100% O₂ before and after these scans. If oxygen saturation dropped below 80%, the safe limit advised by the NVS, animals were to be returned to 100% O₂ and functional scans stopped. Similarly, if animals showed signs of movement on the respiration trace that suggested anaesthesia was too light, isoflurane was switched on and the animal was removed from the scanner and recovered.

2.2.2. Development of fMRI protocol

While BOLD fMRI is an important tool for localisation of brain activity, the BOLD signal is influenced by several factors that are thought to be affected by ageing, at the neuronal level, the vascular level, and in the signalling underlying neurovascular coupling (Ogawa *et al.*, 1992). Because of this, a more comprehensive MRI protocol is required to investigate as many of these factors as possible through non-invasive means. The BOLD signal is comprised of changes in local CBF and CBV, and an increase in local oxygen metabolism due to neuronal activity. Because of this, in addition to imaging changes in the BOLD signal, arterial spin labelling can be added to the protocol to measure changes in resting CBF (Griffin *et al.*, 2010). Measuring neuronal activity itself presents a challenge. Two alternative MRI methods have previously been used to more directly measure neuronal activity using MR. Diffusion-weighted functional MRI (dfMRI) has been used to measure the change in water diffusion with activation, as ion channel activation causes extracellular water to flow into the neuron through osmosis, reducing apparent diffusion coefficient in the active region (Le Bihan *et al.*, 2003; Jin and Kim, 2008; Tsurugizawa *et al.*, 2013). However, this sequence would be confounded in stroke studies by the presence of oedema and the associated increase in free diffusion contributing to the signal. The second option is to use functional MR spectroscopy to measure glutamate turnover (Pritchard *et al.*, 1991; Lin *et al.*, 2012; Stanley and Raz, 2018).

MRS can provide a direct measure of neurotransmitter production to quantify neuronal activity, with the drawback that spatial resolution is limited to a single relatively large voxel covering the region of interest. While MR spectroscopic imaging (MRSI) is possible, in order to image the spatial distribution of metabolites, this technique requires long acquisition times, and so cannot be adapted for functional imaging. While MRS does need a large number of averages, spectra from individual averages can be separated and compiled into 'off' and 'on' blocks, providing a long enough acquisition time in each state. The BOLD fMRI sequence can also be refined to give an improved temporal resolution, allowing changes in the time course of haemodynamic activity to be observed.

Development of the BOLD fMRI protocol typically requires development of an echo planar imaging (EPI) sequence with high temporal and spatial resolution to detect rapid, localised changes in blood flow. EPI is a rapid imaging method which was originally defined in which the complete array of spatial frequencies (k-space) could be sampled in a single excitation (Mansfield, 1977), however this has since been expanded to include sequences using a small number of excitations. At 9.4T, this is complicated by inhomogeneity effects in the magnetic field, which are less pronounced at the 1.5T or 3T field strengths used in human MRI, or the 7T field used in many preclinical studies. Sequences must be adapted to minimise these effects. In EPI sequences used for human imaging at low fields, a single RF pulse is most commonly used to excite a slice, called single-shot EPI. While this is very efficient for temporal resolution, at high field strengths single-shot EPI is highly susceptible to variation in the magnetic field from background gradients or air-tissue interfaces. The main effect of this is distortion of the image, which is extremely pronounced at 9.4T, as increasing the magnetic field amplifies local field changes from magnetic susceptibility effects. Higher resolution also increases distortion relative to the size of the single voxel. Multiple-shot EPI (or segmented EPI) sequences are an alternative to this at high field strengths. Each excitation in a multiple-shot sequence effectively resets the phase differences caused by the inhomogeneity effects, reducing the distortion. Greater spatial resolution is also possible with multiple-shot EPI, as each shot only acquires a portion of the data. Temporal SNR is reduced, as the time between each shot does allow instabilities such as head motion or breathing to affect the signal, however this effect is far smaller than the geometric distortion in single-shot sequences, and is less consequential in anaesthetised animals compared to awake human subjects (Swisher *et al.*, 2012).

To reduce EPI distortion, several two-shot and four-shot EPI sequences were assessed with varying parameters using a spherical water phantom. These sequences were performed using

a 9.4T Small Animal MRI scanner (Agilent Technologies), a 72mm RF volume transmit coil and a 2-channel surface receive coil (Rapid Biomedical, Rimpar, Germany). Parameters that were altered included flip angle, which affects signal-to-noise ratio, K_{zero} , which affects data sampling and image sharpness, repetition time, and data matrix. Spatial signal-to-noise ratios (SNRs) were calculated through dividing the mean intensity of a region in the sphere by the standard deviation of the intensity of the background. In tests with multiple repetitions over five minutes, temporal SNRs were calculated through dividing the mean intensity of a region over time with the standard deviation over time. Tables 2.1 and 2.2 detail the parameters tested and the SNRs calculated. The final sequence uses a 250ms TR with 2 shots, giving a 500ms temporal resolution. The 45° flip angle allows for a shorter TR than 90°, while the reduced K_{zero} reduces distortion at the cost of reduced definition of sharp edges, however this factor is less important in functional images. It is important to note that, while lower and higher TEs were tested, a TE of 22ms was identified for optimal detection of the T_2^* weighted signal. This sequence was then tested in *ex vivo* rat brains, followed by *in-vivo* scanning of young and aged rats. For stimulus-based fMRI, this sequence was used on three slices targeting the somatosensory cortex. For resting-state fMRI, this sequence was adapted for a 1000ms repetition time and used on 22 slices covering the whole brain.

For functional MRS, a LASER sequence was used with a TE of 14.14 and a TR of 2000. This low echo time weights the signal for detection of glutamate (Zhu *et al.*, 2011). Use of the array function allows individual averages to be saved following the scan and compiled into off and on blocks later, using the FID-A MATLAB toolkit (Simpson *et al.*, 2017).

For the arterial spin labelling sequence, a single slice at bregma was imaged for CBF detection. An inversion time of 1500ms was used with a TR of 4529.72ms, with 8 averages compiled into the final image.

Test	TR (ms)	TE (ms)	K_{zero}	Shots	Data Matrix	Flip Angle	Spatial SNR	Ghosting
1	1000	10.84	32	1	64x64	90	311	2.83%
2	1000	15	32	1	64x64	90	330	2.95%
3	1000	20	32	1	64x64	90	328	4.13%

4	1000	22	32	1	64x64	90	205	4.45%
5	1000	22	16	1	64x64	90	244	7.77%
6	1000	22	16	2	64x64	90	136	3.14%
7	1000	22	8	2	64x64	90	169	9.68%
8	1000	30	32	1	64x64	90	117	4.24%
9	1000	36.82	64	1	128x128	90	170	4.31%
10	1000	22	32	1	64x64	45	168	5.27%
11	1000	22	32	1	64x64	30	132	4.54%
12	500	22	32	1	64x64	90	192	4.59%
13	250	22	32	1	64x64	90	151	5.28%
14	500	22	16	2	64x64	90	122	2.75%
15	500	22	32	2	128x128	90	175	2.30%
16	500	22	24	2	192x96	90	193	6.32%
17	500	22	48	2	96x192	90	171	4.09%
18	500	22	24	2	96x96	90	200	3.03%
19	500	22	32	2	128x128	45	149	2.89%
20	500	22	16	2	128x128	45	166	3.53%
21	250	22	16	2	128x128	45	153	0.66%
22	100	22	16	2	128x128	45	126	0.79%
23	100	22	16	2	128x128	30	107	0.93%
24	100	22	16	4	128x128	45	117	4.66%
25	70	22	16	4	128x128	45	103	4.19%
26	70	22	8	4	128x128	45	110	7.96%
27	100	22	8	4	128x128	45	128	5.99%
28	50	22	12	4	96x96	45	117	5.01%
29	50	22	16	4	128x128	45	97	5.54%
30	250	22	32	2	128x128	45	137	0.56%
31	250	22	16	2	128x128	45	162	0.81%

Table 2.1: Spatial SNR of EPI sequences in water phantom. Sequence 21 (repeated as sequence 31) was selected for use based on image quality, temporal resolution and SNR.

Test	TR (ms)	TE (ms)	K _{zero}	Shots	Data Matrix	Flip Angle	Temporal SNR
1	250	22	16	2	128x128	45	114.145
2	500	22	16	2	128x128	45	137.34

3	125	22	16	4	128x128	45	85.55
4	250	20	16	2	128x128	45	117.958
5	250	25	16	2	128x128	45	113.395

Table 2.2: Temporal SNR of EPI sequences in water phantom.

2.2.3. Data Analysis

Raw fMRI data was converted to NIFTI format and processed using FMRIB's Software Laboratory (FSL, Smith *et al.*, 2001). EPI images first undergo motion corrected linear registration using the Motion correction with FMRIB's linear registration tool (MCFLIRT, Jenkinson *et al.*, 2002), minimising the effects of motion such as breathing during the scan. The rat brain extraction tool (rBET, Wood *et al.*, 2013), modified from the human brain extraction tool to assume an oval shape, is then used to remove non-brain structures, allowing registration to structural images or atlases. Following this, the bias field is corrected for. The RF receiver coil, placed over the rat brain has a spatial sensitivity profile, or bias field, which is introduced into the image, giving higher signal in the cortex than in deeper brain structures. The bias field was mapped using the FSL automated segmentation tool (FAST, Zhang *et al.*, 2001) and used to normalise the image. This provides an EPI image ready for analysis (Fig. 2.1).

Following preprocessing, independent component analysis (ICA) is performed using the Multivariate exploratory linear optimized decomposition into independent components (MELODIC, Beckmann and Smith, 2004) tool. This separates the signal scan into separate components based on frequency and spatial patterns over the time course. From this, noise and artefacts can be removed. Using the frequency distribution of each component, components in which the frequency distribution was a single well defined peak were selected as signal, while components of several smaller frequency peaks were determined to be noise. Time series analysis using FMRIB's Expert Analysis Tool (FEAT, Woolrich, 2001), was then performed on this de-noised data to identify significant activity caused by stimulation.

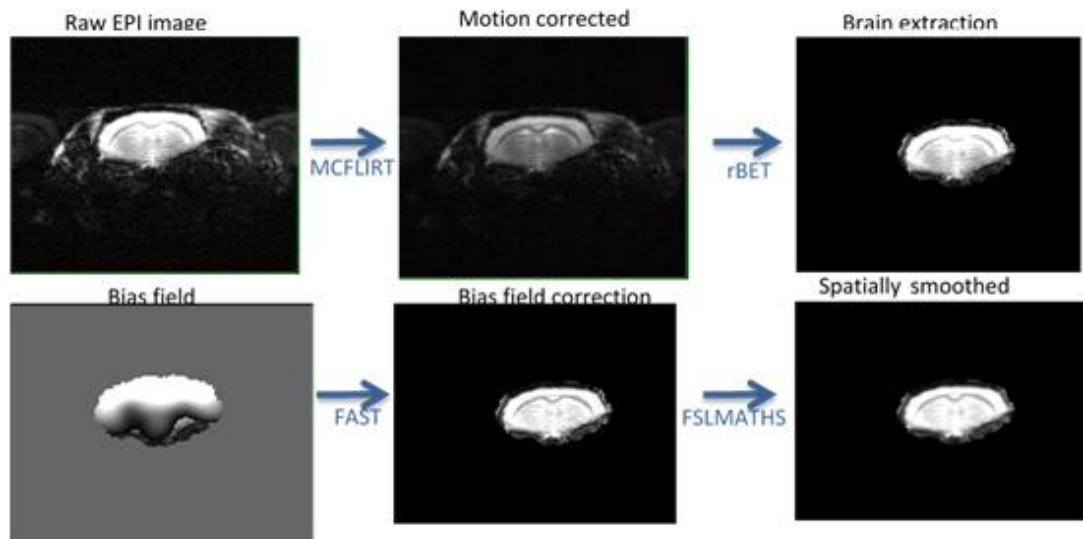


Fig. 2.1. Processing steps to prepare a raw EPI image for time series analysis. First, the image is corrected for motion artefacts. Following this, non-brain tissue is removed. The bias field is mapped and used to correct for the surface coil sensitivity profile, and the image is spatially smoothed.

Resting state fMRI images underwent the same preprocessing steps as stimulus based fMRI. After this, ICA was used to remove noise and identify resting-state components. A group-level ICA was performed on all scans in the study to detect common components between- and within-subjects over time. This component map was used in dual-regression analysis to calculate inter-voxel connectivity in each component. The FSLNets script was then used to create a hierarchy matrix showing how components are connected into networks.

Functional MR spectroscopy data was compiled into stimulus-off and stimulus-on spectra using the FID-A toolkit (Simpson *et al.*, 2017). Bad averages, in which signal power was outside of 2 standard deviations of the mean, were removed, and the first 30 seconds of each off block was discarded to allow metabolite levels to return to baseline following the on block. Spectra were then analysed using the Totally automatic robust quantification in NMR (Tarquin, www.tarquin.sourceforge.net) software package. Spectra were processed using eddy current correction and a lipid filter, then fitted to a Brain + glutathione basis set, to compare levels of glutamate between off and on blocks.

Control and Tag ASL images were first concatenated into a single image of two volumes. The Oxford ASL toolkit for FSL was used to subtract the tag image from the control image to create a difference image. Difference images were thresholded at 0 to remove negative voxels.

FSLmaths was used to double the intensity of control images, and these images were used as inputs in a modified Bloch equation (Williams et al., 1992; Kelly et al., 2010) in order to calculate CBF.

$$f = \frac{\lambda}{T_{1app}} - \frac{M_b^{ctrl} - M_b^{tag}}{2M_b^{ctrl}}$$

Where M_b^{ctrl} is the image intensity of the control image, and M_b^{tag} is the image intensity for labelled images. λ is the ratio of water/g of brain tissue to water/g of blood. T_{1app} is the relaxation time that describes the exponential decrease in M_b . T_{1app} has previously been measured as 2s, and λ has previously been calculated as 0.9 (Williams *et al.*, 1992), and these values are presumed to give the equation:

$$f = 0.45 - \frac{M_b^{ctrl} - M_b^{tag}}{2M_b^{ctrl}}$$

The value f is then converted into ml/g/min to give a CBF map. CBF map images were given an upper threshold of 5 to remove large outliers, and mean and standard deviation across the slice was calculated using FSLstats.

2.2.4. Experimental protocol

The studies in this thesis were conducted in accordance with the UK Animals (Scientific Procedures) Act, 1986 under project licence P7D063834 and following institutional ethical approval by the University of Leicester Animal and Welfare Ethical Review Body. All experiments are reported in accordance with the Animal research reporting of in vivo experiments (ARRIVE) guidelines (Kilkenny et al., 2010). All animals were housed in standard cages, handled regularly, and given daily access to a playpen for a minimum of 2 hours when possible, unless health conditions precluded this (e.g. post stroke). For MRI scanning, animals were initially anaesthetised with 3% isoflurane in 100% oxygen. Tail vein cannulation was performed before transferring the animals to the MRI bed. A bolus of 9mg/kg propofol was administered over 1 minute using a syringe driver (Harvard Apparatus, Cambridge, Massachusetts, United States) and the isoflurane was gradually reduced to 0%, with animals still breathing 100% oxygen. Respiration was monitored using a respiration pillow (Small Animal Instruments Inc. Stony Brook, New York, USA), temperature monitored using a rectal probe and maintained using a fan heater activated when measured temperature dropped below 37°C (Small Animal Instruments Inc. Stony Brook, New York, USA), and heart rate and

blood oxygen saturation monitored using a pulse oximeter (Starr Life Sciences, Oakmont, Pennsylvania, USA). Copper electrodes were inserted subcutaneously into the dorsal surface of the right forepaw between digits 1-2 and 2-3 (Hyder et al., 1994). 3 minutes after the bolus ended, a continuous infusion of propofol was given at 54mg/kg/hr until resting-state fMRI was complete.

MRI scans were performed on a 9.4T Small Animal MRI scanner (Agilent Technologies), using a 72mm RF volume transmit coil and a 2-channel surface receive coil (Rapid Biomedical, Rimpar, Germany). Following a scout scan and manual shimming of the whole brain, a 3D gradient echo volume scout image was taken. A scout scan of the surface of the brain was taken to locate bregma (Fig. 2.2). Using this scout scan, three 1.5mm thick slices were placed centred on bregma. Using the 3D GE image, a 10x9x4.5mm shimming voxel was placed over the slices, covering only brain tissue. This voxel was shimmed to a 50% linewidth <30Hz using FASTMAP, the linewidth was confirmed using a non-water suppressed PRESS MRS test scan, and additional manual shimming was performed if necessary. EPI test scans were taken at each stage to ensure optimal image quality.

Following shimming, animals were switched from breathing oxygen to breathing room air, pumped using an air pump at 3L/min. 9 minutes of fMRI were performed (TR=250ms, TE=22ms, Shots=2, $K_{zero}=16$, flip angle=45, data matrix=128x128). Electrical stimulation of the forepaw was performed in 60 second off, 30 second on blocks, at 10Hz, 10mV, using a stimulator designed by the Joint Biomedical Workshop (Core Biotechnology Services, University of Leicester).

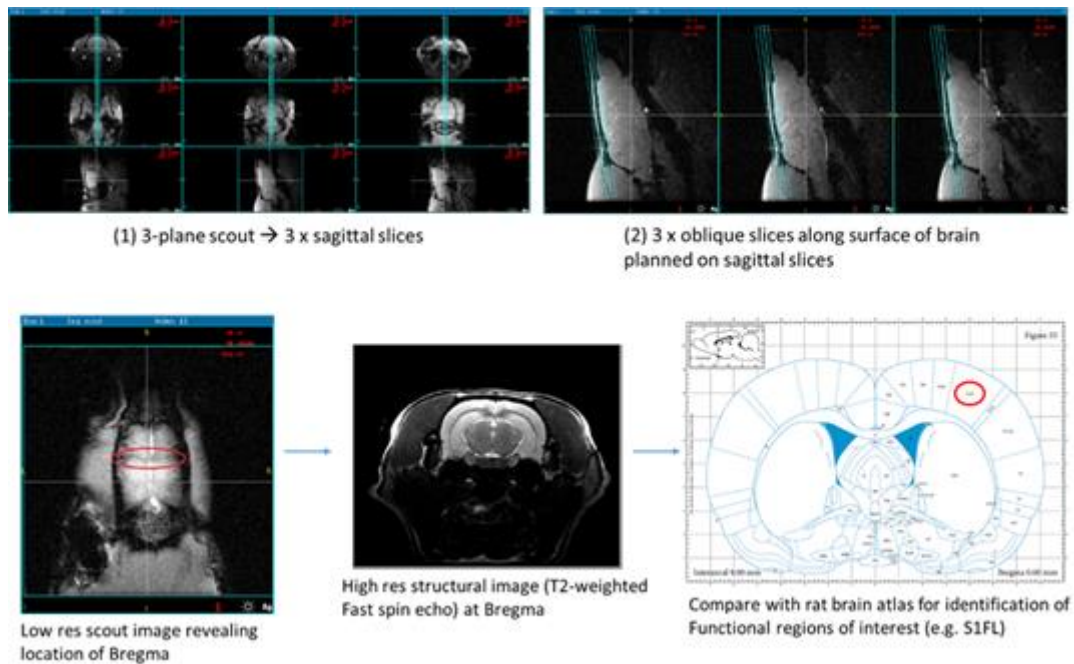


Fig. 2.2. Steps required to locate the region of interest using scout scans. A three plane scout is used to give a whole brain image. Saggital slices are taken down the centre of the brain, allowing the correct plane to be determined to image the brain surface. 3 1mm thick oblique slices are taken along the surface of the brain. If positioned correctly, bregma can be seen as a dark line across the surface of the brain. This is confirmed through comparing a slice taken at bregma with the rat brain atlas (Paxinos and Watson, 2014)

After fMRI, a 4x4x4mm voxel was placed over the somatosensory cortex, shimming was checked and performed again if necessary. 9 minutes of functional MR spectroscopy were performed using a LASER sequence (TR=2000ms, TE=14.14ms), with the array averages function to separate averages, and water suppression using the VAPOR sequence. The same electrical stimulation protocol was applied to this scan as for the fMRI experiment above.

6 minutes of resting-state fMRI was performed over 22 x 1mm thick slices covering the whole brain (TR=1000ms, TE=22ms, Shots=2, K_{zero} =16, flip=45, data matrix=128x128).

Animals were returned to breathing oxygen, and a TOF angiography scan was performed to identify the carotid arteries. A T_2 weighted structural scan was performed. The angiography scan was used to place an inversion plane for arterial spin labelling over the carotid arteries (Bregma-17mm). 6 minutes of ASL were performed (TI=1500ms, TR=4529.72ms) for CBF quantification.

Following this, animals were removed from the scanner and placed in a recovery cage. EMLA cream was applied to the forepaw to prevent any pain from electrode placement/removal. Animals were conscious approximately 10-15 minutes following removal of anaesthesia. Animals were given water and food pellets soaked in water, and were returned to their home cage when they could walk normally without loss of balance, approximately 20-30 minutes following removal of anaesthesia.

2.3. Discussion

The methods presented here were designed to facilitate longitudinal fMRI studies in rats, and improve on current fMRI protocols to study the BOLD signal with improved temporal resolution, as well as functional changes in metabolism and neurotransmitter release, and changes in CBF.

The BOLD fMRI sequence presented here has a temporal resolution of 0.5s, compared to sequences commonly used in most fMRI studies that have a temporal resolution of 1s. This will allow strong statistical power for time-series analysis, as a large number of averages is required for the BOLD signal to have statistical significance. In a 9 minute scan, consisting of 6 stimulus-off blocks of 60s, and 6 stimulus-on blocks of 30s, this gives 720 stimulus-off averages and 360 stimulus-on averages. Additionally, if temporal SNR in a live animal is sufficiently high, analysis of the temporal characteristics of the BOLD signal, including time-to-peak and signal decay over time, would be beneficial to understand how neurovascular reactivity and desensitisation to stimuli may change over time.

The fMRS sequence in such a short scan time on the other hand requires a trade-off between number of averages and minimising scan time. MRS requires a large number of averages to boost SNR. However, due to the novel anaesthetic protocol, and longitudinal study design, scan time has been kept to a minimum where possible to minimise any unexpected harmful effects of propofol on aged, post-stroke or hypertensive rats. For this reason, fMRS scans are kept to 9 minutes with the same stimulus protocol as fMRI, however this does mean only 90 averages are taken and some SNR is sacrificed. The high field strength of the hardware available does offer some advantage to offset this, as MRS signal is stronger, and glutamate and glutamine are better separated as field increases (Ramadan *et al.*, 2013). The LASER sequence has also been shown to have a high degree of tolerance to field inhomogeneity, improving SNR at high field (Godlewska *et al.*, 2017).

The ASL sequence used was a single slice, single inversion time ASL image to quantify resting CBF. While there are many other parameters that may be affected with age, such as capillary transit time (Kelly *et al.*, 2010), or change in CBF with activation, for this study only resting CBF was quantified. Reduced resting CBF may be a marker of arterial stiffness or impaired cerebral autoregulation, both of which impact the BOLD signal (Halani *et al.*, 2016), and so can go some way to explaining any impairment observed in BOLD fMRI. Functional ASL is impractical in this instance, due to the long repetition times and requirement for tag and control scans to be taken for a single image. While the CBF signal is stronger than the BOLD signal, only 12 averages could be taken in 9 minutes using this sequence, which would not be sufficient for statistical significance. Similarly, measurements such as capillary transit time would require similarly long scan times. These measures can be added to future studies once longer scan times are confirmed to be safe.

The methods described here were applied to rat models of healthy ageing (Chapter 3), ischemic stroke (Chapter 4), and hypertension (Chapter 5), with the purpose of understanding how the BOLD signal, neurotransmitter turnover, cerebral blood flow, and functional connectivity change in these conditions over time.

Chapter 3: Longitudinal functional MRI for animal studies of neurovascular coupling in healthy ageing

3.1. Introduction

As life expectancy and the proportion of older people in the population increases, the number of people suffering from mild cognitive impairment, neurodegenerative disease, stroke, or other brain pathologies increases. Even in healthy individuals, changes to the brain and neurovascular system are expected (D'Esposito *et al.*, 1999). While differences between young and old adults have been studied using fMRI and cognitive tests (Heffernan *et al.*, 2018), studying how changes in the brain and neurovascular coupling progress is impractical due to the time scale required. A rodent model of healthy ageing, and a longitudinal fMRI protocol, would be beneficial to study how ageing progresses throughout the lifetime. Additionally,

understanding changes in a healthy brain in a controlled environment would be beneficial to studies of age-related neurological diseases, as currently there are no studies of healthy ageing in rodents to our knowledge. Use of a healthy ageing model in rodent studies would allow known effects of healthy ageing to be factored in to analysis of disease models. Additionally, through use of a multi-parametric fMRI protocol, changes in neuronal metabolism and CBF can be observed in addition to the BOLD signal, and so how neuronal and vascular factors contribute to changes seen in BOLD activity can be studied.

3.1.1. Functional Changes in Normal Ageing

In the process of ageing in healthy individuals, neuronal activity undergoes reorganisation, and the vascular system becomes less efficient. Early human fMRI studies showed a variety of changes in the BOLD response with age. Response amplitude and time-to-peak have both been shown to decrease with ageing. Signal to noise ratio has also been shown to decrease with age (Ross et al., 1997), and the number of activated voxels is up to four times higher in a younger cohort (18-32) than an aged one (61-82) (D'Esposito et al., 1999).

Differences in the BOLD signal vary between different brain regions, with cortical regions displaying decreases in perfusion of varying size, while subcortical regions show a largely intact basal CBF (Chen et al., 2011). The most consistently observed change is in the prefrontal cortex, showing less lateralised activity with ageing. Known as hemispheric asymmetry reduction in older adults (or the HAROLD model), this effect was initially observed in a verbal recall task, and reported as reflecting functional compensation for age-related deficits in processing (Cabeza, 2002). This phenomenon was further characterised and shown to be a global reorganisation rather than task specific. For example, one study looking at both verbal and spatial memory showed greater left hemisphere activation for verbal memory and greater right hemisphere activation for spatial memory in younger adults, while older adults showed equal activation in both hemispheres for both tasks (Reuter-Lorenz et al., 2000). However, other studies have shown that increased bilateral activity can correlate with poorer behavioural outcome, including during inhibition tasks (Colcombe et al., 2005), and naming accuracy tasks (Wierenga et al., 2008).

Studies combining resting-state, activation-state, DTI and behavioural experiments to investigate dorsolateral prefrontal and parietal regions and working memory support this theory. RS-fMRI showed asymmetric reductions in connectivity in these regions, with the left hemisphere preserving connectivity better than the right, and activation in the prefrontal cortex increasing in the right hemisphere. Structural connectivity also shows the same

pattern. Thus, with ageing, reduction in intrahemispheric connectivity is compensated via increased task-related activation of individual regions in the dominant hemisphere, supported by increased proportion of processing shifted to the contralateral region (Cabeza *et al.* 2002).

In animals, age related functional changes are less well characterised. Studies have characterised age related structural changes in the hippocampus, associated with cognitive decline (Driscoll *et al.*, 2006). Functional studies have also shown changes in perfusion associated with cognitive decline. Interestingly, one study showed increased basal perfusion to the hippocampus and reduced reactivity to hypercapnia correlating with memory impairments (Mitschelen *et al.*, 2009). One study has investigated functional asymmetry in ageing rats using optical image spectroscopy, using the LOU/c aging rat model. This study reported a reduction in amplitude of the haemodynamic response to forepaw stimulation, increase in size of the activated area, and delayed time to peak. BOLD responses in the opposite hemisphere remained unaffected with age, correlating with observation of reduced asymmetry in humans (Dubeau *et al.*, 2011). However, healthy ageing has not previously been studied in animals using fMRI. Studies using fMRI would be advantageous due to the non-invasive nature of MRI, the ability to study additional parameters during the same experiment, and the ability to compare data with fMRI studies in humans.

3.1.2. Methodological considerations for preclinical fMRI in ageing rats.

Current preclinical fMRI methods are not optimised for longitudinal studies. In order to perform MRI on rodents, most studies use anaesthesia to ensure the rodent does not move or become distressed (Tremoleda, 2012). Anaesthetics impair neurovascular function to varying degrees (Paasonen *et al.*, 2018). However, extensive training or invasive surgery (e.g. to be able to fix the head in place) is required to prevent an awake rat from moving in the scanner (Lahti *et al.*, 1999; King *et al.*, 2005; Martin *et al.*, 2013). Many previous fMRI studies use injectable anaesthetics, such as urethane or alpha-chloralose, with toxic, carcinogenic or harmful properties (Dijkhuizen *et al.*, 2001; Kennerly *et al.*, 2005) and therefore can only be used in non-recovery studies (Tremoleda *et al.*, 2012). Inhaled anaesthetics, such as isoflurane or halothane, suppress the BOLD signal and shift the balance between capillary and arterial BOLD signal, masking long term changes in activity and artificially increasing the effect of noise or small variations (Schroeter *et al.*, 2014; Tsurugizawa *et al.*, 2016; Paasonen *et al.*, 2018). Medetomidine may be a viable candidate for use in preclinical longitudinal studies, but the variable depth of anaesthesia can cause complications such as increased heart rate (Weber *et al.*, 2006; Tremoleda *et al.*, 2012).

Propofol, an injectable anaesthetic common in veterinary practice, has no known adverse effects from repeated use, and a less pronounced effect on CBF, BOLD signal or the haemodynamic response function when compared to other anaesthetics (Griffin *et al.*, 2010; Kelly *et al.*, 2010; Tremoleda *et al.*, 2012; Schroeter *et al.*, 2014; Paasonen *et al.*, 2018) and thus was selected for this study. Animal welfare is also an important concern in longitudinal studies, and animals' health over their lifetime can have a major impact on study outcomes. For long term health, animals require more space, sensory enrichment and socialisation than allowed by standard rat housing (Hutchinson *et al.*, 2005). Animals kept long term without additional enrichment become obese and develop health problems associated with obesity and inactivity. It has been shown that regular access to a large, multiple level playpen, with access to items promoting burrowing, foraging and gnawing behaviour, and socialisation with the entire cohort, improves animal health in longitudinal studies (Hutchinson *et al.*, 2005). To that end, all animals were given daily access to a playpen for the duration of this study.

Thorough, non-invasive physiological monitoring is also important for longitudinal animal studies. Propofol does cause respiratory depression in large doses, and anaesthetised animals breathing room air can be at risk of hypoxia if their breathing rate is low. A continuous infusion of a low dose of propofol is expected to have minimal effect on breathing rate or oxygen saturation (Griffin *et al.*, 2010). However, MRI of ageing animals has not been previously performed using propofol, so animals were monitored with both a respiration pillow and a pulse oximeter to ensure respiratory depression or hypoxia is identified early and animals can be recovered quickly.

In order to understand the neuronal factors behind the BOLD signal, a non-invasive method of quantifying neuronal activity is required. Electrophysiology methods are invasive and are therefore not practical for longitudinal studies due to their impact on animal welfare. A method that has previously been suggested to give a non-invasive measurement of neuronal activity is functional MR spectroscopy (fMRS). Through taking two spectra with and without stimulation, and subtracting the two, the difference in relative concentrations of the neurotransmitter glutamate can be detected, and used to infer neuronal activity in the region (Gussew *et al.*, 2010). This method is limited in spatial resolution, measuring a voxel several millimetres wide rather than the sub-millimetre resolution provided by preclinical fMRI, however may be useful when paired with fMRI in studies of a single, known region of interest (Stanley and Raz, 2018).

In this chapter, we used fMRI to explore age-related changes in somatosensory cortex activity in response to forepaw stimulation. Understanding age-related changes in healthy animals

using fMRI is important in improving the current understanding of age-related cognitive decline and age-related pathologies. Additional fMRI methods can improve the understanding of how neuronal and vascular components contribute to what is observed with BOLD fMRI.

3.2. Methods

3.2.1. Animal preparation and anaesthesia

This study was conducted in accordance with the UK Animals (Scientific Procedures) Act, 1986 under project licence P7D063834 and following institutional ethical approval by the University of Leicester Animal and Welfare Ethical Review Body. All experiments are reported in accordance with the Animal research reporting of in vivo experiments (ARRIVE) guidelines (Kilkenny et al., 2010). A total of 11 female rats (Wistar Han, Charles River Laboratories); were used in the current study; and all animals completed the study. Rats aged 3 months on arrival were group housed in standard cages. Animals were given daily access to a playpen for 2-6 hours. Animals were first acclimatised to single level playpens in groups of 4 for one week, followed by two weeks of mixing up to 8 animals from two different cages together, then mixing all animals into one playpen. At 12 months of age, the playpen was replaced with a three-storey chinchilla cage kept in an incubator cabinet, maintained at room temperature, with an isolated air supply and red glass doors to block external light sources. Preventing outside air and external light prevents animals from seeing or smelling humans while in the playpen, with the intention of promoting more natural behaviour without anxiety from potential threats.

3.2.2. Experimental schedule

Bench experiments were performed on animals at 5 months old to test the anaesthesia protocol and identify the correct dose rate. The protocol described below was performed, in order to test the initial dose rates of 7.5mg/kg bolus followed by 42mg/kg/hr infusion of propofol (Griffin et al., 2010), without MRI scanning. When this did not induce a sufficient depth of anaesthesia, dose rates were increased in 10% increments until a dose rate of 9mg/kg bolus followed by 54mg/kg/hr infusion was identified as the lowest dose required to maintain anaesthesia once isoflurane had been discontinued.

Animals were weighed prior to all MRI scans, and weighed daily for two days after MRI scans to identify any weight loss related to anaesthesia. Following this, the timepoints used were 7, 9, 12, 15 and 18 months. These time points were chosen to ensure animals were fully mature at the start of the study (equivalent to early 20s in humans), and that, at the end point of the study, animals were old enough to exhibit changes in brain function (equivalent of mid-late 50s in

humans) but that risk of death was minimal. At 18 months old, immediately following the final scan, animals were humanely killed while under propofol anaesthesia. 6 animals were sacrificed using intravenous pentobarbitone. 5 animals were sacrificed using intraperitoneal pentobarbitone, and transcardially perfused with formaldehyde.

3.2.3. Anaesthesia protocol

Animals were initially anaesthetised with 3% isoflurane in 100% oxygen. Tail vein cannulation was performed before transferring the animals to the MRI bed. A bolus of 9mg/kg propofol was administered over 1 minute using a syringe driver (Harvard Apparatus, Cambridge, Massachusetts, US.) and the isoflurane was gradually reduced to 0%, with animals still breathing 100% oxygen. Respiration was monitored using a respiration pillow (Small Animal Instruments Inc. Stony Brook, New York, USA), temperature monitored using a rectal probe and maintained using a fan heater activated when measured temperature dropped below 37°C (Small Animal Instruments Inc. Stony Brook, New York, USA), and heart rate and blood oxygen saturation monitored using a pulse oximeter (Starr Life Sciences, Oakmont, Pennsylvania, USA). Copper electrodes were inserted subcutaneously into the dorsal surface of the right forepaw between digits 1-2 and 2-3 (Hyder et al., 1994). Three minutes after the bolus ended, a continuous infusion of propofol was given at 54mg/kg/hr for the duration of the scan. Following the scan, animals were allowed to recover in a separate cage. Analgesic cream (EMLA cream, Aspen Pharma, Dublin, Ireland) was applied to the forepaw where electrodes had been removed, and animals were provided with water and wet food pellets to prevent dehydration after anaesthesia. Animals were awake within 15 minutes following removal of anaesthesia, and moving freely within 30 minutes, at which point they were returned to their home cage.

3.2.4. MRI protocol

MRI scans were performed on a 9.4T Small Animal MRI scanner (Agilent Technologies), using a 72mm RF volume transmit coil and a 2-channel surface receive coil (Rapid Biomedical, Rimpar, Germany). Coronal scout images were used to locate bregma, and three 1.5mm slices were selected with bregma in the middle slice. A shimming voxel with dimensions 10x9x4.5mm was positioned to cover the centre of all three slices, excluding non-brain tissue or tissue outside the slices of interest. Fast, automatic shimming technique by mapping along projections (FASTMAP, Gruettter, 1992) was used to shim these slices to a 50% water linewidth between 20-35Hz. Rats were switched from breathing oxygen to room air, pumped at 2L/min using an air pump (Wiz-Air, Clarke Tools, Dunstable, UK). Functional MRI was performed for 9 minutes using a gradient echo EPI sequence (TR=250ms, TE=22ms, $K_{zero}=8$, shots=2, data matrix

=128x128). The forepaw was stimulated at 10mV, 10Hz, pulse width 1 μ s, with a block design of 60s off, 30s on. Following this, a 4x4x4mm voxel was positioned over the left somatosensory cortex at bregma, and manual shimming was performed to a 50% water linewidth of <25Hz. A Localisation by adiabatic selective refocusing (LASER, Slotboom et al., 1993) MR spectroscopy sequence (TR=2000ms, TE=14.54ms, 270 arrayed averages) was used to perform functional MRS over 9 minutes, using the same forepaw stimulation paradigm used for fMRI. For analysis, the first 30 seconds of each "off" block were discarded to allow time for metabolites to return to baseline levels. 6 Minutes of resting-state fMRI were performed (TR=1000ms, TE=22ms, shots=2, K_{zero} =16, data matrix=128x129, slices=22, slice width=1mm) for analysis of functional connectivity. Oxygen saturation was maintained above 80% during functional experiments (Tremoleda et al., 2012). Animals were switched back to 100% oxygen after all functional scans were complete. After being returned to 100% oxygen, a time-of-flight angiography scan and a T₂ weighted structural scan were performed. Using the TOF angiography image, the carotid artery was located and a tagging slice placed with a gap of -17mm from bregma. 6 minutes of continuous arterial spin labelling (CASL) was performed on a single 1.5mm slice placed over bregma (TI=1500ms, TR=2500ms, TE=10ms, shots=1, K_{zero} =16, data matrix=128x128).

3.2.5. Data analysis

A fMRI analysis pipeline was developed using FSL (www.fmrib.ox.ac.uk/fsl, Smith et al., 2001). MCFLIRT (Jenkinson et al., 2002), rBET (Wood et al., 2013), and FAST (Zhang et al., 2001) were used for motion correction, brain extraction and bias field correction respectively. Independent component analysis for artefact removal, using MELODIC (Beckmann and Smith, 2004) were performed prior to time-series analysis in FEAT (Woolrich, 2001) to visualise the BOLD response. Cluster analysis was performed on the first-level FEAT outputs to determine number of active voxels, maximum % signal change within the cluster, and mean % signal change across the cluster. In each scan, time to peak was calculated for each of the six stimulus blocks and averaged, with a temporal resolution of 0.5 seconds (Baumann *et al.*, 2010).

Functional MRS spectra were separated into "off" and "on" blocks and averaged using the MATLAB FID-A toolkit (Simpson et al., 2017). The two spectra were analysed using the TARQUIN MRS analysis package (www.tarquin.sourceforge.net) to determine relative concentrations of glutamate. Metabolite concentrations from "off" blocks were subtracted from "on" blocks to determine the difference in glutamate concentration, and difference in glutamate change (Δ Glu) was averaged across subjects. "Off" blocks were also used to quantify NAA and Inositol, used as markers of neuronal viability and inflammation, respectively.

Resting-state fMRI underwent the same preprocessing steps as fMRI, followed by a group level independent component analysis (MELODIC) to detect regions of low-frequency activity. The independent component maps generated were used for dual regression analysis to map voxel-wise connectivity for each component. These dual regression maps were fed into network analysis using FSLNets to build a hierarchy matrix, determining functional connectivity between components and organising components into functional networks. Stage 3 dual regression analysis comparing 6 months and 18 months was used to determine changes in voxel-wise connectivity with age.

Control and tag ASL images were first concatenated into a single image of two volumes. The Oxford ASL toolkit for FSL was used to subtract the tag image from the control image to create a difference image. FSLmaths was used to apply a modified Bloch equation (Williams et al., 1992) to the data in order to quantify CBF in absolute units.

CBF map images were given an upper threshold of 5 to remove large outliers. This was determined based on the histogram of voxel intensities, in which some scans displayed a small number of single voxels with large intensities between 5 and 80 having a large influence on the mean. Non-zero mean and standard deviation CBF were calculated using FSLstats.

Statistical analysis was performed in Graphpad Prism (Version 7, www.graphpad.com). Data are shown as mean +/- standard deviation (SD). Changes over time were analysed using a repeated measures ANOVA, with a mixed effects model to account for any missing data points, and the criterion for statistical significance was $P < 0.05$. Where statistically significant differences were found, post-hoc testing to compare individual time points was performed using the Tukey-Kramer multiple comparisons test.

3.3. Results

3.3.1. Animal body weight

Body weight significantly increased with age (Repeated measures ANOVA, $F = 14.19$, $P < 0.0001$), from 253 +/- 20.26g at 7 months old to 310 +/- 24.61g at 18 months, and remained within the expected weight range for healthy Wistar Han rats (Fig. 3.1). Post-hoc comparisons showed significant differences when comparing 7 months vs 9 months ($P = 0.0012$) 7 vs 12 months ($P = 0.012$), 7 vs 15 months ($P = 0.0002$), 7 vs 18 months ($P = 0.0001$), 9 vs 15 months ($P = 0.0196$), 9 vs 18 months ($P = 0.0004$), 12 vs 15 months ($P = 0.0047$), 12 vs 18 months ($P = 0.0004$), and 15 vs 18 months ($P = 0.012$). During scanning, while breathing room air, oxygen saturation remained above 80%, which has been previously defined as safe (Tremoleda et al., 2012).

Breathing rate remained steady at 60 +/- 5 bpm while animals were breathing room air, with transient increases to 73 +/- 13 bpm during stimulus blocks. Breathing rate during scanning did not change with age.

3.3.2. Functional MRI

First-level analysis of BOLD fMRI data was performed in FEAT (Fig. 3.2) and was used to quantify three aspects of the BOLD signal: number of active voxels in S1FL, maximum % signal change in S1FL, and mean % signal change in S1FL (Fig. 3.3).

The number of active voxels was found to significantly decrease with age ($F(4, 27) = 3.727, P = 0.0153$), with the number decreasing from 399.5 +/- 356.8 at 7 months to 76.7 +/- 37.0 at 18 months old. Post-hoc testing found that there was a significant decrease in the number of active voxels between the ages of 9 months (532.8 +/- 570.3) and 15 months (114.7 +/- 46.91m $P = 0.0367$), and between 9 months and 18 months (76.7 +/- 37, $P = 0.0286$). Standard deviation was also shown to significantly decrease with age (Brown-Forsythe test, $P = 0.0001$). No significant difference was found in the maximum BOLD signal change ($F(4, 27) = 0.1963, P = 0.9381$) or mean BOLD signal change ($F(4, 36) = 1.422, P = 0.2465$) with age. Time-to-peak of the BOLD signal was not found to significantly change with age ($F(4, 27) = 2.210, P = 0.0946$, Fig. 3.4).

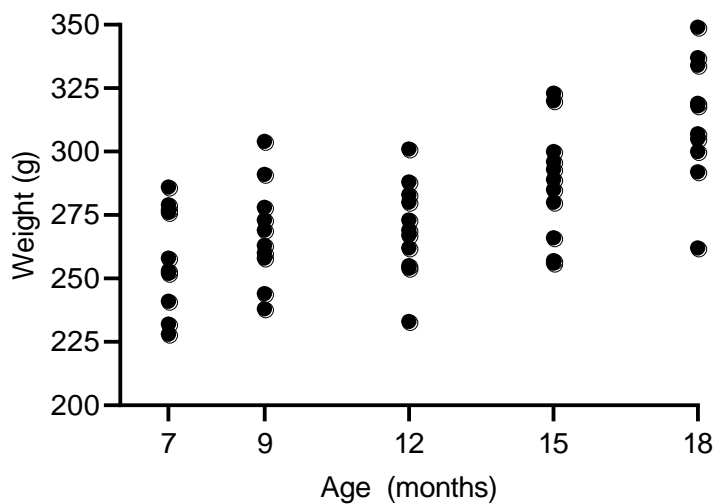


Fig. 3.1. Individual rat weights at 7, 9, 12, 15 and 18 months (n=11)

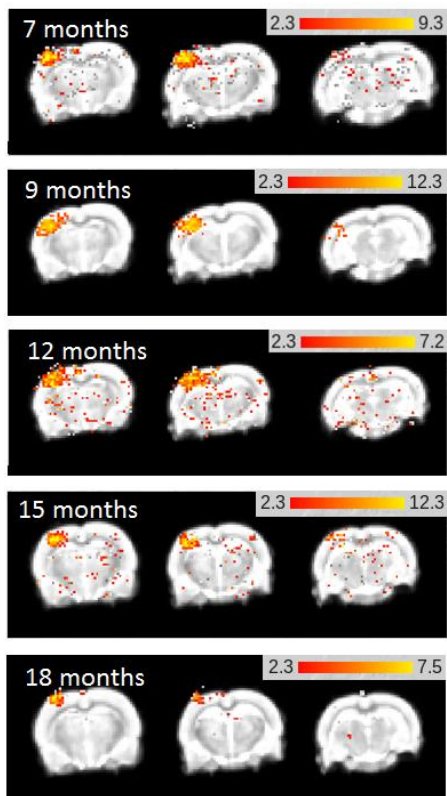


Fig. 3.2. Example BOLD fMRI images displaying S1FL activation in response to forepaw stimulation in a representative rat at 7, 9, 12, 15 and 18 months old. Coloured bar indicates Z statistic of active voxels. Slices (from left to right) are bregma + 1.5mm, bregma, bregma - 1.5mm

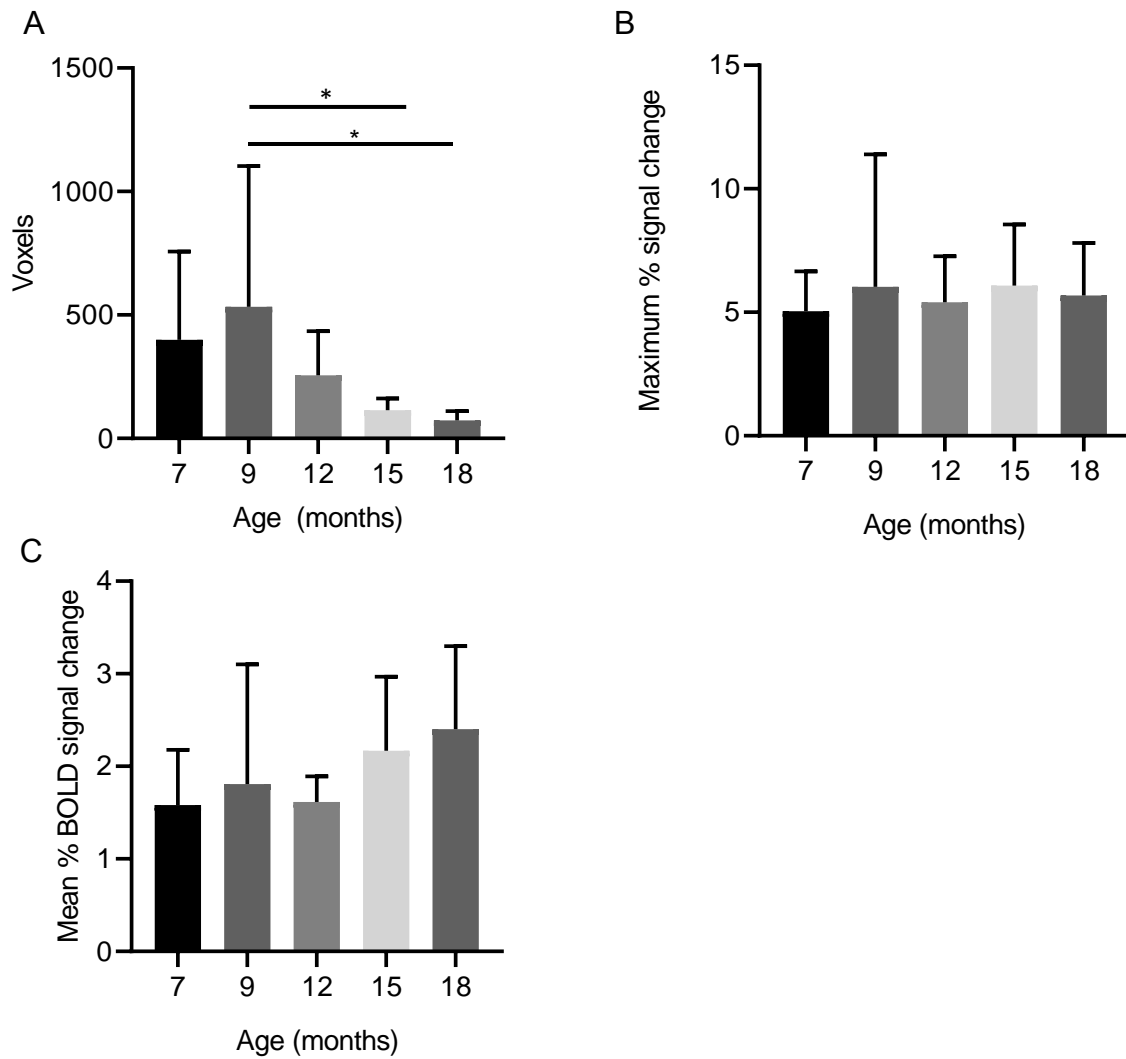


Fig. 3.3. Effect of age on various aspects of the BOLD signal in response to forepaw stimulation including the maximum BOLD signal change in S1FL, the mean BOLD signal change of all active voxels in S1FL, and the number of active voxels in S1FL. A significant decrease in the number of active voxels was observed with age (* $P = 0.05$). Data is displayed as mean \pm SD, $n = 8, 8, 8, 10,$ and 7 at $7, 8, 12, 15$ and 18 months respectively.

Time-To-Peak of BOLD signal

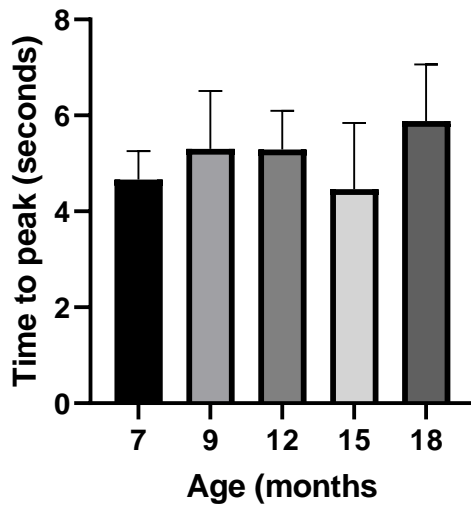


Fig. 3.4: Time-to-peak of BOLD signal in response to forepaw stimulation with age. TTP is taken from the voxel with the highest Z statistic. No significant change is seen between any time points. Data is displayed as mean \pm SD, n = 8, 8, 8, 10, and 7 at 7, 8, 12, 15 and 18 months respectively.

3.3.3. Functional MR Spectroscopy

The change in glutamate signal between off and on blocks (Δ Glu) decreased significantly ($F(4, 37) = 4.018, P = 0.0083$) from 7 months (73.4 ± 103.6 AU) to 18 months (-1.08 ± 1.19 AU). Post-hoc testing showed significant differences between 7 and 9 months ($P=0.0447$), 7 and 12 months ($P=0.0162$) and 7 and 15 months ($P=0.009$). From 12 months onwards, the glutamate signal change became negative, showing an overall decrease in glutamate with activation (Fig. 3.5). NAA and Inositol were also quantified (Fig. 3.6). Quantification of NAA displayed a significant decrease ($F(4, 27) = 5.267, P = 0.0025$) in NAA from 36.50 ± 28.46 AU at 7 months to 8.41 ± 14.40 AU at 18 months, with post-hoc testing showing significant decreases between 7 months and 9 months ($P = 0.0076$), 12 months ($P = 0.0083$), 15 months ($P = 0.0029$) and 18 months ($P = 0.048$). Inositol was found to significantly decrease ($F(4,41) = 1.68, P = 0.0417$) from 118.53 ± 168.3 AU at 7 months to 21.7 ± 58.1 AU at 18 months. 7 months and 15 months (8.63 ± 15.54 AU) were found to be significantly different in post-hoc testing ($P = 0.036$).

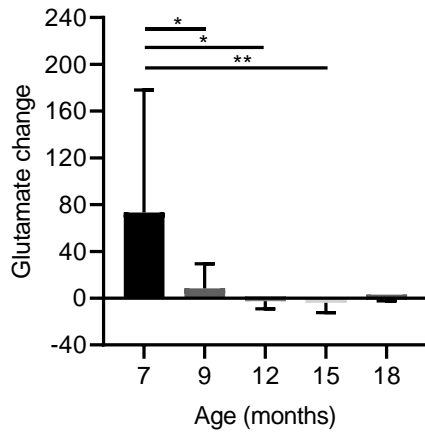


Fig. 3.5. Effect of age on glutamate change in S1FL in response to forepaw stimulation quantified using LASER fMRS. There was a significant decrease in the glutamate signal change with increasing age (* $P = 0.05$, between various times points). Data is displayed as mean \pm SD, $n = 8, 10, 9, 11,$ and 4 at $7, 8, 12, 15$ and 18 months respectively.

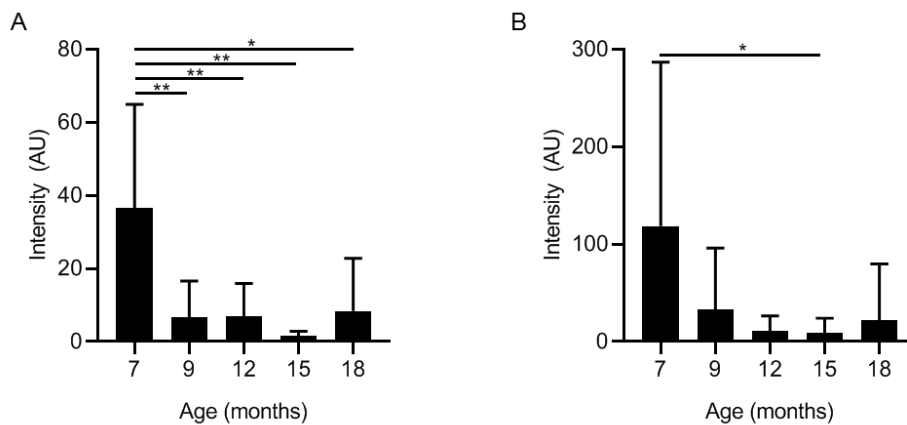


Fig. 3.6. Effect of age on intensity of NAA (A) and Inositol (B) levels with age in the somatosensory cortex quantified using LASER MRS. Both NAA and Inositol levels significantly decreased with increasing age (* $P = 0.05$, between various times points). Data is displayed as mean \pm SD, $n = 8, 10, 9, 11,$ and 4 at $7, 8, 12, 15$ and 18 months respectively.

3.3.4. Resting state fMRI

Independent component analysis and dual regression detected 19 independent components. These included left and right caudate nucleus, nucleus accumbens, hypothalamus, left and right somatosensory cortex, cingulate cortex, retrosplenial cortex, superior colliculus, globus pallidus, cerebellum, visual cortex, and entorhinal cortex. These components were sorted into

a hierarchy matrix (Fig. 3.7) by FSLNets, which separated them into three networks. The first network consisted of somatosensory and motor cortices, the cingulate cortex, the caudate, thalamus, nucleus accumbens and hypothalamus, and was identified as the sensorimotor network. The second network consisted of the superior colliculus, retrosplenial cortex, cerebellum, globus pallidus and anterior hypothalamus, and is thought to be the default mode network. The third network consisted of the visual cortex, secondary somatosensory or premotor regions and the entorhinal cortex, and is thought to be the visual network. Stage 3 Dual Regression was also performed in order to identify changes in intra- and inter-component connectivity. Of the 19 components, 11 displayed a significant (multiple-comparison corrected P (corr) < 0.01) change in connectivity with another region (Table 3.1). All 11 of these components displayed an increase in connectivity with another region, while one component also displayed a decreased connectivity with another region.

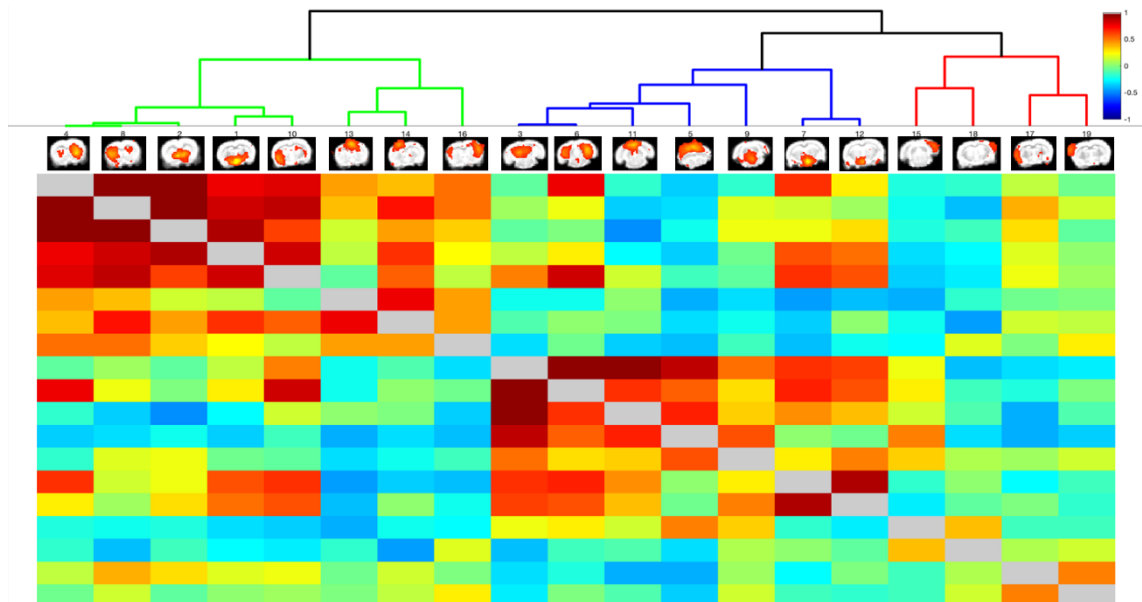


Fig. 3.7: Hierarchy matrix displaying connectivity between 19 components detected by ICA and dual regression analysis. Each square represents the correlation between two components, with components displayed on the horizontal axis. Darker red indicates a stronger positive correlation between components, darker blue indicates a stronger negative correlation. Components are organised into three groups based on inter-component connectivity. The sensorimotor network, displayed by green lines, includes somatosensory and motor cortices, superior colliculus, globus pallidus and caudate nuclei. The default Mode network, displayed by blue lines, includes the retrosplenial cortex, cerebellum, and mesencephalic nuclei. The visual network, displayed by red lines, includes visual and entorhinal cortexes.

Component	Connection to:	Increase/Decrease
Nucleus Accumbens	Superior Colliculus	Increase
Left Caudate/secondary somatosensory/Globus Pallidus	Globus pallidus	Decrease
Left Caudate/secondary somatosensory/Globus Pallidus	Dorsal Hippocampus	Increase
Cerebellum	Cerebellum, right caudate	Increase
Left posterior caudate	Ventral tegmental area	Increase
Retrosplenial cortex	Cerebellum	Increase
Left motor/somatosensory cortex	Superior Colliculus	Increase

Table 3.1. Changes in functional connectivity with age. Dual regression was performed on resting-state components identified with ICA to identify voxels showing a significant (corr $p < 0.01$) increase in connectivity to each component, comparing data from the 7 month and 18 month time points. The table shows the component of interest, region to which connectivity changed, and whether that change with age was an increase or decrease.

3.3.5. Arterial Spin Labelling

Mean CBF across the slice did not change significantly between 7 and 18 months ($P=0.28$), with low variability between subjects (fig. 3.8). Mean CBF at all time points was within a standard deviation of the expected value of 2.33ml/g/min observed in some previous rodent experiments (Thomas et al., 2006).

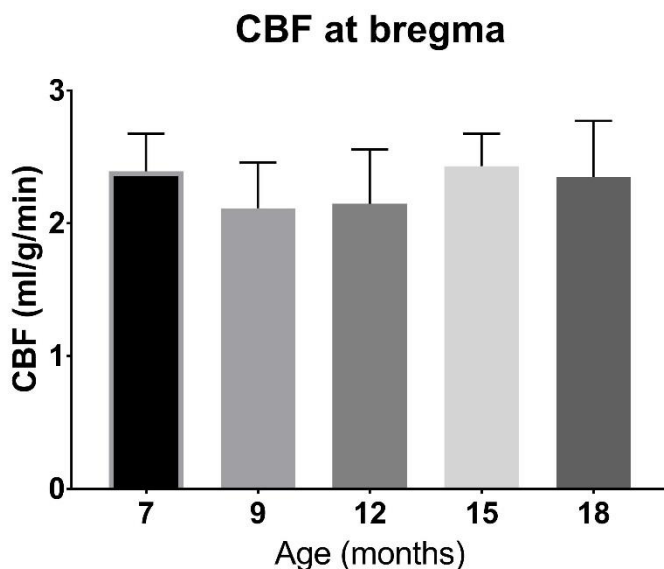


Fig. 3.8: The effect of age on resting CBF at bregma, quantified using ASL MRI. There was no significant differences in resting CBF at bregma at any of the time points measured. Data is displayed as mean \pm SD, n = 11, 11, 11, 11, and 10 at 7, 8, 12, 15 and 18 months respectively.

3.4. Discussion

This study investigated changes in the BOLD signal, glutamate turnover and CBF with age in healthy rats using fMRI. Propofol was determined to be a suitable anaesthetic for longitudinal studies, causing no detrimental effects to animal health and allowing detection of a strong BOLD signal compared to observations using other anaesthetics (Schroeter et al., 2014). The size of the BOLD signal in the somatosensory cortex decreased with age. Functional MR spectroscopy showed a reduction in Δ Glu (Glutamate during stimulation – glutamate during rest) from 9 months onwards, with glutamate change becoming negative at 12 months old. Arterial spin labelling showed that resting CBF remained constant for the duration of the study.

Here we report, for the first time, a decrease in the BOLD signal during ageing in rodents which is consistent with human task-based fMRI studies comparing young and aged groups, where the active region is significantly reduced in size during motor tasks (Huettel et al., 2001; Ances et al., 2009). The maximum and mean signal change remained constant over all time points, and was consistently located in the centre of the ROI, which is consistent with human studies where the BOLD signal amplitude remains consistent in healthy aged subjects while the spatial extent of the BOLD response is reduced (D'Esposito et al., 1999; Huettel et al., 2001). Time-to-peak of the BOLD signal also remained constant at all time points. While the reduction in size of the active region is consistent with human studies, the reduction in variability between subjects with age is not consistent with human studies (D'Esposito et al., 1999). Aged human subjects show a greater variability in task-related BOLD signal than young subjects (Kannurpatti et al., 2010). Our data shows a reduction in variability between 12-18 months. In healthy volunteers, there is uncontrolled variability in lifestyle factors and medical history, whereas in our study, all animals, as is standard in preclinical studies, experience the same highly controlled environment. Careful control of lifestyle factors in this manner provides an excellent platform for future treatment studies involving longitudinal functional MRI.

Reduction in size of an active region may be due to a number of factors, including synaptic plasticity, neuronal death, reduction of neurovascular signalling, or reduced vascular reactivity (Girouard and Iadecola, 2006). In normal learning and development, or during recovery following ischaemic stroke, task-related activity may shrink over time as connections are formed and become more efficient (Penhune and Doyon, 2005). While this is unlikely in an ageing group

of animals, animals in our study were provided novel stimuli as part of the animals' enrichment, which is thought to be beneficial for somatosensory cortex function. Animal welfare is also an important concern in longitudinal studies, and animals' health over their lifetime can have a major impact on study outcomes. For this reason, access to an enriched environment providing more space, sensory enrichment and socialisation than allowed by standard rat housing was provided in accordance with previously identified requirements (Hutchinson et al., 2005). Neuronal death, reduced neuronal activity, reduced neurovascular signalling and reduced neurovascular activity are all elements of age related changes to the brain, with varying effects depending on overall health (Girouard and Iadecola, 2006). Thus, the reduction in size of the active region is likely an effect of healthy ageing, while the low variability is likely due to the beneficial effects of the enrichment protocol.

A limitation of BOLD fMRI is that the BOLD signal is not a direct measure of neuronal activity. Impairment of neurovascular coupling or changes in vascular reactivity can confound interpretation of the BOLD signal. For this reason, a more direct measure of neuronal activity can be beneficial. Glutamate is the most common neurotransmitter in the brain (Walls et al., 2014), and so direct quantification of glutamate turnover may complement BOLD fMRI data when investigating neurovascular coupling. MR spectroscopy is the least invasive method of measuring neurotransmitter levels in vivo, and though there are limitations with respect to spatial and temporal resolution, this method has previously been applied to quantify task- or stimulus-based changes in glutamate and lactate (Gussew et al., 2010, Stanley and Raz, 2018).

Here, we describe age-related changes in glutamate levels becoming negative from 12 months onwards, which may be due to decreasing efficiency of glutamate turnover mechanisms with age. Glutamate is normally stored in vesicles and released with activation. As glutamate is released, increased glutamate production occurs to refill the vesicles and glutamate is recycled with sustained activity through the glutamine-glutamate cycle (Walls et al., 2014). If this cycle is impaired with age, and glutamate production does not exceed or keep up with glutamate release, this may be measured as a net decrease in glutamate. If this is the case, it can also explain the reduction in BOLD signal observed with age. Glutamatergic receptors on astrocytes are an important mediator of neurovascular coupling (MacVicar and Newman, 2019), and reduced glutamate turnover would lead to reduced glutamate diffusion outside the synaptic cleft. However, due to the low SNR of this method when using a short scan time, caution must be exercised in interpreting their findings, and further studies using longer scan times or alternative MRS techniques are required to confirm this hypothesis.

We also measured changes in the levels of the metabolites, NAA and inositol, as they are correlated with age-related cognitive decline in humans. NAA is reported to a neuronal marker and an indicator of neuronal integrity as others have reported a correlation between NAA and neuronal density in patients with Alzheimer's disease (Cheng et al., 2002). With respect to aging others have demonstrated a decrease in NAA levels in human studies (Boumezbeur et al., 2010; Lim and Spielman, 1997; Schmitz et al., 2018) which is consistent with the age-related decline in NAA we observed here and may be indicative of reduced neuronal density or neuronal function. However, changes in NAA levels in humans may be regionally dependent (Eylers et al., 2016) which we did not assess here and further studies could correlate changes in such levels with alterations in cognitive function. Inositol, or myo-inositol, is considered to be a putative glial marker (Martin, 2007) and higher levels are seen in patients with, for example, Alzheimer's disease frontotemporal dementia, which might be expected in conditions associated with higher gliosis (Ernst et al., 1997). However, it is still not clear what changes in absolute levels of inositol represent – it may be that changes, as reported here, reflect changes in glial metabolism (Marajanska et al., 2017). The decrease in NAA and glutamate turnover after 7 months may suggest that this is the point where rodent brains mature from young adulthood to middle age, as some human studies have shown a decrease in NAA at this time as formation of new pathways slows down (Chichocka and Beres, 2018), however, further study in humans and rodents is needed to fully understand such changes.

As well as examining stimulus-related activity, resting-state activity was also studied. 19 independent components were detected, more than previously detected in rats anaesthetised with medetomidine or isoflurane (Jonckers *et al.*, 2008). Some independent components did include multiple adjacent regions (e.g a component in the caudate extending into the globus pallidus and lower layers of the secondary somatosensory cortex). Using FSLNets, a hierarchy matrix was created which determined that these components were organised into three networks, thought to be the sensorimotor network, default mode network, and visual network. Of these components, 8 displayed no change in functional connectivity with age, while 11 displayed an increase in inter-component connectivity. Studies in humans have shown increased cross-hemispheric connectivity with age in some cortical regions, known as the hemispheric asymmetry reduction in older adults, or HAROLD, model (Cabeza *et al.*, 2002). More recently, studies have shown that this is not limited to cross-hemispheric connectivity, but also includes additional connectivity to supplementary areas within each hemisphere. This more generalised model is known as the compensatory-related utilisation of neural circuits hypothesis, or CRUNCH (Berlingeri *et al.*, 2013). In this study, no cross-hemispheric increases in

connectivity were observed. All increases in connectivity were either within the same hemisphere, or connectivity to central regions, mainly the superior colliculus. No regions in the right hemisphere displayed an increase in connectivity. It is possible that this is due to rats showing a dominant hemisphere for sensorimotor activity. Alternatively, it is possible that this is due to reinforcement of pathways involved with sensory processing in the left hemisphere, due to repeated experiments in which the right forepaw is stimulated. To understand this further, a study focusing only on resting-state measures is needed.

Arterial spin labelling, as used here, allows imaging of cerebral perfusion. No changes were seen in mean CBF across the lifespan of the animals studied here, and values were similar to those reported in previous studies (Thomas et al., 2006), however some studies do report a lower value (Wegener et al., 2007) which may be variation between strains. This would suggest that mechanisms of cerebral autoregulation remained intact in these animals. Human studies have varied in whether ageing affects resting perfusion, showing either no change in CBF (Meltzer et al, 2000) or a decrease in CBF with age (Tarumi and Zhang, 2018). In this study, the consistent level of perfusion taken with the change in glutamate suggests that changes in the BOLD signal are caused by neuronal factors rather than vascular factors. As time-to-peak remained consistent with age, this also suggests that vascular reactivity was not impaired, which also suggests that the change in BOLD signal was caused by neuronal factors.

To our knowledge, this study for the first time shows age-related changes in stimulus-induced BOLD signal in a longitudinal study of rats. Through use of a novel anaesthesia protocol, which overcomes the limitations of other anaesthetics, a large active region was detected in the somatosensory cortex of young rats, which decreased in size over the animals' lifetime. This is consistent with the difference in BOLD signal between young and old human volunteers. In contrast to human studies, the aged animals showed very low between-subject variability, which may be due to the animal cohort all experiencing the same living environment, while lifestyles in human volunteers are variable. A further study with a larger cohort may allow the age at which changes to the BOLD signal begin to be identified. There are some methodological issues in the current study to consider in terms of the short TR used, which, combined with limitations in shimming an adequate volume, did limit scans to three slices over the region of interest without loss of image quality. While this allowed for a high temporal resolution and a large number of repeats, while keeping scan time to 9 minutes, the limited field of view did prevent image registration to high-resolution T₂ weighted images or to a standard space. Because of this, images had to be analysed at first level, then number of active voxels and signal intensity recorded, and group level comparisons were performed manually. Whole-brain fMRI

would facilitate registration of images to a standard structural space, thus allowing voxel-wise group level analysis to be performed. As we have demonstrated the utility of the anaesthesia protocol, future studies can incorporate longer scan times, and whole brain images can be obtained either through improved shimming or a longer TR and additional stimulus blocks. Functional MR spectroscopy also suffered from low SNR due to the need for a short scan time, as the total length of the protocol was kept to approximately one hour to minimise risk from the novel anaesthetic protocol, which may be improved on in future studies.

Combining results from all MRI techniques, the reduction in size of the active BOLD region, shift to a negative glutamate change, while CBF and NAA levels remained constant, offers an explanation of how neurovascular coupling may change with age. It is possible that the reduced glutamate turnover is the cause of the observed reduction in size of the BOLD signal, without significant neuronal death or impairment of cerebral autoregulation. These methods have application in the study of neurodegenerative, neurological and vascular diseases and may enable longitudinal preclinical studies which are relevant for progressive diseases such as stroke or Alzheimer's disease to improve the translational relevance of such preclinical models (Sauter et al., 2002; Dijkhuizen et al., 2003; Hu et al., 2004; Sangahalli et al., 2013). In addition, the combination of a multi-parametric fMRI protocol may enable factors influencing neurovascular coupling in response to aging and neurodegenerative conditions to be further explored. These methods also represent a refinement to animal welfare, in that animals can be kept healthy for most of their lifespan, and animal numbers can also be reduced, which will benefit animal research as a whole. In Chapters 4 and 5, I applied these methods to investigate changes in neurovascular coupling during recovery following experimental stroke (Chapter 4), and as hypertension develops in spontaneously hypertensive rats (Chapter 5).

Chapter 4: Longitudinal functional MRI of recovery following experimental stroke in rats

4.1. Introduction

Ischaemic stroke is one of the most common causes of death or disability. Survivors often develop motor deficits, and the effectiveness of physical therapy on motor recovery varies greatly between patients. Clinical studies commonly use fMRI as an outcome measure in conjunction with motor task performance. Through these methods, changes in brain activity correlating with good or poor motor recovery have been observed. As patients begin to relearn lost motor skills, a larger region of the brain is recruited, including areas close to the damaged region and supplementary areas elsewhere in the brain, known as the recruitment phase (Feydy *et al.*, 2002; Tombari *et al.*, 2004). In patients showing poor recovery of motor skills, brain activity remains in this phase. In patients showing improvement in motor performance, these active regions are reduced over time, and a full recovery can be defined as showing an active region the same size as a healthy control, shifted to account for lost tissue, and similar task performance. This second phase is known as the focusing phase (Feydy *et al.*, 2002; Tombari *et al.*, 2004). However, this pattern has not previously been observed in rodents, and if rodents are to be used as a preclinical model for developing therapeutics, it is important to determine whether post-stroke recovery follows a similar progression in rodents.

Very few preclinical stroke recovery studies have used fMRI as an outcome measure (summarised in Table 4.1), which may be due to limitations of equipment availability, financial cost, technical expertise, and uncertainty regarding the fMRI protocol with regards to appropriate anaesthesia. Human stroke patients are typically awake during fMRI scanning but it is common practice for animals to be anaesthetised. Thus, in rodents, fMRI typically requires the use of an appropriate anaesthetic protocol that allows for detection of a haemodynamic response and for animals to recover so that they may be scanned at sequential time points and/or used for additional outcome measures, such as behaviour. Because of this, preclinical fMRI studies of post-stroke recovery have tended to use different groups of animals for each time point, introducing an additional source of variability and limiting the ability to monitor the progression of pathology and/or recovery in brain function over time.

Study	Rat Strain/sex/age	Longitudinal?	Anaesthetic	Stroke model	Outcome measures
-------	-----------------------	---------------	-------------	--------------	---------------------

Dijkhuizen et al., 2001	Sprague-Dawley, male, adult	No	Alpha-chloralose	Permanent MCAO	Cerebral blood volume fMRI (3/14 days post-MCAO), behaviour, lesion volume.
Abo et al., 2001	Sprague-Dawley, male, young adult	No	0.5% Isoflurane, muscle relaxant	Photochemical	Cerebral blood volume fMRI (3 weeks post-stroke), behaviour.
Sauter et al., 2002	Fischer, male, not specified	No	2% Isoflurane/Nitrous oxide	Permanent MCAO	CBF fMRI, lesion volume (1/2/5/12 days post-MCAO), apparent diffusion coefficient (ADC). Placebo vs neuroprotection with isradipine.
Dijkhuizen et al., 2003	Sprague-Dawley, male, adult	No	Alpha-chloralose	2 hr MCAO	CBV fMRI (1/3/14 days post-MCAO), neurological score, lesion volume, ADC
Markus et al., 2006	Not specified, not specified, 25 months	No	Not specified	Permanent MCAO	CBV fMRI (8 weeks post-MCAO), Behaviour, effect of novel therapeutic
Sicard et al., 2006	Sprague-Dawley, male, not specified	Yes	1% isoflurane	20 minute MCAO	BOLD fMRI, behaviour, lesion vol, ADC (0mins/30

					mins/180mins/1 day/7 days/21 days post-MCAO)
Kim et al. 2005	Sprague-Dawley, male, adult	No	Alpha-chloralose	2 hour MCAO	BOLD and CBV fMRI (2 weeks post-MCAO), lesion volume
Kim, et al., 2007	Sprague-Dawley, male, not specified	No	Alpha-chloralose	90 min MCAO	BOLD and CBV fMRI (2 weeks post-MCAO), lesion volume, effect of IV albumin.
Weber et al., 2008	Wistar, male, not specified	Yes	Medetomidine	1 hr MCAO	BOLD fMRI, electrophysiology (2/7/14/28/49 days post-MCAO)
Van Meer et al., 2010	Sprague-Dawley, male, not specified	No	1% isoflurane	90 min MCAO	RS-fMRI, manganese-enhanced MRI
Van Meer et al., 2010	Wistar, male, not specified	Yes	1.8% isoflurane	90 min MCAO	RS-fMRI (3, 7, 21, 70 days post-MCAO), lesion volume, manganese-enhanced MRI, behaviour
Van Meer et al., 2012	Sprague-Dawley, male, young adult	Yes	1% isoflurane	90 min MCAO	RS-fMRI (3, 7, 21, 49, 70 days post-MCAO), lesion volume, EEG, behaviour
Shih et al., 2014	Sprague-Dawley, male, adult	Yes	1% isoflurane	20 mins or 45 mins MCAO	CBV fMRI, electrophysiology (0/7/21 days post-MCAO)

Lake et al., 2017	Sprague-Dawley, male, adult	Yes	Propofol	Endothelin-1 injection	CBF fMRI with hypercapnic stimulus, electrophysiology with forepaw stimulus (7, 21 days post-MCAO)
Lake et al., 2017	Sprague-Dawley, male, adult	Yes	Propofol	Endothelin-1 injection	CBF fMRI with hypercapnic stimulus (7, 21 days post-MCAO), effect of COX-1 inhibitor
Shim et al., 2017	Sprague-Dawley, not specified, adult	No	Alpha-chloralose	2 hour MCAO	BOLD fMRI, RS-fMRI, Diffusion-weighted MRI, lesion volume (6 months post-MCAO)

Table 4.1: Summary of methods and outcome measures of recent preclinical fMRI studies of experimental stroke in rats.

In most preclinical stroke studies, stroke is induced through surgical or pharmacological methods. While Spontaneously Hypertensive stroke-prone rats are an option, allowing stroke to occur naturally in animals, these are better suited for studies into the risk factors of stroke and stroke prevention (Doggrell and Brown, 1998). The most common method of experimental stroke is middle cerebral artery occlusion (MCAO, Longa *et al.*, 1989). For this method, an incision is made into the common carotid artery, and a filament is advanced up the internal carotid artery until the middle cerebral artery is occluded. The incision is then closed. The occlusion can be permanent, or the filament can be removed between 20 minutes and 3 hours following occlusion. This method reliably causes stroke in the somatosensory regions of the brain, making it advantageous for preclinical fMRI, in which sensory stimulation is used (Durukan and Tatlisumak, 2007).

Initial fMRI studies performed in rats, using non-recovery anaesthesia and invasive monitoring protocols, showed low levels of contralesional activity in response to forepaw stimulation in groups scanned at 3 days and 14 days post-stroke, which was not seen in sham animals, and

an initial reduction in ipsilesional activity at 3 days, followed by a slight increase at 14 days post-stroke (Dijkhuizen *et al.*, 2001; 2003). This initial increase in contralesional activity, followed by a decrease as ipsilesional activity is restored, is similar to the changes seen in human stroke patients (Ward *et al.*, 2003a;b; Tombari *et al.*, 2004). However, in human studies, contralesional activity is higher at the early stage post-stroke, and ipsilesional hyperactivity is exhibited as recovery progresses (Feydy *et al.* 2002), rather than the low levels reported in rodents. Similar findings were reported in a subsequent study by the same group, although both studies report high inter-subject variability, which was also seen when animals were exposed, under isoflurane, to non-recovery scans post-stroke. Studies using a single time-point also detected contralesional activity, using CBV-weighted or contrast-enhanced MRI sequences (Abo *et al.*, 2001; Markus *et al.*, 2005; Kim *et al.*, 2005; 2007). These methods, when applied to studies of novel therapeutics with behavioural outcome measures, showed benefits of modulating pathways involved with plasticity in the thalamus and the contralesional cortex on outcome in the chronic phase (Kim *et al.*, 2005; 2007). Single time-point studies such as this are beneficial when performed in conjunction with longitudinal behavioural studies, in understanding how differences in activation patterns correlate with long-term behavioural outcome. However, their ability to infer the mechanisms behind functional recovery is limited.

Advances in post-stroke fMRI in rodents have been assisted with the development of suitable anaesthetic protocols for longitudinal functional studies, for example, using a subcutaneous infusion of medetomidine (Weber *et al.*, 2006). A longitudinal study using this method showed three different patterns of activity following induction of experimental stroke via MCAO (Weber *et al.*, 2008). All animals underwent the same MCAO procedure, however one group of animals showed no loss of BOLD response to forepaw stimulation and one group showed a complete loss of activity in the forepaw region of the ipsilesional somatosensory cortex (S1FL). These results suggested that there is high variability in the effects of MCAO on the injured hemisphere. Across all groups, Somatosensory evoked potential (SSEP) signals were consistent with the observed BOLD activity, suggesting preservation of neurovascular coupling. In contrast to previous studies, there was no contralesional somatosensory cortex activity in response to impaired forepaw stimulation. Lesion volume over time correlated with changes in BOLD and SSEP signals, with small subcortical lesions causing no significant deficit, and loss and recovery of the BOLD response correlating with size and recovery of the lesion. Thus, this tended to suggest three different severities of stroke as a consequence of the same MCAO procedure – minimal damage, severe damage with recovery and severe damage with no

recovery (Weber *et al.*, 2008). The group exhibiting complete loss of activity in the ipsilesional cortex contrasts with human studies, as impaired forepaw stimulation did not evoke contralesional activity, and there was no period of ipsilesional hyperactivity as observed in humans. The variability in lesion volume and outcome, despite all rats undergoing the same MCAO surgery, suggests an inherent problem associated with such experimental stroke models. Although attempts are being made to try and reduce the variability in outcome measures, such as lesion volume, associated with the MCAO model of experimental stroke (Trotman-Lucas *et al.*, 2017), this does emphasise the importance of performing longitudinal fMRI studies to account for within-group variability caused by the MCAO method, and minimising sources of variability in the imaging protocol.

A recent study compared fMRI with local field potential (LFP) responses, using continuous arterial spin labelling MRI to measure the CBF response to hypercapnia under propofol anaesthesia (Lake *et al.*, 2017a). While the CBF and LFP responses in this case were not directly compared, as forepaw stimulation was performed for LFP experiments while CBF responses were induced with hypercapnia, the two modalities did show changes in post-stroke activity resembling those observed in humans (Feydy *et al.*, 2002; Tecchio *et al.*, 2006; Lake *et al.*, 2017a). Resting perfusion in the ipsilesional hemisphere showed an initial increase, and returned to baseline at days post-stroke. Reactivity to hypercapnia in the ipsilesional hemisphere was raised at both time points. This was attributed to injury induced angiogenesis, triggered following ischemia, leading to a higher vascular density at seven days, with excess vessels pruned back in the following weeks (Hayward *et al.*, 2011). This supports fMRI data in humans showing increased neuronal recruitment followed by focusing of activity (Feydy *et al.*, 2002). As new pathways are recruited, additional blood flow is required to support the increased activity, and as these pathways become more efficient, less blood supply is needed (Arai *et al.*, 2009). LFP data showed altered organisation in the ipsilesional somatosensory cortex compared to the contralesional cortex. In the undamaged hemisphere, response amplitude to stimulation decreased with distance from Bregma, correlating with the responses mapped in the cortex of healthy rats (Hosp *et al.*, 2008). Following stroke, this correlation is lost, and as recovery progresses, the reverse is true, with peak responses observed at the furthest distance from Bregma (Lake *et al.*, 2017a). This supports the previous data shown in humans of reorganisation, where the peak activity detected is shifted compared to healthy controls as recovery progresses.

In recent years, resting-state fMRI has become a more common outcome measure in both clinical and preclinical research. The ability to examine connectivity between brain regions is

beneficial to the understanding of recovery following stroke, as supplementary regions compensate for ischemic tissue and alternative pathways are formed. Sources of variability related to an external stimulus, such as sensitisation of the paw from electrode placement, artefacts from the electrical current, or habituation in the brain to the stimulus paradigm, are also avoided. As with stimulus-based fMRI, there has been a mix of single time-point and longitudinal resting state fMRI studies performed (Van Meer *et al.*, 2010; 2012; Shim *et al.*, 2017). Results of RS-fMRI studies show more consistency than stimulus-based fMRI, and the progression of recovery in rodent RS-fMRI studies shows more features of the progression seen in humans. For example, increase in recruitment in early stages followed by focusing of activity as recovery progresses can be seen in one study of functional connectivity, in which connectivity between the somatosensory and motor cortices in the ipsilesional hemisphere is increased above baseline at 3 weeks, before returning to baseline at 10 weeks (Van Meer *et al.*, 2010). Other studies show a correlation between improved interhemispheric functional connectivity in the chronic phase and improved functional connectivity (Shim *et al.*, 2017; Van Meer *et al.*, 2012), and this is supported by a study treating experimental stroke with mesenchymal stem cells (MSCs), in which MSC treated groups show improved interhemispheric connectivity and behavioural outcome (Nagahama *et al.*, 2018). The high variability between studies, discrepancies between human and rodent studies, and differences between electrophysiological and imaging results, show that preclinical imaging protocols need to be refined for stroke studies. Longitudinal studies should reduce inter-subject variability and allow for progression of individual animals to be tracked, however they require an appropriate anaesthetic protocol for imaging. BOLD imaging supplemented with CBF imaging and functional MR spectroscopy may also help to address the differences between electrophysiology and fMRI results. Through improving on these aspects of the methodology, preclinical fMRI studies will be better able to determine the progression of post-stroke recovery in rats, and whether it shares similarities with recovery observed in humans. Use of an optimised anaesthesia protocol for BOLD fMRI, combined with additional spectroscopy and imaging methods to investigate metabolism and CBF, may give new insight into how recovery progresses in rodents, and the mechanisms underlying changes observed in the BOLD signal.

This study applies the propofol anaesthesia protocol and multi-parametric MRI protocol that is described in Chapters 2 and 3 to a rodent model of ischaemic stroke. Through use of these methods to quantify changes in BOLD activity, neurotransmitter turnover, CBF, and the addition of lesion volume measurement, this study aims to determine how activity in the somatosensory cortex, metabolism, and perfusion change as recovery progresses.

4.2. Methods

4.2.1. Animals

This study was conducted in accordance with the UK Animals (Scientific Procedures) Act, 1986, under project licence P7D063834 and following institutional ethical approval by the University of Leicester Animal and Welfare Ethical Review Body. 11 male Sprague-Dawley rats (supplied by Charles River Laboratories) aged 3 months were housed in standard cages and given daily access to a playpen to promote social and physical enrichment. After acclimatisation to the unit, animals underwent MRI scanning at least one week prior to undergoing experimental stroke by middle cerebral artery occlusion (MCAO). Animals underwent MCAO at 3-4 months old. Animals underwent MRI scanning at 2, 7, 14, 21 and 42 days post-MCAO.

4.2.2. MCAO surgery

Animals were anaesthetised with 5% isoflurane in 100% oxygen, and maintained on 3% isoflurane during surgery. Animal temperature was monitored by rectal probe and maintained at $37\pm 1^{\circ}\text{C}$ for the duration of surgery. An incision was made into the skin over the temporalis muscle and a Laser Doppler probe was inserted to monitor cerebral blood flow. A midline incision was made on the ventral surface of the neck, and the right common carotid arteries were isolated and ligated. The internal carotid artery was temporarily occluded using a microvascular clip. A nylon monofilament was inserted through an incision in the common carotid artery, and advanced approximately 10mm distal to the carotid bifurcation. Occlusion was confirmed through a drop in cerebral blood flow. The incision was sutured, animals were recovered from anaesthetic kept in recovery cages on a heated shelf at 28°C for 60 minutes. After 60 minutes, animals were re-anaesthetised and the filament was withdrawn up the common carotid artery to allow reperfusion to occur. For 72 hours after MCAO, animals were kept in the post-op room in recovery cages at 28°C . Animals were monitored for weight, behaviour, food intake and other signs of poor wellbeing twice daily for 72 hours post-MCAO. Food pellets were weighed and counted before being placed in the cage, and remaining pellets were weighed and counted again during the next check up to monitor intake. Animals were observed for coat condition, eye or nasal fluid discharge, vocalisation, hunching behaviour, and other signs of poor wellbeing in this time.

4.2.3. MRI anaesthesia protocol

Animals were initially anaesthetised with 3% isoflurane in 100% oxygen. Tail vein cannulation was performed before transferring the animals to the MRI bed. A bolus of 9mg/kg propofol was

administered over 1 minute using a syringe driver (Harvard Apparatus, Cambridge, Massachusetts, United States.) and the isoflurane was gradually reduced to 0%, with animals still breathing 100% oxygen. Respiration was monitored using a respiration pillow (Small Animal Instruments Inc. Stony Brook, New York, USA), temperature monitored using a rectal probe and maintained using a fan heater activated when measured temperature dropped below 37°C (Small Animal Instruments Inc. Stony Brook, New York, USA), and heart rate and blood oxygen saturation monitored using a pulse oximeter (Starr Life Sciences, Oakmont, Pennsylvania, USA). Copper electrodes were inserted subcutaneously into the dorsal surface of the right forepaw between digits 1-2 and 2-3 (Hyder *et al.*, 1994). 3 minutes after the bolus ended, a continuous infusion of propofol was given at 54mg/kg/hr until resting-state fMRI was complete. For the duration of the TOF angiography, T₂ weighted structural scan and ASL scan, animals were given 1.5% isoflurane in 100% oxygen. Following the scan, animals were allowed to recover in a separate cage. EMLA cream was applied to the forepaw where electrodes had been removed, and animals were provided with water and wet food pellets to prevent dehydration after anaesthesia. Animals were awake within 15 minutes of removal of anaesthetic, and moving normally within 30 minutes, at which point they were returned to their home cage.

4.2.4. MRI protocol

MRI scans were performed on a 9.4T Small Animal MRI scanner (Agilent Technologies), using a Rapid 72x2 RF volume transmit coil and surface receive coil (Rapid Biomedical). Coronal scout images were used to locate bregma, and three 1.5mm slices were selected with bregma in the middle slice. A shimming voxel with dimensions 10x9x4.5mm was positioned to cover the centre of all three slices, excluding non-brain tissue or tissue outside the slices of interest. FASTMAP was used to shim these slices to a 50% linewidth between 20-35Hz. Rats were switched from breathing oxygen to room air and fMRI was performed for 9 minutes using a rapid EPI sequence (TR=250ms, TE=22ms, K_{zero}=8, shots=2, data matrix =128x128). The forepaw was stimulated at 10mV, 10Hz, pulse width 1us, with a block design of 60s off, 30s on. Following this, a 4x4x4mm voxel was positioned over the left somatosensory cortex at bregma, and manual shimming was performed to a 50% linewidth of <25Hz. A LASER MR spectroscopy sequence (TR=2000ms, TE=14.54ms, 270 arrayed averages) was used to perform functional MRS over 9 minutes, using the same forepaw stimulation paradigm used for fMRI. For analysis, the first 30 seconds of each off block were discarded to allow time for metabolites to return to baseline levels. 6 Minutes of resting-state fMRI were performed (TR=1000ms, TE=22ms, shots=2, K_{zero}=16, data matrix=128x129, slices=22, slice width=1mm) for quantification of low-frequency fluctuations throughout the brain and analysis of functional connectivity. Animals were switched back to

100% oxygen after all functional scans were complete. Oxygen saturation was maintained above 80% throughout the time on room air (the safe limit defined by the Named Veterinary Surgeon). After being returned to 100% oxygen, a TOF angiography scan and a T₂ weighted structural scan were performed. Using the TOF angiography image, the carotid artery was located and a tagging slice placed with a gap of -17mm from Bregma. 6 minutes of Arterial spin labelling was performed on a single 1.5mm slice placed over Bregma (TI=1500ms, TR=2500ms, TE=10ms, shots=1, K_{zero}=16, data matrix=128x128).

4.2.5. Behavioural Assessment

Behaviour deficits caused by stroke were assessed using a 28 point neurological score system (Hunter *et al.*, 2000). Animals were assessed at 48 hours, and then at 1, 3 and 6 weeks following MCAO. Animals were placed in an empty cage and assessed for circling motion and exploration of the cage walls. Animals were then tested for grip strength when holding on to the edge of the cage while being gently lifted away from the edge, and ability to hang from or climb onto the edge of the cage. Response to tactile whisker stimulation was tested. Forepaw sensory ability was tested through holding the animal and gently moving them backwards along the edge of a table, and number of attempts to place the impaired forepaw was counted. Visual ability was tested through raising and lowering the animal near a table edge and observing how many times an animal reached for the ledge.

4.2.6. Data analysis

A standard fMRI analysis pipeline was performed using FSL (www.fmrib.ox.ac.uk/fsl). Motion correction (MCFLIRT), brain extraction (rBET), bias field correction (FAST) and independent component analysis for artefact removal (MELODIC) were performed prior to time-series analysis in FEAT to visualise the BOLD response.

Functional MRS spectra were separated into “off” and “on” blocks and averaged using the MATLAB script FID-A. The two spectra were analysed using TARQUIN (www.tarquin.sourceforge.net) to determine relative concentrations of glutamate. Off blocks were subtracted from on blocks to determine the difference in glutamate concentration, any negative results were removed as outliers, and difference in glutamate was averaged.

Control and Tag ASL images were first concatenated into a single image of two volumes. The Oxford ASL toolkit for FSL was used to subtract the tag image from the control image to create a difference image. Difference images were thresholded at 0 to remove negative voxels. FSLmaths was used to double the intensity of control images, and these images were used as

inputs in a modified Bloch equation (Williams *et al.*, 1992; Kelly *et al.*, 2010) in order to calculate CBF.

$$f = \frac{\lambda}{T_{1app}} - \frac{M_b^{ctrl} - M_b^{tag}}{2M_b^{ctrl}}$$

Where M_b^{ctrl} is the image intensity of the control image, and M_b^{tag} is the image intensity for labelled images. λ is the ration of water/g of brain tissue to water/g of blood. T_{1app} is the relaxation time that describes the exponential decrease in M_b . T_{1app} has previously been measured as 2s (ref), and λ has previously been calculated as 0.9 (ref), and these values are presumed to give the equation:

$$f = 0.45 - \frac{M_b^{ctrl} - M_b^{tag}}{2M_b^{ctrl}}$$

The value f is then converted into ml/g/min to give a CBF map. CBF map images were given an upper threshold of 5 to remove large outliers, and mean and standard deviation across the slice was calculated using FSLstats.

T_2 weighted images were analysed using the 3Dslicer software package. Areas of high intensity corresponding to lesions were identified and all voxels were highlighted. Lesion volume in mm³, maximum signal intensity and mean signal intensity were then calculated.

Statistical analysis was performed in Graphpad Prism (Version 7, www.graphpad.com). Data are shown as mean +/- standard deviation (SD). Changes over time were analysed using a repeated measures ANOVA, applying a mixed effects model to account for any missing data points, and the criterion for statistical significance was $P < 0.05$. Where statistically significant differences were found, post-hoc testing to compare individual time points was performed using the Tukey-Kramer multiple comparisons test.

4.3. Results

Due to surgical complications, one animal had to be humanely killed during surgery. One animal died within 48 hours of surgery. One animal developed a lesion covering the entire right hemisphere, and displayed severe behavioural impairment, and was euthanised after the 48 hour scan. All other animals displayed weight loss after MCAO surgery to a maximum of

25%, with animals regaining weight at different rates (Fig. 4.1). No animals displayed any adverse effects from the propofol anaesthetic protocol for MRI scanning.

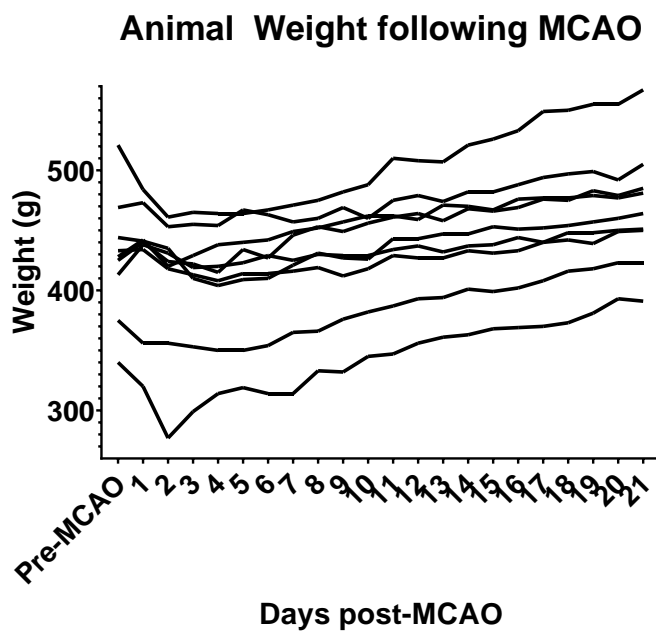


Fig. 4.1: Individual weights of animals prior to MCAO and for 3 weeks post-MCAO

4.3.1. Behavioural assessment

Behavioural assessment through a 28 point neurological score was taken at 2 days, 1 week, 3 weeks and 6 weeks post-MCAO (Fig. 4.2). Neurological score was shown to change significantly over time ($F(1.599, 11.73) = 12.71, P = 0.0018$). Post-hoc testing showed that there was a significant increase between 2 days and 1 week ($P = 0.0468$), 3 weeks ($P = 0.0126$) and 6 weeks ($P = 0.0153$). No significant differences were observed between other timepoints.

Neurological score following MCAO

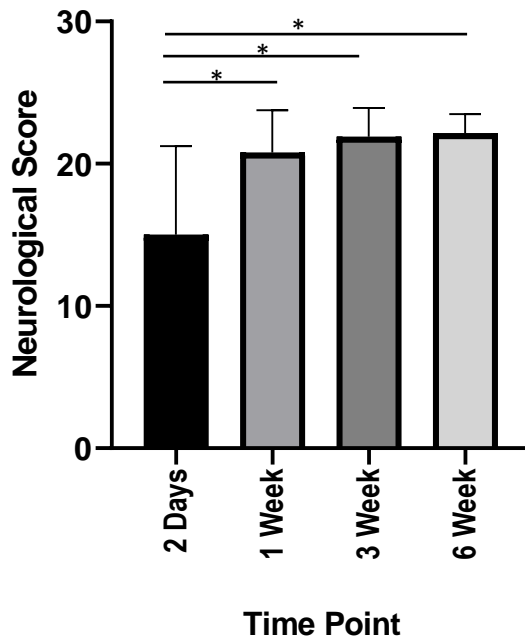


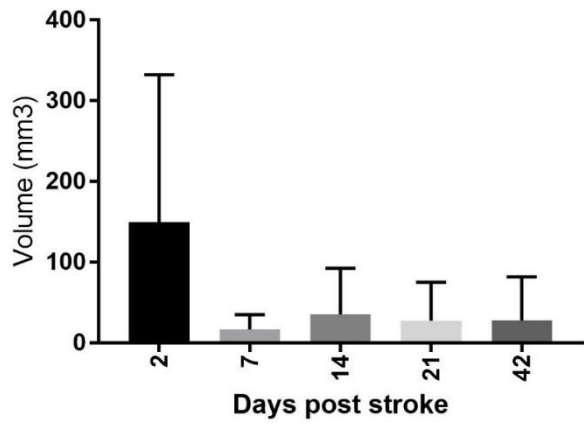
Fig 4.2: Mean neurological score at 2 days, 1 week, 3 weeks and 6 weeks post-MCAO.

Neurological score increased after 2 days (* indicates $P < 0.05$). Data is displayed as mean \pm SD, $n = 10, 10, 10,$ and 8 at 2 days, 1, 3, and 6 weeks, respectively.

4.3.2. Lesion Volume

Animals showed high variability in lesion volume and intensity. One animal displayed a lesion which injured the entire right hemisphere (582.324mm^3), while two animals exhibited lesions smaller than 20mm^3 at 48 hours post-stroke. All animals showed a decrease in lesion volume over time ($F(4,26) = 5.933, P = 0.0016$, Fig. 4.3), however the rate of change in lesion volume was variable. In four animals, lesion volume decreased to 0 at different time points, with one animal showing no lesion at 1 week onward, one animal at 3 weeks onwards, and two animals at 6 weeks.

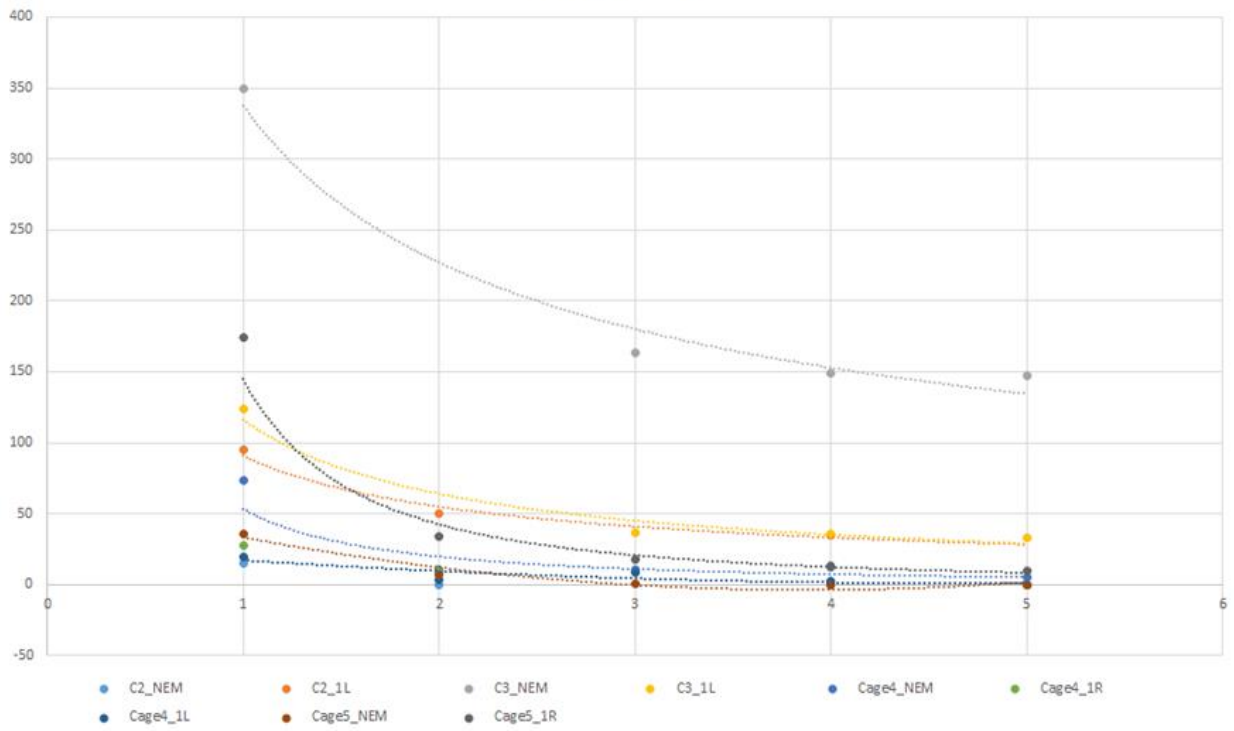
Lesion volume



A

B

Lesion volume over time



C

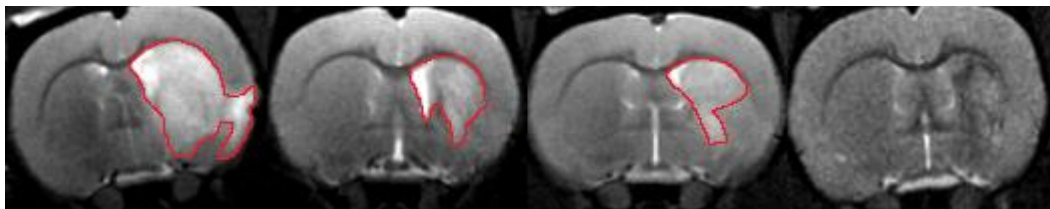


Fig. 4.3: (A) Mean lesion volume quantified by T₂ weighted structural imaging over time. Significant change over time was observed using repeated measures ANOVA, however no significant difference was found between individual time-points using post-hoc testing. Data is displayed as mean ± SD, n = 10, 7, 7, 9, and 7 at 2 days, 1 week, 2 weeks, 3 weeks and 6 weeks, respectively. (B) Change in lesion volume in each animal over time. (C) T₂ weighted images displaying lesion progression in an example animal, showing a large lesion at 2 days post-MCAO (left), which shrinks at 1 and 2 weeks post-MCAO (centre left and centre right), and no visible lesion at 3 weeks (right). Lesion is outlined in red

4.3.3 BOLD fMRI

In all but one animal, the BOLD response in the injured hemisphere to contralesional forepaw stimulation was completely eliminated 2 days post MCAO, before recovering at later time points in most animals. However, number of active voxels in S1FL was not found to be significantly different between pre-stroke and any post-stroke time points ($F(2.565, 10.26) = 0.2.186, P = 0.1558$, Fig. 4.4). The time at which the BOLD response returned in these animals varied between 1 week and 6 weeks (Table 4.2). Due to this variability in the rate of recovery, the time factor was removed and data was analysed to compare lesion volume with number of active voxels. Functional MRI scans were divided into bins according to their corresponding lesion volume, with bin sizes 0-20, 21-40 and >40, and compared with pre-stroke fMRI scans for number of active voxels. However, this also showed no significant difference in number of active voxels between pre-stroke animals or any post-stroke time point ($F(3, 33) = 0.6806, P = 0.3602$, fig. 4.5).

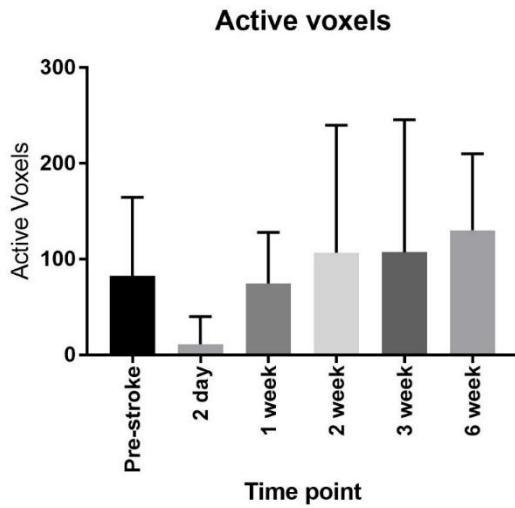


Fig. 4.4: Mean number of active voxels in response to forepaw stimulation in S1FL over time quantified with BOLD fMRI. Time points are displayed as pre-stroke or days/weeks post stroke. No significant change over time was found. Data is displayed as mean \pm SD, $n = 10, 7, 6, 6, 8,$ and 6 at pre-stroke, 2 day, 1, 2, 3 and 6 week time points, respectively.

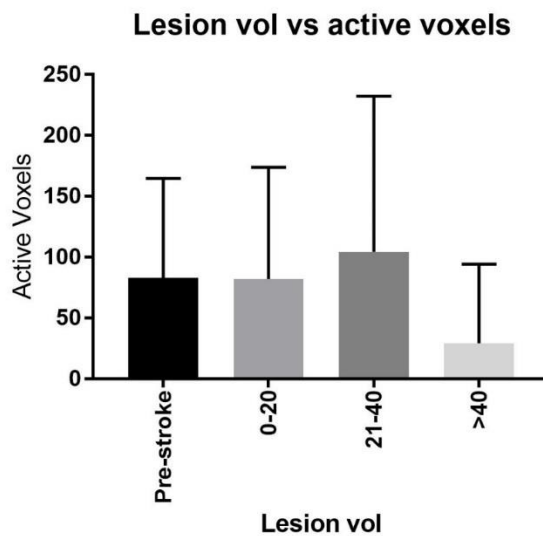


Fig. 4.5: Comparison of mean BOLD signal between pre-stroke animals, and post stroke scans at all time points grouped by lesion volume. No significant difference between groups was found. Data is displayed as mean \pm SD, $n = 10, 13, 8$ and $11,$ respectively.

Animal	First BOLD signal detection post-MCAO
C2_NEM	3 weeks
C2_1L	1 week
C3_NEM	6 weeks
C3_1L	2 weeks
Cage4_NEM	1 week
Cage4_1R	1 week
Cage4_1L	2 days
Cage5_NEM	None
Cage5_1R	1 week
Cage5_1L	None

Table 4.2: Time point at which first BOLD response was detected post-MCAO.

4.3.4. Functional MRS

Glutamate turnover showed no significant change at any time point ($F(1.393,6.6873) = 0.7613$, $P = 0.4574$, Fig. 4.6). Variability in this data was high, particularly at 2 days post-stroke, with a mean value of 266.2 AU and an SD of 651.1, and individual animals did not show a consistent increase in glutamate change as recovery progressed.

NAA levels also showed no significant change at any time point ($F(1.012, 4.860) = 1.004$, $P = 0.3649$, Fig. 4.7). Variability was high at 2 days post stroke, with a mean value of 155.9 AU and an SD of 380.7, due to one large outlier. No significant change was observed if this outlier was removed.

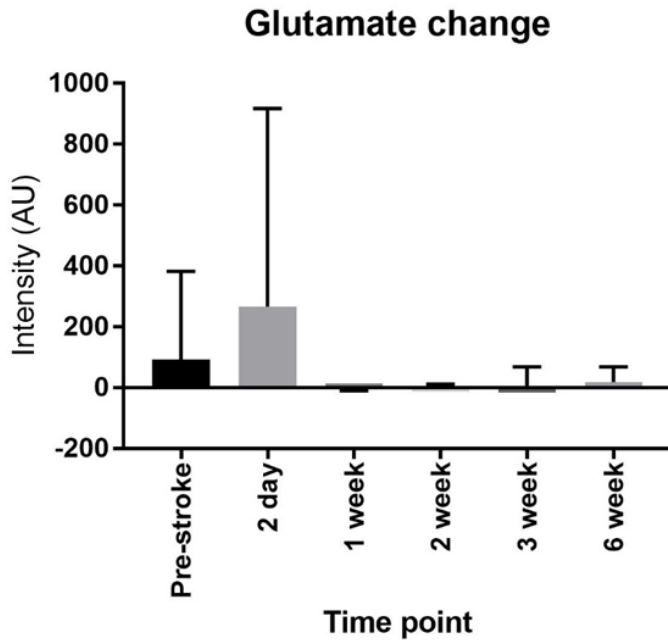


Fig. 4.6: Mean glutamate signal change in response to forepaw stimulation in S1FL over time quantified using LASER fMRS. Time points are displayed as pre-stroke or days/weeks post stroke. No significant change over time was found. Data is displayed as mean \pm SD, $n = 10, 6, 5, 5, 8$ and 5 , respectively.

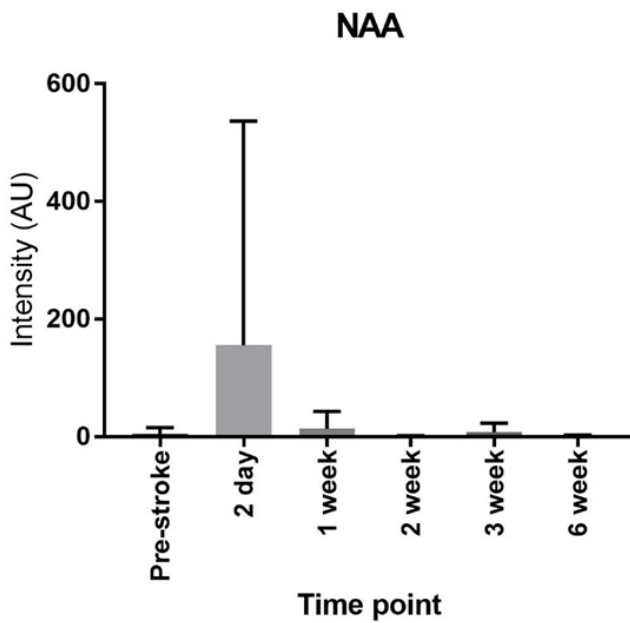


Fig. 4.7: Mean NAA signal in S1FL over time quantified using LASER MRS. Time points are displayed as pre-stroke or days/weeks post stroke. No significant change over time was found. Data is displayed as mean \pm SD, $n = 10, 6, 5, 5, 8$ and 5 , respectively.

4.3.5. Arterial spin labelling

Cerebral blood flow pre-stroke had a mean value of 2.03 ± 0.48 ml/g/min prior to stroke, and this did not change significantly over time following stroke ($F(1.592, 7.006) = 1.822$, $P = 0.2285$, Fig. 4.8).

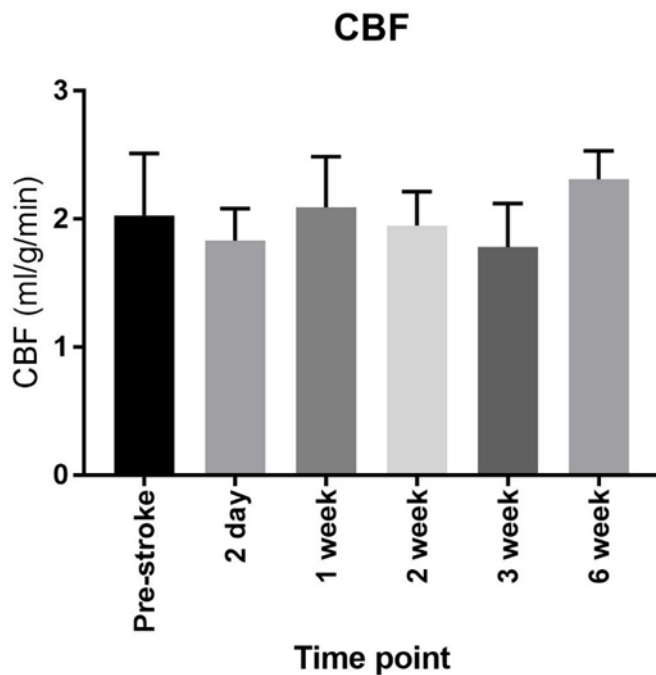


Fig. 4.8: Mean CBF at bregma over time. Time points are displayed as pre-stroke or days/weeks post stroke. No significant change over time was found. Data is displayed as mean \pm SD, $n = 10, 5, 5, 5, 7$ and 5 , respectively.

4.4. Discussion

This study uses the propofol anaesthesia protocol and longitudinal, multi-parametric fMRI to investigate changes in the rat brain for 6 weeks following experimental stroke. T_2 weighted scans showed that all animals displayed a stroke lesion, which recovered at a variable rate over time. Animals displayed a high variability in BOLD signal and glutamate turnover post-stroke. Due to this, no significant changes were found in these measures at any time point post-stroke. Comparison of lesion volume and BOLD signal also showed no significant difference between pre-stroke animals and any lesion volume group. A trend towards increased activation was observed in the $21\text{-}40\text{mm}^3$ group, however this was not significant, possibly due to the small number of animals. Individual animals did exhibit increased

activation when the BOLD signal was restored after the 48 hour time point, similar to that observed in humans (Feydy *et al.*, 2002), however due to the low animal numbers and high variability, this could not be shown within the group as a whole. Previous studies that did not use a longitudinal design showed similarly varied results (Dijkhuizen *et al.*, 2001; 2003; Sauter *et al.*, 2002). These studies used 10 animals per time point, however, from the data presented here, 10 animals is not sufficient to draw meaningful conclusions in this model.

4.4.1 Lesion Volume

Lesion volume was highly variable between animals, even at the first time point post stroke. Variability is expected with MCAO (Durukan and Tatlisumak, 2007; Weber *et al.*, 2008; Trotman-Lucas *et al.*, 2017), however this high variability does highlight the need for larger animal groups even in a longitudinal study. Many factors can affect variability in the MCAO model. Some of these factors can be easily controlled, such as occlusion time and filament size (Abraham *et al.*, 2002). Infarct size is also influenced by how far the filament is advanced. A significant increase in lesion volume is observed between groups of animals with the filament advanced 22mm beyond the CCA bifurcation, versus a group with an advancement of only 18mm (Zarow *et al.*, 1997), suggesting that some variability within a group can be due to small differences in filament placement. Variation in the animals' cerebral vasculature is another potential source of variability, as human studies have shown that patients with a higher number of collateral arteries supplying the circle of Willis develop less severe lesions (Alastruey *et al.*, 2007; Zhou *et al.*, 2016), however this has not yet been studied in rats.

When plotted individually, lesion volume for all animals shrank exponentially, with a highly variable rate, however as a group average there was no significant difference in lesion volume between 1 week post-stroke and later time points. Lesion volumes could be broadly split into three groups, 0-20, 21-40 and >40mm³ (Weber *et al.*, 2008), which was used for analysis comparing lesion volume with BOLD signal, however this type of analysis requires larger groups to determine changes based on lesion volume.

4.4.2 BOLD fMRI

While BOLD signal change following stroke was not significantly different from baseline, this can be attributed to the high variability between animals. Previous studies have shown that BOLD responses following stroke can range from no significant impairment to complete loss of response (Weber *et al.*, 2008). Our data showed a similar range of BOLD responses. One animal did not exhibit impairment to the BOLD signal even at 48 hours post-stroke, one animal

showed no BOLD response until 6 weeks post-stroke, one animal showed no BOLD response until 3 weeks post stroke, and one animal showed a BOLD response at 1 week post stroke, but not at any subsequent time point. However, the number of animals in this study was too small to divide into groups as with previous studies.

Our previous data in healthy ageing animals (Chapter 3) show that the anaesthesia and fMRI protocol gives a highly reproducible BOLD signal. Here, our data shows that, despite using a reproducible longitudinal fMRI method, there was still high variability in recovery between post-stroke rats. Thus, because of such high variability in the stroke model, previous studies using multiple groups (Dijkhuizen *et al.*, 2001; 2003) or a less reproducible anaesthesia protocol (Kim *et al.*, 2005; 2007) may introduce additional confounding factors to the results. Comparison of pre-stroke s1FL activation with 1st post-stroke activation and 2nd post stroke activation showed a trend towards hyperactivation (max. BOLD signal changes: 5.097% pre-stroke, 8.57% post-stroke), however due to the low number of animals this was not statistically significant. Combination of this minimally invasive anaesthesia protocol and factoring in change in lesion volume over time into analysis may help minimise variability in the stroke model, and allow progression of stroke recovery to be studied using fewer animals than previous stroke studies.

4.4.3 Functional MRS

Functional MRS was also not conclusive in this study. No significant change was observed in glutamate change following stroke or during recovery. Individual animals did not show a clear progression, nor was there any correlation between lesion volume and glutamate change.

The animal which displayed the largest lesion at 2 days post-stroke, covering the entire right hemisphere, also displayed the largest glutamate change, and the largest glutamate signal during “off” blocks. A possible explanation of this is as a result of spreading depolarisation and excitotoxicity. In stroke, particularly in cases where the blood brain barrier is disrupted and oedema is present, disrupted ion homeostasis prevents activity of sodium-potassium pumps and the maintenance of resting membrane potential (Dreier, 2011). This can lead to hyperexcitability that, combined with glutamate release, can lead to a cascade of excitatory potentials that spread throughout the injured region, with disruption to inhibitory mechanisms that would ordinarily restore resting membrane potential and prevent further glutamate release (Shin *et al.*, 2006; Kramer *et al.*, 2016). The size of the lesion in this animal suggests complete loss of both perfusion and the neurovascular response. The forepaw stimuli during the BOLD fMRI and fMRS scans trigger glutamate release without hyperaemia and

increased oxygen delivery. Increased acidity from lactate production exacerbates the disrupted ion homeostasis, as does lack of energy to drive sodium/potassium pumps, together making a cascade of spreading depolarisations more likely (Zhou *et al.*, 2010; Kramer *et al.*, 2016). The other animals showed either a low positive glutamate change, or in most cases, a negative glutamate change. In all but one animal, no BOLD signal was observed at 2 days post-stroke. In these animals, it is possible that ischaemia caused impairment of neuronal activity during the acute stage. However, it is also possible that neurovascular coupling was disrupted, but neuronal activity was still present. In which case, the negative glutamate change would represent disruption to glutamate recycling mechanisms. To further understand this, studies combining BOLD fMRI, metabolic analysis and electrophysiology would be required.

4.4.4 Arterial spin labelling

Arterial spin labelling showed no significant change in CBF across all time points. This finding was unexpected, as some studies show that the stroke lesion is characterised by severe hypoperfusion, particularly in the lesioned hemisphere (Richardson *et al.*, 2011). However, some rodent studies have shown the opposite, with one study showing CBF in both hemispheres increased compared to sham animals from one day post-stroke, remaining high for two weeks (Lin *et al.*, 2002). No correlation was observed between lesion volume and CBF following stroke, and some animals showed a lower CBF at later time points as lesion volume decreased. Some studies have suggested that a higher vascular density, and so higher CBF, pre-stroke may reduce infarct volume, however comparison between pre-stroke CBF and lesion volume at 2 days showed no correlation

4.4.5 Conclusions

While this study did allow post-stroke animals to undergo repeated fMRI scanning with no harmful effects, the variability observed in the results of all MRI sequences used prevented meaningful conclusions from being drawn. A previous study has shown that it is possible to broadly categorise post-stroke animals into three groups, mild, moderate and severe, based upon lesion volume (Weber *et al.*, 2008). These three groups of animals each shows a different progression of recovery. Power calculations may factor in this categorisation of lesion severity, allowing functional recovery to be analysed based on both lesion volume and time post-stroke. In this study, individual animals recovered at different rates, contributing to the high variability and confounding analysis based solely on time. When data from this study was grouped based on lesion volume, split into three groups as per Weber *et al.*, and groups chosen based on the range of the data, significant differences in functional or vascular

measures were still not seen, due to the small group sizes. While use of longitudinal methods is intended to reduce the number of animals required, this study suggests that a larger cohort is needed in order to account for the high variability in ischaemic stroke.

In order to reduce animal numbers, methods to reduce or account for the variability observed in lesion volume will be needed. If the factors determining the severity of an individual animal's lesion can be identified, animals can be screened for expected lesion severity prior to experimental stroke. Human studies suggest that collateral flow surrounding the middle cerebral artery is a determinant of stroke severity. More collateral arteries supplying the regions surrounding the MCA allow tissue to receive oxygen in the event of an occlusion, increasing the likelihood that tissue within the lesion penumbra can be recovered (Hoksbergen *et al.*, 2003). MR angiography studies have imaged collateral vessels in stroke patients, showing a larger number of collateral arteries in patients with less severe strokes (Alastruey *et al.*, 2007; Zhou *et al.*, 2016). In rodents, studies using Laser Doppler perfusion monitoring and histological analysis of lesion volume showed an inverse relationship between local CBF and lesion volume at 24 hours (Riva *et al.*, 2012; Beretta *et al.*, 2015). It has also been shown that perfusion imaging during MCAO can be used as a predictor of lesion severity, and separate animals into groups accordingly (Cuccione *et al.*, 2017). Further stroke studies in rodents may make use of high resolution MRA scans prior to MCAO, allowing animals to be divided by prospective stroke severity prior to surgery. This will allow for variability to be better controlled, the influence of lesion volume to be better accounted for, and reduce animal numbers. If numbers required for each group are calculated prior to the beginning of the study, excessive animals that fit into each group can be discounted before unnecessary surgery is performed.

Additionally, refinements to the MCAO surgery method can also reduce variability. Studies in mice have shown that refining the MCAO method to repair the external carotid artery and so allow reperfusion directly through the MCA, rather than rely solely on reperfusion through collateral flow, greatly reduce variability between subjects (Trotman-Lucas *et al.*, 2017). Combination of this improved MCAO method with pre-stroke angiography imaging may allow for lesion volume to be controlled, and study of the effects of varying lesion size to be performed.

Through refining the preclinical model of stroke, rodent experimental stroke can be made to better match the presentation and progression of human ischaemic stroke. Individual animals in this study did display hyperactivation during recovery. Human studies have shown that, as

the damaged region recovers following ischaemia, functional recovery relies on the disinhibition of previously redundant connections, followed by reinforcing these new pathways in a similar manner to learning in the healthy brain (Manganotti *et al.* 2002). During this process, hyperactivation in the region of interest is observed after the initial restoration of activity, representing the larger number of synapses required to process the task or stimulus (Tombari *et al.*, 2004). As these pathways learn the function of the lost pathways, the level of activity decreases back towards baseline. This is known as the “recruitment and focusing” model (Feydy *et al.*, 2002). In previous rodent studies, this progression has not previously been observed, instead seeing an initial drop in activity with a slow increase approaching baseline activity. This altered pattern of activity can be down to high variability in non-longitudinal studies (Dijkhuizen *et al.*, 2001;2003; Sauter *et al.*, 2002), or the effect of isofluane on the BOLD signal in longitudinal studies (Van Meer *et al.*, 2010; 2012). In this study, while the group did not show a significant change as a whole, individual animals did show the recruitment and focusing pattern. This suggests that, in a larger cohort, separated by stroke severity, observing the recruitment and focusing pattern seen in humans may be possible through this method.

The addition of functional spectroscopy, with the aim of quantifying glutamate turnover as a measure of neuronal activity separate from the BOLD signal, further confounded analysis due to the highest signal being observed in the animal with the largest stroke lesion. This may be caused by poor SNR, exacerbated by strong water signal due to oedema, or by a large increase in glutamate due to spreading depolarisation and excitotoxicity. Further study using longer MRS scan times or alternative MRS sequences will be required to understand how glutamate activity changes post-stroke, and any significance this measure may have in recovery.

Neurological scoring in this cohort could only confirm that animals’ sensorimotor abilities improved between 2 days and 1 week. If animals were grouped by stroke severity, progression may be altered depending on severity of lesion. Additionally, while this neurological scoring gives a simple measure of overall impairment, to truly link behaviour to lesion volume or fMRI, a more in-depth series of behavioural tests will be required.

This study demonstrates that 10 animals is not sufficient to determine a significant effect of stroke on BOLD signal. For a future study, a larger group is required. To calculate a more appropriate group size, certain assumptions must be made. An effect size for post-stroke hyperactivation can be estimated at 30% (Ward *et al.*, 2004). Due to the effect of lesion volume previously described (Weber *et al.*, 2008), a high standard deviation value must be

estimated. Using a mean change of 30%, SD of 40% of the mean, aiming for 5% significance with 5 comparisons (Pre-stroke vs 5 post stroke time points), an n of 42 is required to achieve significance. If methods of controlling lesion volume can be developed, through predicting lesion volume based on CBF and cerebrovascular anatomy, or through further refinements to the MCAO method, future studies can then estimate effect size and standard deviation for a set stroke severity, and reduce animal numbers accordingly.

While this study did not give conclusive results, it did show that current models of stroke are highly variable even when using an anaesthetic and MRI protocol previously shown to give highly reproducible results in a healthy model (Chapter 3). This suggests that, when using previous anaesthesia protocols not optimised for longitudinal fMRI, variability is high enough that conclusions drawn may not truly represent changes in the rat brain following stroke. Through the refinements used in this study, with further refinements as suggested to reduce variability and better account for lesion severity, studies of functional recovery following stroke can be refined to better represent stroke as seen in humans, with the end goal of developing an animal model suitable for the testing of therapeutics.

Chapter 5: Longitudinal functional MRI imaging changes in the BOLD response of Spontaneously Hypertensive Rats

5.1. Introduction

In recent decades, evidence has shown a role for the vascular system in age-related cognitive decline, and age-related neurodegeneration (Cooper *et al.*, 2016). Hypertension is now widely accepted as a risk factor for cognitive decline and neurodegenerative disease (Iadecola and Gottesman, 2019). Functional MRI studies in humans have shown impaired CBF and diminished BOLD response in a number of brain regions in hypertensive subjects, as well as disruption to functional connectivity (Jennings *et al.*, 1998). The mechanisms behind these changes in neurovascular coupling are currently unclear. Examining fMRI in a rodent model of hypertension (Doggrell and Brown, 1998) may reveal how vascular changes correlate with changes in neuronal activity as hypertension progresses.

As evidence for a vascular component to many neurodegenerative disease was discovered, hypertension patients were also observed to have an increased risk of developing neurodegeneration (Iadecola *et al.*, 2019). Chronic hypertension has been shown to correlate with mild cognitive impairment. Adaptive responses to acute hypertension, which are protective in the short term, cause impairments in functional hyperaemia in the long term, leading to hypoxia in neurons, contributing to factors such as oxidative damage (Thorin-Trescases *et al.*, 2018).

Arterioles and capillaries exhibit adaptation to acute hypertension shortly after onset, and these adaptations are thought to maintain cerebral autoregulation and be neuroprotective in the short term. The initial phase of remodelling, eutrophic remodelling, is thought to improve the vessel wall's resistance to stress and reduce CBF to healthy levels for short periods of time (Heagerty *et al.*, 1993). This phase does not include an increase in the mass of smooth muscle or pericytes, and is reversible if hypertension is resolved. In chronic hypertension, permanent changes occur due to hypertrophic remodelling, in which smooth muscle and pericytes grow thicker due to collagen deposition. While this prevents damage from increased stress, and reduces CBF, this increased thickness reduces vascular reactivity and functional hyperaemia, as well as BBB permeability (Schriffin 2012).

5.1.1 Functional imaging in hypertension

Studies using PET imaging hypothesised that findings of thicker vascular walls and narrowing of the lumen (Jiang *et al.*, 1992; Hadju *et al.*, 1993) in cerebral vessels would be reflected in a

reduced rCBF response to a cognitive task. In regions primarily associated with the cognitive task, rCBF response was reduced in hypertensives compared to controls, with the deficit increasing in response to increased task difficulty (Jennings et al., 1998), and a reduction in resting state functional connectivity was also observed in these regions (Mentis et al., 1994). Brain activity was also shown to be less lateralised in hypertensive subjects, with activity in the left hemisphere observed in hypertensives that was not observed in controls. This correlated with a later model of healthy ageing, in which a reduced rCBF response in cognitive regions with age is compensated for by reduced lateralisation as activity is distributed to supplementary regions (Jennings et al., 1998; Cabeza et al., 2002; Berlingeri et al., 2013). Subsequent studies supported this, consistently showing reduced rCBF responses and functional connectivity in cognitive regions, even in patients showing normal cognitive performance or with treated hypertension (Jennings et al., 2005; Dai et al., 2007; Beason-Held et al., 2007; Li et al., 2015).

More recently, studies into the effects of hypertension on the brain have found that measures of brain function can also be predictive of the effectiveness of blood pressure treatment (Jennings et al., 2008; Jennings et al., 2017). Structural and functional indices of brain ageing in hypertensive patients were found to correlate strongly with responses to treatment over two years, with patients exhibiting higher brain atrophy and greater CBF impairment being less responsive to treatment (Jennings et al., 2008). Performance in cognitive tasks was also found to predict response to treatment (Jennings et al., 2017). Taken together, this suggests that the interplay between vascular and cognitive function in hypertension, and the influence on the development of dementia, is more complex than originally thought, possibly involving feedback mechanisms originating in the brain.

In fMRI studies, hypertension has been shown to affect task-related BOLD response, and genetic risk of hypertension has an impact on the BOLD response even before onset. One study of normotensive patients with family history of hypertension showed a significant decrease in BOLD signal intensity in three cognitive regions during a visuospatial task, compared to controls with no history of hypertension (Haley *et al.*, 2008). However, another study showed increased BOLD signal in middle-aged hypertensive patients in multiple regions during a cognitive task, and recruited additional cortical regions not observed in controls (Naumczyk *et al.*, 2017). However, brainstem activity in simple motor tasks shows a significant negative correlation with blood pressure (Coulson *et al.*, 2015). This suggests that there are multiple compensatory and pathological changes as hypertension progresses, making it clear

that a preclinical model of progressive hypertension is required to understand how neurovascular activity changes over time.

Other MRI outcome measures have also been shown to be affected by hypertension. Analysis of functional connectivity also gave mixed results, showing reduced functional connectivity between the right inferior parietal lobe, left precuneus, and left angular regions of the left frontoparietal network, but increased functional connectivity between the left inferior parietal lobe and left triangle inferior frontal gyrus areas of this network (Li *et al.*, 2015). These changes correlated with impaired performance in verbal cognitive tasks. This suggests a combination of pathological and compensatory changes even in the same cohort as hypertension progresses. This is also supported by CBF imaging, showing impaired CBF in the right cortex, with compensatory increases in CBF in the left cortex (Jennings *et al.*, 1998). Cerebral glucose uptake is also impaired in cognitive regions (Fujishima *et al.*, 1995). To fully understand how these changes occur as hypertension develops, a longitudinal preclinical imaging model would be beneficial.

While functional imaging is becoming increasingly common in clinical research into hypertension, rodent studies still mostly focus on either behavioural measures or more invasive methods. These studies have provided insights into changes in vascular properties with hypertension, as well as the neuronal and glial mechanisms influenced as hypertension progresses (Razaida *et al.*, 1990; Tang *et al.*, 1993; Chi *et al.*, 1997; Tomassoni *et al.*, 2004a; b; Liu *et al.*, 2015). Microstructural and electrophysiological studies of the spontaneously hypertensive rat (SHR) cortex also support findings in human imaging of long term remodelling of the brain in hypertension that mimics the ageing brain. However, functional imaging studies in hypertensive rodents are still quite rare, with those that do exist either focusing on transient hypertension, or focusing on a single time point after the onset of hypertension (Wang *et al.*, 2006; Reimann *et al.*, 2018; Chen *et al.*, 2017). SHRs have been shown to exhibit disrupted functional connectivity in the hippocampus compared to Wistar Kyoto controls (Chen *et al.*, 2017), similar to disrupted FC in humans with hypertension (Jennings *et al.*, 2008, Dai *et al.*, 2007). This disrupted connectivity in SHRs was found to be reversible with taurine (Chen *et al.*, 2017). Taken together with human studies showing that changes in the brain are not reversed when BP is treated, this suggests long term changes at the neuronal level that are still not yet understood.

5.1.2. Spontaneously Hypertensive Rats

Spontaneously hypertensive rats (SHRs) are a strain bred from Wistar Kyoto rats to select for high blood pressure. These animals are normotensive for the first 6-8 weeks of life, with systolic BP between 100-120mmHg, and develop hypertension between 2 months and 5 months, reaching blood pressures of 160mmHg in females and 180mmHg in males when measured by tail cuff (Adams and Korner, 1989). Telemetry measurements show higher readings, 200mmHg in females and 250mmHg in males (Davidson *et al.*, 1995). The life span of SHRs is between 1.5-2 years, with one study of a group of 49 SHRs showing 90% survival rate at 12 months old, compared to 100% survival of Wistar Kyotos (Mori *et al.*, 1995).

Hypertension plateaus at 6 months, and the survival rate at this time is approx. 98%, dropping to 96% at 8 months. This strain is a suitable model for the development of hypertension, as the gradual onset of hypertension without the requirement of any invasive procedures, and the well documented blood pressure range over time, limit any external sources of variation.

In this study, an MRI protocol investigating the BOLD signal, resting CBF, changes in metabolite and neurotransmitter levels, and functional connectivity will be used to study SHRs from 2 months old (normotensive) to 6 months old (chronic hypertension). Through this protocol, changes to neuronal and vascular activity as hypertension progresses can be investigated.

5.2. Methods

5.2.1 Animals

This study was conducted in accordance with the UK Animals (Scientific Procedures) Act, 1986 under project licence P7D063834 and following ethical approval by the University of Leicester Animal and Welfare Ethical Review Body. All experiments are reported in accordance with the Animal research reporting of in vivo experiments (ARRIVE) guidelines (Kilkenny *et al.*, 2010). A total of 8 female Spontaneously Hypertensive Rats (Envigo, Shardlow, Derbyshire, UK) aged 3 weeks on arrival were housed in standard cages in groups of 4. Animals were given daily access to a playpen for 2-6 hours. After one week of acclimatisation to the animal unit, animals underwent two weeks of acclimatisation to blood pressure monitoring equipment, and blood pressure was taken weekly from 5 weeks onwards.

5.2.2 Experimental schedule

After a week's acclimatisation to the animal unit, animals were acclimatised to the playpen in groups of 4 over two days, before putting the entire cohort into one playpen from day 3 onwards. For one week, animals were acclimatised to the blood pressure monitoring equipment, first by acclimatising them to the tube, followed by the nose cone, followed by tube,

nose cone and tail cuff. Blood pressure was then taken weekly for the duration of the study. Animals were weighed prior to all MRI scans. The first MRI scan was performed between 6 weeks and 2 months of age, prior to the onset of hypertension, and subsequent scans were performed at 4 months and 6 months of age. Immediately following the final scan, animals were humanely killed using intraperitoneal pentobarbitone, and transcardially perfused with formaldehyde.

5.2.3. Blood pressure monitoring

Blood pressure was taken using a Kent Scientific Coda 4.1 BP monitoring system (Kent Scientific Corporation, Torrington, CT, United States). Animals were trained to enter a plastic tube, after which they were sealed in with a nose cone at one end and cover with a tail hole at the other. The nose cone was adjusted to prevent the rat turning round but not to cause discomfort. Two cuffs were placed over the tail, the occlusion cuff at the base and the detection cuff at the tip. 15 averages were taken, with the first 5 discarded as acclimatisation to the system, and any averages with motion artefacts discarded. Systolic, Diastolic and pulse pressure were averaged each month and compared using a repeated measures Anova.

5.2.4. Anaesthesia protocol

Animals were initially anaesthetised with isoflurane (5% induction, 2-3% maintenance) in 100% oxygen. Tail vein cannulation was performed before transferring the animals to the MRI bed. A bolus of 9mg/kg propofol was administered over 1 minute using a syringe driver (Harvard Apparatus, Cambridge, Massachusetts, United States.) and the isoflurane was gradually reduced to 0%, with animals still breathing 100% oxygen. Respiration was monitored using a respiration pillow (Small Animal Instruments Inc. Stony Brook, New York, USA), temperature monitored using a rectal probe and maintained using a fan heater activated when measured temperature dropped below 37°C (Small Animal Instruments Inc. Stony Brook, New York, USA), and heart rate and blood oxygen saturation monitored using a pulse oximeter (Starr Life Sciences, Oakmont, Pennsylvania, USA). Copper electrodes were inserted subcutaneously into the dorsal surface of the right forepaw between digits 1-2 and 2-3 (Hyder *et al.*, 1994). 3 minutes after the bolus ended, a continuous infusion of propofol was given at 54mg/kg/hr until resting-state fMRI was complete. For the duration of the TOF angiography, T₂ weighted structural scan and ASL scan, animals were given 1.5% isoflurane in 100% oxygen. Following the scan, animals were allowed to recover in a separate cage. Analgesic cream (EMLA, AstraZeneca, UK) was applied to the forepaw where electrodes had been removed, and animals were provided with water and wet food pellets to prevent dehydration after anaesthesia. Animals were awake

within 15 minutes of removal of anaesthetic, and moving normally within 30 minutes, at which point they were returned to their home cage.

5.2.5. MRI protocol

MRI scans were performed on a 9.4T Small Animal MRI scanner (Agilent Technologies, Santa Clara, CA, United States), using a RF volume transmit coil and a 2-channel surface receive coil (Rapid Biomedical, Rimpar, Germany). Coronal scout images were used to locate bregma, and three 1.5mm slices were selected with bregma in the middle slice. A shimming voxel with dimensions 10x9x4.5mm was positioned to cover the centre of all three slices, excluding non-brain tissue or tissue outside the slices of interest. FASTMAP (fast, automatic shimming technique by mapping along projections, Gruettter, 1992) was used to shim these slices to a 50% linewidth between 20-35Hz. Rats were switched from breathing oxygen to room air, pumped at 2L/min using an air pump (Clarke Wiz-Air, Clarke Tools, Dunstable, Bedfordshire, UK). Functional MRI was performed for 9 minutes using a gradient echo EPI sequence (TR=250ms, TE=22ms, $K_{zero}=8$, shots=2, data matrix =128x128). The forepaw was stimulated at 10mV, 10Hz, pulse width 1us, with a block design of 60s off, 30s on. Following this, a 4x4x4mm voxel was positioned over the left somatosensory cortex at bregma, and manual shimming was performed to a 50% linewidth of <25Hz. A LASER (Slotboom *et al.*, 1991) MR spectroscopy sequence (TR=2000ms, TE=14.54ms, 270 arrayed averages) was used to perform functional MRS over 18 minutes, using the same forepaw stimulation paradigm used for fMRI. For analysis, the first 30 seconds of each off block were discarded to allow time for metabolites to return to baseline levels. Animals were switched back to 100% oxygen after all functional scans were complete. Oxygen saturation was maintained above 80% throughout the time on room air (Tremoleda *et al.*, 2012). After being returned to 100% oxygen, a time-of-flight angiography scan and a T₂ weighted structural scan were performed. Using the TOF angiography image, the carotid artery was located and a tagging slice placed with a gap of -17mm from bregma. 6 minutes of continuous arterial spin labelling (CASL) was performed on a single 1.5mm slice placed over bregma (TI=1500ms, TR=2500ms, TE=10ms, shots=1, $K_{zero}=16$, data matrix=128x128).

5.2.6. Data analysis

A fMRI analysis pipeline was developed using FSL (www.fmrib.ox.ac.uk/fsl, Smith *et al.*, 2001). MCFLIRT (Jenkinson *et al.*, 2002), rBET (Wood *et al.*, 2013), and FAST (Zhang *et al.*, 2001) were used for motion correction, brain extraction and bias field correction respectively. Independent component analysis for artefact removal, using MELODIC (Beckmann and Smith, 2004) were

performed prior to time-series analysis in FEAT (Woolrich, 2001) to visualise the BOLD response. Cluster analysis was performed on the first-level FEAT outputs to determine number of active voxels, maximum % signal change within the cluster, and mean % signal change across the cluster.

Functional MRS spectra were separated into “off” and “on” blocks and averaged using the MATLAB FID-A toolkit (Simpson et al., 2017). The two spectra were analysed using the TARQUIN MRS analysis package (www.tarquin.sourceforge.net) to determine relative concentrations of glutamate. Metabolite concentrations from “off” blocks were subtracted from “on” blocks to determine the difference in glutamate concentration, and difference in glutamate change (ΔGlu) was averaged across subjects. “Off” blocks were also used to quantify NAA and Inositol, used as markers of neuronal viability and inflammation, respectively.

Control and tag ASL images were first concatenated into a single image of two volumes. The Oxford ASL toolkit for FSL was used to subtract the tag image from the control image to create a difference image. FSLmaths was used to apply a modified Bloch equation (Williams et al., 1992) to the data in order to quantify CBF in absolute units.

CBF map images were given an upper threshold of 5 to remove large outliers. This was determined based on the histogram of voxel intensities, in which some scans displayed a small number of single voxels with large intensities between 5 and 80 having a large influence on the mean. Non-zero mean and standard deviation CBF were calculated using FSLstats.

Statistical analysis was performed in Graphpad Prism (Version 7, www.graphpad.com). Data are shown as mean +/- standard deviation (SD). Changes over time were analysed using a repeated measures ANOVA, with a mixed effects model applied to account for any missing data points, and the criterion for statistical significance was $P < 0.05$. Where statistically significant differences were found, post-hoc testing to compare individual time points was performed using the Tukey-Kramer multiple comparisons test.

5.3. Results

5.3.1. Blood pressure and body weight

Animals showed a consistent increase in systolic ($F(2,452) = 8.822$, $P < 0.0001$) and diastolic ($F(2,452) = 9.82$, $P < 0.0001$) blood pressure over the duration of the study (Fig. 5.1). Systolic BP increased 28% between 2-4 months ($P < 0.0001$), and increased 11% between 4-6 months ($P < 0.0001$). Diastolic BP increased 22% between 2-4 months ($P < 0.0001$), and increased 27% between 4-6 months ($P < 0.0001$). Pulse pressure changed significantly over time ($F(2, 452) =$

12.8, $P < 0.0001$), increasing by 61% between 2-4 months ($P < 0.0001$), and decreasing by 49% between 4-6 months ($P < 0.0001$). Animals' weight increased over time in line with their expected development.

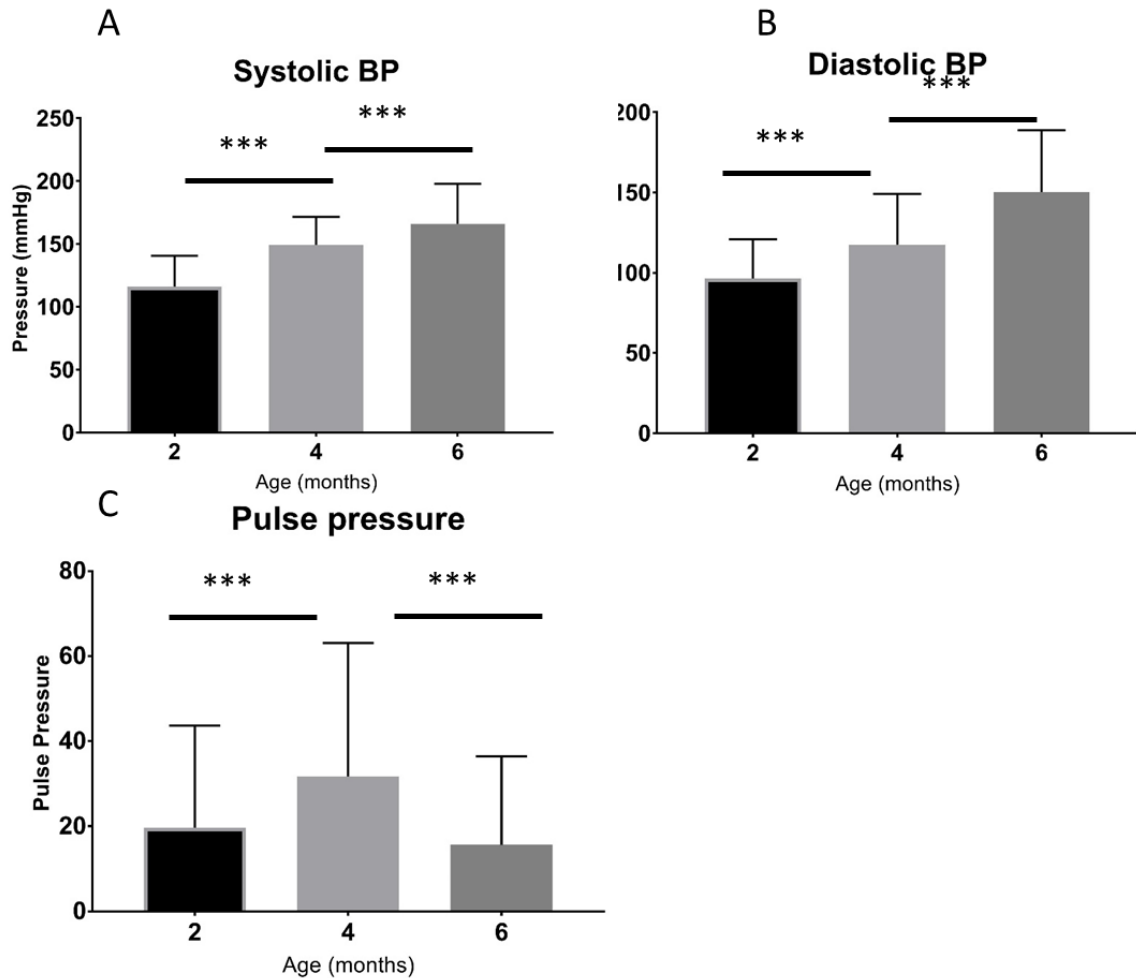


Fig. 5.1. Average rat systolic blood pressure (A), diastolic blood pressure (B), and pulse pressure (C) over time. Systolic and diastolic blood pressure both significantly increase at both time points ($***P < 0.001$). Pulse pressure significantly increased between 2 and 4 months ($***P < 0.001$) and significantly decreased between 4 and 6 months ($***P < 0.001$). Data is displayed as mean \pm SD, $n = 8$.

5.3.2. BOLD fMRI

First-level analysis of BOLD fMRI data was performed using FEAT was used to quantify three aspects of the BOLD signal: number of active voxels in S1FL, maximum % signal change in S1FL, and mean % signal change in S1FL (Fig. 5.2).

The number of active voxels in S1FL significantly decreased over time ($F(2, 16) = 4.834$, $P = 0.0228$, Fig. 5.3) with post-hoc testing showing a significant decrease between 4 and 6 months from 71 ± 32 voxels to 29 ± 26 voxels ($P = 0.0254$). Maximum and mean % BOLD signal change showed no significant change over time (Max $F(2, 16) = 2.139$, $P = 0.1502$. Mean $F(2, 16) = 2.827$, $P = 0.0888$).

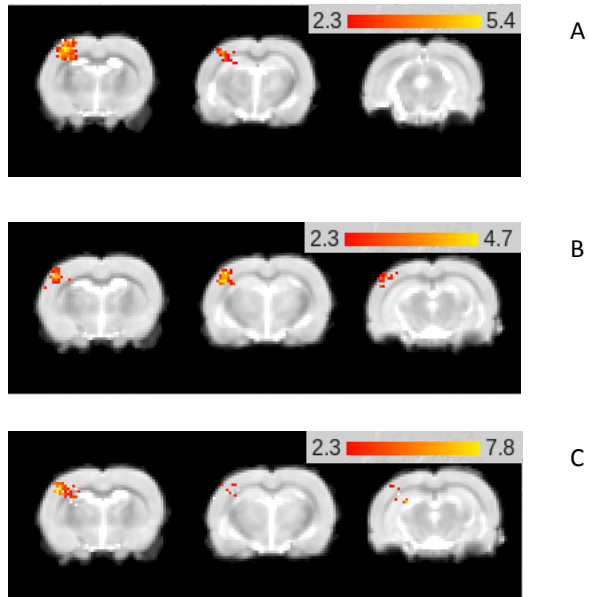


Fig. 5.2. Example images displaying S1FL activation in response to forepaw stimulation in a representative rat at 2 months (A), 94 months (B) and 6 months (C). Coloured bar indicates Z statistic of active voxels. Slices (from left to right) are bregma + 1mm, bregma, bregma – 1mm.

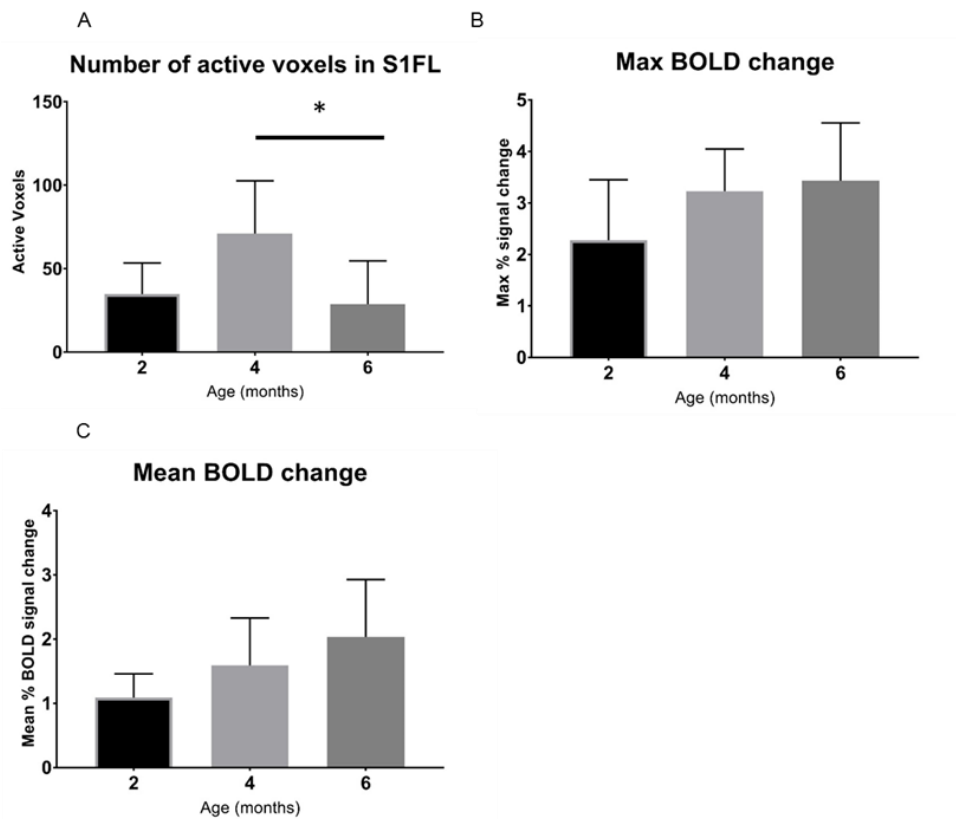


Fig. 5.3. Bar graphs showing number of active voxels in S1FL (A), maximum BOLD signal change in S1FL (B), and mean BOLD signal change of all active voxels in S1FL (C), quantified using BOLD fMRI in response to forepaw stimulation. Number of active voxels significantly decreased between 4 and 6 months (* $P < 0.05$). Data is displayed as mean \pm SD, $n = 6, 6,$ and 7 at 2, 4, and 6 months respectively

5.3.3. Functional MR Spectroscopy

At the first time point, mean glutamate change with activation (ΔGlu) was 0.99645 ± 1.69 . No significant change was observed over time ($F(2, 11) = 1.317, P = 0.3071$, fig. 5.4). Analysis was also performed on the NAA signal, which was 1.58 ± 2 at 2 months and did not change significantly over time ($F(2, 14) = 1.086, P = 0.3642$, Fig. 5.5).

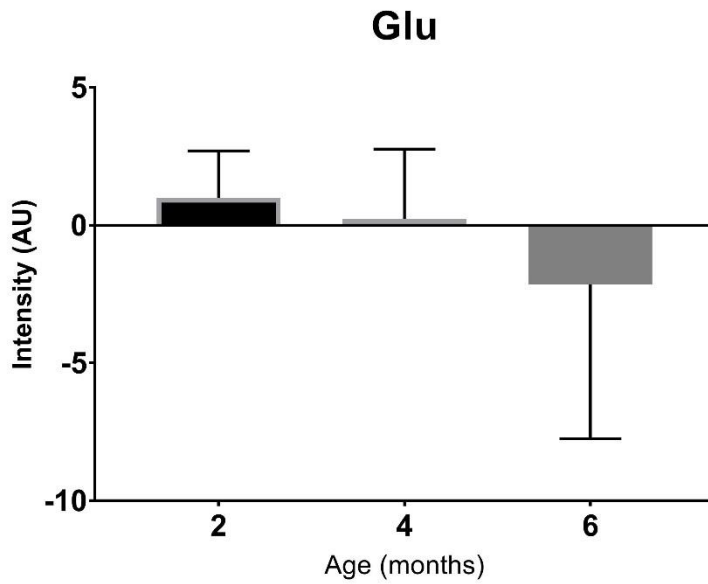


Fig. 5.4: Glutamate turnover in S1FL in response to forepaw stimulation over rats' lifetime, quantified using LASER fMRS. Data is displayed as mean \pm SD, n = 6, 8, and 7 at 2, 4 and 6 months respectively.

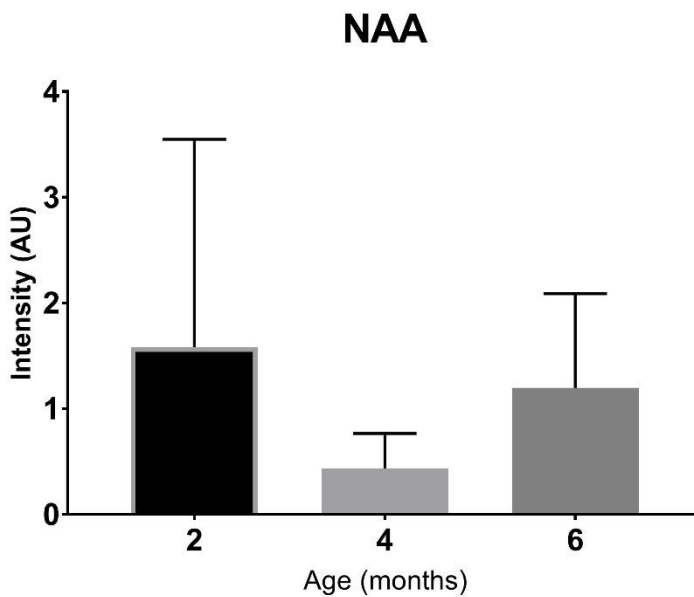


Fig. 5.5: NAA levels in somatosensory cortex over time, quantified using LASER MRS. Data is displayed as mean \pm SD, n = 6, 8, and 7 at 2, 4 and 6 months respectively.

5.3.4. Arterial Spin Labelling

Mean CBF significantly changed over time ($F(2, 18) = 8.738, P = 0.017$, Fig. 5.6). Post-hoc testing showed a significant increase from 1.616 ± 0.253 ml/mg/min at 2 months old to 2.422 ± 0.486 at

4 months old ($P = 0.0285$). CBF at 6 months was also significantly greater than 2 months ($P = 0.0110$)

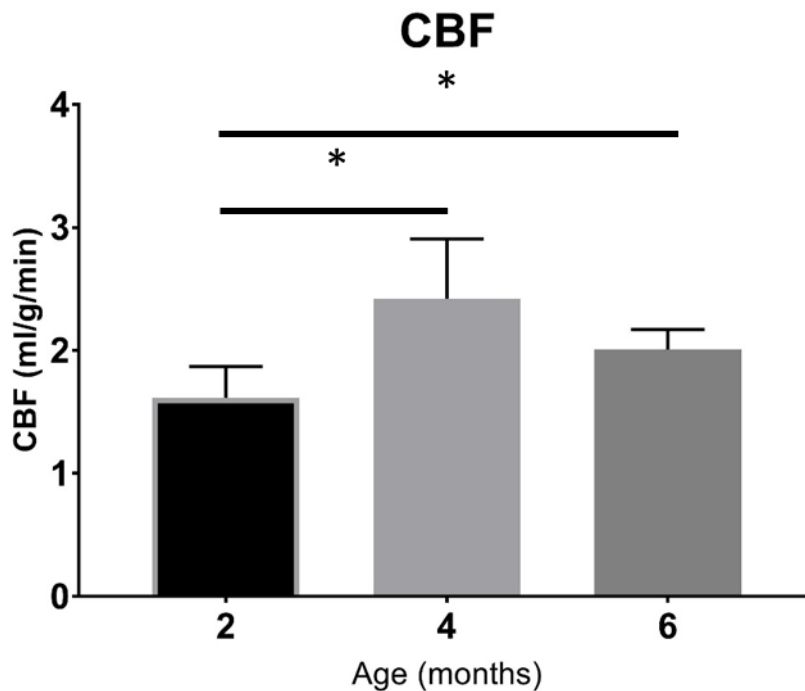


Fig. 5.6. Resting CBF at bregma, quantified using ASL MRI. CBF significantly increased between 2 and 4 months, and CBF at 6 months was significantly greater than CBF at 2 months ($*P < 0.05$). Data is displayed as mean \pm SD, $n = 7$.

5.4. Discussion

This study used fMRI to investigate changes in the BOLD signal, glutamate turnover and CBF over time in spontaneously hypertensive rats, as animals progressed from normotensive to chronic hypertension. Propofol was determined to be a suitable anaesthetic for detection of the BOLD signal, and with no detrimental effects on animal health. Animals' blood pressure increased significantly between each time point. Systolic blood pressure and diastolic blood pressure increased at different rates, causing pulse pressure to increase between 2 and 4 months and return to baseline between 4 and 6 months. This change in blood pressure correlated with previous measurements of SHRs (Adams and Korner, 1989). The size of the BOLD signal in S1FL increased between 2 and 4 months and also returned to baseline between 4 and 6 months. Cerebral blood flow was found to increase between 2 and 4 months, and remained high at 6 months old. Functional MR spectroscopy showed no significant change in glutamate turnover.

In the acute stage of hypertension, i.e. ~4 months in SHR_s (Adams and Korner, 1989; Mori *et al.*, 1995) adaptive changes are thought to occur in the brain's vasculature (Fujishima *et al.*, 1995; Naumczyk *et al.*, 2017). As the BOLD response is not impaired at the 4 month time point, when pulse pressure is highest, these adaptations may be linked to pulse pressure rather than the increased systolic blood pressure. The decrease in pulse pressure, as diastolic BP increases more rapidly, may then be the point in which adaptive changes to the vasculature become pathological. Previous studies suggest that SHR_s have been shown to favour eutrophic remodelling, in which muscle in the arteries rearranges to narrow the lumen, rather than hypertrophic remodelling, in which growth of new smooth muscle and perivascular cells occurs (Heagerty *et al.*, 1993; Schriffin, 2012), and these results suggest that eutrophic remodelling may occur in the acute stage, to preserve vascular reactivity, while hypertrophic remodelling occurs in the chronic stage and decreases reactivity.

It is important to note that the BOLD signal at two months old, when animals are still normotensive, is much lower than observed in our previous work in healthy 7 month old rats (Chapter 3). A possible explanation for this is that vascular or signalling changes observed in SHR_s may be genetic, and begin prior to the onset of hypertension. This is supported by evidence seen in human studies that suggests a hereditary component to neurovascular adaptive or pathological changes in hypertension (Haley *et al.*, 2007). However, to investigate this, further study comparing 2 month old SHR_s with age matched Wistar Kyotos would be required. An alternative explanation may be that the rat somatosensory cortex is not yet fully developed before 6 months old, and Wistar Kyoto rats may exhibit the same low baseline. If this is the case, WK rats will be expected to exhibit an increase in size of the BOLD signal at both time points.

Arterial spin labelling for CBF quantification showed an increase in CBF from 4 months onwards, with no change at 6 months. This suggests that at this stage, cerebral autoregulation cannot compensate for the sustained increase in BP. In healthy animals, transient systemic blood pressure increases are counteracted by mechanisms of cerebral autoregulation to prevent hyperperfusion, which can be damaging to the brain. The elevated CBF observed here suggests that these mechanisms are less effective at this time point, either through inhibition of signalling, or through reduced sensitivity of remodelled vessels. This supports previous observations in rodents, in which two-photon microscopy in 40 week old SHR_s showed a sustained increase in CBF (Calcinaghi *et al.*, 2013). However, these findings in SHR_s contradict previous research in humans, in which autoregulation is shifted in hypertensive subjects to counteract the effect of hypertension. When studying cerebral autoregulation between

normotensive and hypertensive subjects, CBF has been shown to be the same in both groups when measured at each group's mean blood pressure (Iadecola and Gottesman, 2019). In the longer term, human studies have shown that CBF is reduced below baseline, due to thickening of vascular smooth muscle and collagen deposition in arteries and veins which reduces lumen diameter and distensibility (Jennings *et al.*, 1998; Schriffin *et al.*, 2004). Whether this occurs in SHR's may require studying animals for 12 months or more (Calcinaghi *et al.*, 2013). If CBF remains high throughout the lifetime of SHR's, then an alternative model of hypertension may be more appropriate for future studies (Doggrell and Brown, 1998).

No significant changes were seen in ΔGlu at any time point. If synaptic activity or neuronal metabolism were impaired, a decrease in glutamate would be expected. This would represent either a decrease in glutamate release, or decrease in metabolic activity behind glutamate turnover (Walls *et al.*, 2015). Impairment of neurovascular coupling, reducing delivery of oxygen and glucose during neuronal activity, would be expected to reduce neuronal energy production (Stanimirovic and Friedman, 2012), which would impair cellular processes such as glutamate turnover. That a change in glutamate is not observed would suggest that the changes shown in blood pressure, CBF and vascular reactivity are not impairing neuronal metabolism or synaptic activity at this point. NAA levels, a marker for neuronal viability, also do not change, suggesting that neuronal death does not occur at this stage. While further study using longer scans is needed, as SNR using this method was poor, preservation of glutamate turnover rate and synaptic activity at 6 months suggests that the neuronal damage and cognitive deficits develop more slowly than chronic hypertension. If further time points were investigated and SNR could be improved, the time point at which synaptic impairment and neuronal death begin can be determined, indicating the possibility of a window in which neuroprotective strategies may be of benefit in chronic hypertension.

This study shows a clear change in BOLD response to forepaw stimulation and resting CBF in spontaneously hypertensive rats as animals age and hypertension develops. CBF increases at 4 months and remains high at 6 months, while the BOLD signal does not change at 4 months, followed by a decrease at 6 months. This suggests that while cerebral autoregulation is impaired in the acute stage of hypertension, protective mechanisms are active which preserve the BOLD response at this stage, and the BOLD response is only impaired in the chronic stage as pathological changes occur, and that neuronal damage does not occur at this stage. To our knowledge, this study is the first longitudinal fMRI study in hypertensive rats. The methods, which were initially developed using a rat model of healthy aging (Chapters 2 and 3) did require one adaptation to SHR physiology. During anaesthetic testing prior to experiments, after

cannulating the tail vein, the tail vein rapidly constricted and blocked application of propofol. As this was observed before hypertension developed, this is likely an inherent trait of the SHR strain, similar to other inherited adaptive traits seen in humans with family history of hypertension (Haley *et al.*, 2008). This was mitigated through application of lidocaine to the base of the tail, preventing the vein from constricting and allowing for one hour of propofol application before animals were returned to isoflurane. This may prevent longer scans from being performed, and so other scans may need to be removed to allow time for longer MRS scans in future experiments if this limitation cannot be overcome.

An alternative solution to this may be to use another model of hypertension, for example salt and mineralocorticoid induced hypertension in Wistar rats (Doggrell and Brown, 1998). This removes any hereditary factors that may be present in SHRs, which should remove the need for lidocaine to prevent vein constriction. Additionally, this allows the age of onset of hypertension to be determined by the researcher, rather than by the animals' genetics. Animals can then be allowed to reach full maturity before onset of hypertension, removing any confounding factors relating to normal development. Disease progression can also more accurately reflect the progression of hypertension in humans, which is normally observed in older adults. Comparison between animals with induced hypertension versus genetic hypertension, with normotensive controls, could then be used to investigate how hereditary factors versus lifestyle factors affect progression, cause cognitive decline, and be used to identify risk factors or develop treatments.

Chapter 6: Discussion and Conclusions

6.1. Development, validation and applications of methods – Anaesthetic protocol

The studies presented used a novel anaesthetic protocol with the aim of preserving the BOLD signal under anaesthesia, and causing no long term detrimental effects to animal welfare, to facilitate a longitudinal study design. In all studies, propofol was deemed to be safe for long term use. One animal died due to an error causing an overdose, which was reported to the Home Office Inspector and deemed to have not caused additional suffering, and in accordance with Schedule 1. All other animals experienced no harmful effects from the anaesthetic for the duration of the three studies. No behavioural changes or unexpected weight loss were observed in any animal following anaesthesia at any time point.

In aging Wistar Han rats, the dose given (54mg/kg/hr) provided effective sedation while allowing for a strong BOLD signal change. Breathing rate decreased under propofol compared to isoflurane, however this did not cause hypoxia, and oxygen saturation remained within the safe limit given by the Named Veterinary Surgeon (>80%). The required dose was higher than expected from previous studies of Wistar rats (Griffin *et al.*, 2010; Kelly *et al.*, 2010), and the correct dose rate for these experiments was obtained through experiments anaesthetising animals with isoflurane, applying the dose rate previously used (45mg/kg/hr), reducing isoflurane to zero, and monitoring the animal for signs of waking up. The dose rate was increased in 10% increments until anaesthesia could be sustained with propofol alone. The animal was then recovered. These bench experiments were performed under the supervision of the NVS. At 54mg/kg/hr, a strong BOLD signal change (~6%) was observed in S1FL in response to 10mV forepaw stimulation at all time points. Strong resting CBF signal was also observed, and consistent with expected values (Kelly *et al.*, 2010).

In Sprague-Dawley rats, the 54/mg/kg/hr dose rate gave a less consistent signal, with higher noise in healthy and post-stroke animals, and some animals showing no BOLD response at all. This highlights an aspect of method development that was not considered – variable sensitivity to propofol between strains. However, in both pre- and post-stroke SD rats, anaesthesia caused no harmful effects during or after experiments, with no unexpected weight change and oxygen saturation being maintained during scanning. This study does at least confirm that propofol is safe to use on post-stroke animals for longitudinal experiments, and while use of a lower dose or another strain may improve results for future stroke studies, some conclusions could still be drawn from the data.

Spontaneously Hypertensive rats showed better BOLD signal change than SD rats, but more noise than Wistar Han rats, suggesting a small reduction in dose rate may be needed for future studies. This strain also displayed no detrimental effects from multiple experiments under propofol anaesthesia. However, experiments in SHR's did highlight another difficulty in applying methods developed in healthy models to a disease model. After cannulation, SHR's tail veins would constrict and prevent propofol entering circulation, and animals had to be recovered. This was solved by applying 10µl Lidocaine subcutaneously to the base of the tail, preventing a response to the cannulation. This dose lasted an hour, and so after fMRI, fMRS and RS-fMRI, animals were returned to 1.5% isoflurane for the TOF, T₂ and ASL scans to prevent the animal from waking up. This does highlight the need for bench testing of the anaesthetic regime on any new strain or disease model, particularly those with a systemic vascular effect, and difficulty with cannulation in models of neurovascular disease is likely to be the main disadvantage of propofol vs gaseous anaesthetics going forward. It may be possible to overcome this disadvantage through intraperitoneal or subcutaneous injection rather than IV. Propofol has previously been tested using a single IP dose, giving 30 mins of anaesthesia at 200mg/kg, and has been used in short surgeries in smaller doses combined with medetomidine and fentanyl (Alves *et al.*, 2010). However motion was still observed in some animals under IP propofol, so testing of an IP continuous infusion would be required to ensure a stable depth of anaesthesia can be reached without harmful effects. Medetomidine anaesthesia can be used both IV and subcutaneously (Weber *et al.*, 2006; Pawela *et al.*, 2009), so subcutaneous infusion may also be possible with propofol.

6.2. Development, validation and applications of methods – MRI protocol

The MRI protocol was designed to study multiple functional parameters in the rodent brain. The BOLD signal is comprised of changes in oxyhaemoglobin to deoxyhaemoglobin ratio, and changes in local CBF, and while BOLD activity is a proxy for neuronal activity, changes in neurovascular coupling may cause changes in BOLD activity that do not reflect neuronal activity. Because of this, a functional MRS sequence was developed to calculate changes in glutamate with stimuli, and resting CBF was calculated using arterial spin labelling. Additionally, network analysis was performed using resting-state fMRI images. This was intended to give a comprehensive picture of changes at the local level, improving understanding of the mechanisms behind BOLD signal change, as well as observe changes at the whole-brain level using resting state.

The BOLD fMRI sequence was developed to give minimal distortion, with high spatial and temporal resolution at 9.4T. A 2 shot, 250 millisecond TR sequence was chosen from the sequences tested as a trade-off between optimum SNR and temporal resolution. Shortening the TR to 125ms did not cause distortion but did reduce SNR.

In Wistar Han rats (250-350g) and SHRs (200-300g), strong signal change was detected in the majority of scans. Some scans were discounted due to lack of signal, however this is more likely due to human error or variation in individual animals. Images in Sprague-Dawley rats were more likely to show distortion, possibly due to the animals' larger size (400-500g) making shimming more difficult. After confirming the long term safety of the anaesthetic protocols in aging and disease models, future studies can spend more time on shimming to remove this distortion in larger animals, and to extend the coverage of the protocol to whole brain rather than 3 slices. Whole-brain fMRI will also improve image registration for group analysis.

While the chosen sequence gave a good temporal resolution, temporal SNR was not sufficient for analysis of the BOLD time series. There was a high variability in the intensity of individual averages, and between subjects, which may have affected analysis of signal decay rate and time-to-peak. Neither parameter showed a trend towards increase or decrease with age.

While this cohort may not have exhibited any changes in time-to-peak or signal decay, studying these parameters may offer important insights in the future. Time-to-peak may be an indicator of vascular reactivity, which is thought to change with age and with vascular disease. Reduced vascular reactivity may be an indicator of vessel stiffening, and neurovascular uncoupling. Decay rate may be an indicator of neurovascular signalling. If decay rate increases without change to the stimulus, this would support the explanation that neurotransmitter turnover rate decreases, thus the initial level of signalling is not sustained. However, to measure this, the temporal SNR of the BOLD fMRI sequence must be improved.

The functional MRS sequence can be improved in a number of ways. The simplest change would be an increase in scan time and so an increase in the number of averages. An increase to a 27 minute sequence would give 270 averages each for the off and on conditions. In MRS, signal increases in proportion to the number of averages, while noise increases in proportion to the square root of the number of averages (Alger, 2011), and so three times the amount of averages would increase the signal by a factor of 3, but only increase noise by a factor of 1.7. As well as reducing variation in detection of glutamate turnover, NAA and Inositol, this would also allow other metabolites with a weaker signal to be studied. Of particular interest would be lactate as a marker of anaerobic respiration. An increase in lactate change with age, stroke,

or hypertension would be an indicator of neurovascular uncoupling, as higher lactate production would suggest that oxygen delivery is not keeping up with demand.

An alternative sequence may also be beneficial to fMRS. A Point Resolved Spectroscopy Sequence (PRESS) uses a spin-echo sequence, in which two 180 degree refocusing pulses are used following the initial 90 degree pulse to remove field inhomogeneity effects. While this is advantageous for SNR, particularly at high field strengths, this does require a longer echo time (Zhu *et al.*, 2011). This may reduce the signal strength of the glutamate and glutamine peaks, due to their short T_2 , and eliminate the lactate peak entirely. This was why PRESS was not selected for these studies. This can be compensated for, using a method known as TE averaging, however this does reduce the signal of other metabolites (Ramadan *et al.*, 2013). Alternatively, if neurotransmitters are the only metabolite of interest, spectral editing may be beneficial. Both PRESS and LASER can be modified to remove peaks that are not of interest, using Mescher-Garwood Point Resolved Spectroscopy Sequence (MEGA-PRESS) or Mescher-Garwood Localisation by Adiabatic Selective Refocusing (MEGA-LASER) sequence (Mescher *et al.*, 1998). These sequences use two pulses, one designed to amplify the signal for gamma-aminobutyric acid (GABA), an inhibitory neurotransmitter, and one regular pulse. The detected signals are then subtracted, leaving only GABA, and the adjacent NAA and Glutamate peaks (Mullins *et al.*, 2014). Removing other peaks in this way gives a stronger glutamate signal relative to NAA, as well as allowing quantification of GABA. Quantification of GABA, and thus quantification of inhibitory neuron activity, would be particularly useful where disinhibition is thought to play a role in the changes observed, such as hyperexcitability following stroke (Manganotti *et al.*, 2002), or increased cross-hemispheric connectivity to compensate for deficits (Cabeza *et al.*, 2002). However, due to the low SNR for GABA, the spatial resolution of this technique is limited, and so may be impractical for preclinical studies (Mullins *et al.*, 2014).

CBF quantification in this study, while limited to a single slice, did give important information. In this case, that CBF with age did not change in the cohort, and in the hypertensive group, CBF did increase at the early stage of hypertension. Further refinement of the ASL sequence would allow for a number of other parameters to be measured. For example, use of multiple inversion times can be used to study both CBF and arterial arrival time (AAT). AAT may be particularly useful in stroke studies, as this parameter has a low variance in individual regions in healthy subjects, and changes in AAT are an indicator of haemodynamically compromised tissue (McIntosh *et al.*, 2010). Quantification of AAT may be of use in understanding sources of variation in post-stroke animals, both through quantification of tissue in the lesion penumbra,

and potentially of identifying differences in perfusion pre-stroke that may indicate risk of more severe lesions.

ASL can also be used for fMRI. The main advantages of this method are that CMRO₂ does not contribute to the signal, and so signal change can be quantified in terms of CBF rather than arbitrary units, and better localisation due to the lack of weighting from deoxyhaemoglobin, and thus surrounding veins do not contribute to the signal (Petcharunpaisan *et al.*, 2010). However, these advantages do come at the cost of temporal resolution, which can often be higher than 10 seconds, and so more stimulus blocks are required for sufficient averages to be taken. The studies presented here have shown that propofol does not have adverse effects within the scan time, and so longer experiments to incorporate longer fMRS and ASL fMRI scans into the protocol are feasible. With ASL fMRI and improved fMRS, the contributions of neurotransmitter activity and CBF to the BOLD signal change can be better quantified.

6.3. Limitations of the current studies

Due to the novel nature of this work and many methods used, the conclusions that can be drawn are limited. An important consideration in all animal work is to keep animal numbers to a minimum, which is why the longitudinal study design was used in this research. However, where methods do cause high inter-subject variability, and multiple comparisons are used in analysis, reducing animal numbers too much can reduce the statistical power of a study. In future studies using these methods, assumptions made in power calculations must be altered to allow for this.

For the ageing study, an effect size of >50% was observed in the change in BOLD signal. However, earlier time points had a high standard deviation. While this is thought to be due to human error at earlier time points, and can be compensated for by spending more time on shimming and tuning the MRI scanner, calculations must factor in this high SD. Using an effect size of 50%, a standard deviation of 50% of the mean, a type 1 error rate of 5%, and 10 pairwise comparisons, a group size of 27 animals is needed to give a power of 0.8. Decreasing the type 1 error rate to 1% increases the animals needed to 34. However, if standard deviation can be reduced, as shown at later time points, and a 40% standard deviation is assumed, a 50% effect size with a 1% type 1 error rate can be seen in 22 animals. Increasing the number of animals for a future study according to these calculations will give an appropriate statistical power to better determine differences between individual time points, and investigate at what age changes in BOLD activity and neurotransmitter turnover begin.

In the hypertension study, a decrease of ~60% was observed in the BOLD signal between 4 months and 6 months. Factoring in a 50% standard deviation, to give a 5% type 1 error rate of 5% and power of 0.8, 15 animals are needed with the current study design, increasing to 20 if the type 1 error rate is reduced to 1%. In this case, number of time points can be increased to 4 or 5 with only a small increase in the number of animals to 22 or 24, respectively, allowing the effects of chronic hypertension to be studied over a longer time period.

6.4. Future directions

Future studies can build on these methods in a number of ways. Additional MRI sequences can be used to further investigate the different mechanisms behind neurovascular coupling. Different animal models can be used to apply these protocols to other neurovascular diseases. Ageing animals can be used to study the impact of lifestyle on the ageing brain, and models of stroke and hypertension can be refined.

Diffusion-weighted MRI can complement the methods used here in a number of ways. A common use of diffusion-weighted imaging is the mapping of white matter tracts using diffusion tensor imaging (DTI). Diffusion tensor imaging quantifies the property of fractional anisotropy (FA) of brain water, defined as the level of non-randomness, and used as a measure for directionality of tissue. Freely diffusing water has zero FA, while water in a highly ordered tissue, such as white matter tracts, has high FA (Baliyan *et al.*, 2016). This method allows for structural evaluations such as axon integrity, which is thought to be lost with ageing. Degradation of white matter tracts is thought to occur with age (Mosely, 2002) and can be measured using DTI. The extent of white matter damage correlates with cognitive decline in humans (Jokinen *et al.*, 2013). DTI has also been used in a mouse model of vascular cognitive impairment to observe changes in structural connectivity with cognitive decline (Boehm-Sturm *et al.*, 2017), a method which would complement functional connectivity measures using resting-state fMRI. Local glutamate concentration has also been shown to correlate with connectivity within a region, and so the effect of structural connectivity on neurotransmitter turnover with age would also provide novel insight into ageing (Duncan *et al.*, 2013).

Diffusion-weighted fMRI may also complement the other functional measures used here. Through measuring changes in diffusion with high temporal resolution, water diffusion during neuronal activity in response to a stimulus can be detected and used for functional imaging (Le Bihan, 2006). This sequence has some advantages over BOLD, in that activity is more localised, and that the signal originates from neuronal terminals, so has a shorter delay and

does not rely on neurovascular coupling being intact (Nunes *et al.*, 2019), however disadvantages such as SNR and high gradient load mean that it is currently not commonly used. It would however complement BOLD and ASL fMRI, allowing BOLD signal, CBF change and synaptic water diffusion to be mapped under the same stimulus protocol, and both neuronal and vascular aspects of neurovascular coupling to be observed.

Other animal models that would benefit from these longitudinal methods include Alzheimer's disease (AD) or other forms of dementia, and multiple sclerosis (MS). Studies of Alzheimer's disease in rodents do not routinely use a longitudinal study design (Sanganahalli *et al.*, 2013), however some groups are moving towards using a longitudinal model (Sharp *et al.*, 2019). It has been suggested, from an optical image spectroscopy study, that some previously observed deficits in neurovascular coupling in AD (Lacoste *et al.*, 2013; Park *et al.*, 2014) may be due to the stresses of an acute experiment, as the haemodynamic response was preserved in a longitudinal study (Sharp *et al.*, 2019). Through use of the longitudinal study protocol presented here, aspects of neuronal function and neurovascular coupling can be imaged non-invasively in an AD model to study AD progression, without confounding factors that may affect acute experiments. Multiple sclerosis is another progressive disease in which neurovascular coupling is impaired, affecting vascular reactivity and oxygen metabolism (Ge *et al.*, 2012; Marshall *et al.*, 2014). Increased glial activity is also a component of MS (Metea and Newman, 2006). Studies combining BOLD, CBF and MRS as presented here would provide insight into how these measures change as MS progresses.

The model of healthy ageing used here can be further refined to compare healthy vs unhealthy ageing. The animals in this study remained healthy until 18 months old. The benefit of playpen access for lab animals can be studied using fMRI, and comparing enrichment vs non enrichment groups. If a large difference is observed, this could then lead to different levels of enrichment, or different amounts of time in the playpen. This would have the dual benefit of improving animal welfare by demonstrating the benefits of enrichment, and allowing the effect of exercise on neurovascular coupling to be studied, which may explain the high variation seen in aged human cohorts (D'Esposito *et al.*, 1999).

In future studies, it is also important to study changes in cognitive ability using behavioural testing. In human subjects, the effects of ageing, stroke and hypertension on outcome measures seen with MRI are correlated with changes in working memory or visuomotor skills. In ageing and hypertension, working memory and visuomotor task performance becomes poorer over time, and correlates with changes described including reductions in BOLD activity,

compensatory increases in cross-hemispheric connectivity, and altered neuronal metabolism (Harrington *et al.*, 2000; Colcombe *et al.*, 2005; Wirenga *et al.*, 2008; Zahr *et al.*, 2013). In stroke, behavioural outcome has been shown to correlate with progression from the 'recruitment' stage to the 'focusing' stage (Feydy *et al.*, 2002; Tombari *et al.*, 2004). The goal in studying these conditions is to improve quality of life, through minimising cognitive and sensorimotor impairment. Thus, understanding how ageing and hypertension correlate with cognitive function, and how recovery post-stroke correlates with motor ability, is highly important. Combining imaging and behaviour in rats will allow the link between fMRI outcome and task ability to be studied in a controlled environment, and the effect of novel therapeutics to be investigated (for example, Markus *et al.*, 2006). Sensorimotor tests developed for stroke compare ability between impaired and unimpaired forelimbs, for example in reaching or tactile response (Dijkhizen *et al.*, 2001; Markus *et al.*, 2006). Future stroke studies can apply these tests at each time point to compare with lesion volume, S1FL activation, and glutamate turnover to determine the structural, neuronal and neurovascular changes affecting performance. For ageing and hypertension, tests can include examining sensorimotor function through exploratory activity in novel environments, balance, gait analysis and tactile response (Altun *et al.*, 2007), or spatial working memory through a water maze test (Rapp *et al.*, 1987) or a radial maze test (Oler and Markus, 1998). This form of testing at each time point can be used to understand how MRI outcomes correlate with behavioural ability.

The studies presented here represent a refinement to the methodology of preclinical functional imaging. Through use of non-invasive anaesthesia and a longitudinal study design, the number of animals required has been reduced. Use of the playpen and non-invasive imaging is beneficial to animal welfare, and the combination of multi-parametric imaging, non-invasive methodology, a longitudinal study design and improved animal welfare has provided new insights into neurovascular coupling. While there are still aspects of the study that need improving, these methods can provide a foundation for future studies into neurovascular coupling in a broad range of conditions.

References

- Abernethy, W. B., Bell, M. A., Morris, M. and Moody, D. M. (1993) 'Microvascular density of the human paraventricular nucleus decreases with aging but not hypertension', *Exp Neurol*, 121(2), pp. 270-4.
- Abo, M., Chen, Z., Lai, L. J., Reese, T. and Bjelke, B. (2001) 'Functional recovery after brain lesion--contralateral neuromodulation: an fMRI study', *Neuroreport*, 12(7), pp. 1543-7.
- Adams, H. P., Bendixen, B. H., Kappelle, L. J., Biller, J., Love, B. B., Gordon, D. L. and Marsh, E. E. (1993) 'Classification of subtype of acute ischemic stroke. Definitions for use in a multicenter clinical trial. TOAST. Trial of Org 10172 in Acute Stroke Treatment', *Stroke*, 24(1), pp. 35-41.
- Adams, H. P. and Biller, J. (2015) 'Classification of subtypes of ischemic stroke: history of the trial of org 10172 in acute stroke treatment classification', *Stroke*, 46(5), pp. e114-7.
- Adams, M. A., Bobik, A. and Korner, P. I. (1989) 'Differential development of vascular and cardiac hypertrophy in genetic hypertension. Relation to sympathetic function', *Hypertension*, 14(2), pp. 191-202.
- Aksenov, D. P., Li, L., Miller, M. J., Iordanescu, G. and Wyrwicz, A. M. (2015) 'Effects of anesthesia on BOLD signal and neuronal activity in the somatosensory cortex', *J Cereb Blood Flow Metab*, 35(11), pp. 1819-26.
- Alarcon-Martinez, L., Yilmaz-Ozcan, S., Yemisci, M., Schallek, J., Kiliç, K., Can, A., Di Polo, A. and Dalkara, T. (2018) 'Capillary pericytes express α -smooth muscle actin, which requires prevention of filamentous-actin depolymerization for detection', *Elife*, 7.
- Alastruey, J., Parker, K. H., Peiró, J., Byrd, S. M. and Sherwin, S. J. (2007) 'Modelling the circle of Willis to assess the effects of anatomical variations and occlusions on cerebral flows', *J Biomech*, 40(8), pp. 1794-805.
- Alger, J. R. (2010) 'Quantitative proton magnetic resonance spectroscopy and spectroscopic imaging of the brain: a didactic review', *Top Magn Reson Imaging*, 21(2), pp. 115-28.
- Altun, M., Bergman, E., Edström, E., Johnson, H. and Ulfhake, B. (2007) 'Behavioral impairments of the aging rat', *Physiol Behav*, 92(5), pp. 911-23.

- Alves, H. N., da Silva, A. L., Olsson, I. A., Orden, J. M. and Antunes, L. M. (2010) 'Anesthesia with intraperitoneal propofol, medetomidine, and fentanyl in rats', *J Am Assoc Lab Anim Sci*, 49(4), pp. 454-9.
- Ances, B. M., Liang, C. L., Leontiev, O., Perthen, J. E., Fleisher, A. S., Lansing, A. E. and Buxton, R. B. (2009) 'Effects of aging on cerebral blood flow, oxygen metabolism, and blood oxygenation level dependent responses to visual stimulation', *Hum Brain Mapp*, 30(4), pp. 1120-32.
- Arai, K., Jin, G., Navaratna, D. and Lo, E. H. (2009) 'Brain angiogenesis in developmental and pathological processes: neurovascular injury and angiogenic recovery after stroke', *FEBS J*, 276(17), pp. 4644-52.
- Armstead, W. M. (2016) 'Cerebral Blood Flow Autoregulation and Dysautoregulation', *Anesthesiol Clin*, 34(3), pp. 465-77.
- Attwell, D. and Laughlin, S. B. (2001) 'An energy budget for signaling in the grey matter of the brain', *J Cereb Blood Flow Metab*, 21(10), pp. 1133-45.
- Austin, V. C., Blamire, A. M., Allers, K. A., Sharp, T., Styles, P., Matthews, P. M. and Sibson, N. R. (2005) 'Confounding effects of anesthesia on functional activation in rodent brain: a study of halothane and alpha-chloralose anesthesia', *Neuroimage*, 24(1), pp. 92-100.
- Bakker, E. N., van der Meulen, E. T., van den Berg, B. M., Everts, V., Spaan, J. A. and VanBavel, E. (2002) 'Inward remodeling follows chronic vasoconstriction in isolated resistance arteries', *J Vasc Res*, 39(1), pp. 12-20.
- Balardin, J. B., Zimeo Morais, G. A., Furucho, R. A., Trambaiolli, L., Vanzella, P., Biazoli, C. and Sato, J. R. (2017) 'Imaging Brain Function with Functional Near-Infrared Spectroscopy in Unconstrained Environments', *Front Hum Neurosci*, 11, pp. 258.
- Baliyan, V., Das, C. J., Sharma, R. and Gupta, A. K. (2016) 'Diffusion weighted imaging: Technique and applications', *World J Radiol*, 8(9), pp. 785-798.
- Banks, W. A., Farr, S. A. and Morley, J. E. (2000) 'Permeability of the blood-brain barrier to albumin and insulin in the young and aged SAMP8 mouse', *J Gerontol A Biol Sci Med Sci*, 55(12), pp. B601-6.

- Baron, J. C. (2001) 'Perfusion thresholds in human cerebral ischemia: historical perspective and therapeutic implications', *Cerebrovasc Dis*, 11 Suppl 1, pp. 2-8.
- Baumbach, G. L. and Hajdu, M. A. (1993) 'Mechanics and composition of cerebral arterioles in renal and spontaneously hypertensive rats', *Hypertension*, 21(6 Pt 1), pp. 816-26.
- Baumbach, G. L. and Heistad, D. D. (1989) 'Remodeling of cerebral arterioles in chronic hypertension', *Hypertension*, 13(6 Pt 2), pp. 968-72.
- Beason-Held, L. L., Moghekar, A., Zonderman, A. B., Kraut, M. A. and Resnick, S. M. (2007) 'Longitudinal changes in cerebral blood flow in the older hypertensive brain', *Stroke*, 38(6), pp. 1766-73.
- Beckmann, C. F. and Smith, S. M. (2004) 'Probabilistic independent component analysis for functional magnetic resonance imaging', *IEEE Trans Med Imaging*, 23(2), pp. 137-52.
- Bell, M. A. and Ball, M. J. (1981) 'Morphometric comparison of hippocampal microvasculature in ageing and demented people: diameters and densities', *Acta Neuropathol*, 53(4), pp. 299-318.
- Bell, M. A. and Ball, M. J. (1990) 'Neuritic plaques and vessels of visual cortex in aging and Alzheimer's dementia', *Neurobiol Aging*, 11(4), pp. 359-70.
- Beretta, S., Cuccione, E., Versace, A., Carone, D., Riva, M., Padovano, G., Dell'Era, V., Cai, R., Monza, L., Presotto, L., Rousseau, D., Chauveau, F., Paternò, G., Pappadà, G. B., Giussani, C., Sganzerla, E. P. and Ferrarese, C. (2015) 'Cerebral collateral flow defines topography and evolution of molecular penumbra in experimental ischemic stroke', *Neurobiol Dis*, 74, pp. 305-13.
- Berlingeri, M., Danelli, L., Bottini, G., Sberna, M. and Paulesu, E. (2013) 'Reassessing the HAROLD model: is the hemispheric asymmetry reduction in older adults a special case of compensatory-related utilisation of neural circuits?', *Exp Brain Res*, 224(3), pp. 393-410.
- Berwick, J., Johnston, D., Jones, M., Martindale, J., Redgrave, P., McLoughlin, N., Schiessl, I. and Mayhew, J. E. (2005) 'Neurovascular coupling investigated with two-dimensional optical imaging spectroscopy in rat whisker barrel cortex', *Eur J Neurosci*, 22(7), pp. 1655-66.

- Bishop, N. A., Lu, T. and Yankner, B. A. (2010) 'Neural mechanisms of ageing and cognitive decline', *Nature*, 464(7288), pp. 529-35.
- Biswal, B., Yetkin, F. Z., Haughton, V. M. and Hyde, J. S. (1995) 'Functional connectivity in the motor cortex of resting human brain using echo-planar MRI', *Magn Reson Med*, 34(4), pp. 537-41.
- Boehm-Sturm, P., Füchtmeier, M., Foddiss, M., Mueller, S., Trueman, R. C., Zille, M., Rinnenthal, J. L., Kypraios, T., Shaw, L., Dirnagl, U. and Farr, T. D. (2017) 'Neuroimaging Biomarkers Predict Brain Structural Connectivity Change in a Mouse Model of Vascular Cognitive Impairment', *Stroke*, 48(2), pp. 468-475.
- Boero, J. A., Ascher, J., Arregui, A., Rovainen, C. and Woolsey, T. A. (1999) 'Increased brain capillaries in chronic hypoxia', *J Appl Physiol (1985)*, 86(4), pp. 1211-9.
- Boorman, L., Kennerley, A. J., Johnston, D., Jones, M., Zheng, Y., Redgrave, P. and Berwick, J. (2010) 'Negative blood oxygen level dependence in the rat: a model for investigating the role of suppression in neurovascular coupling', *J Neurosci*, 30(12), pp. 4285-94.
- Boumezbeur, F., Mason, G. F., de Graaf, R. A., Behar, K. L., Cline, G. W., Shulman, G. I., Rothman, D. L. and Petersen, K. F. (2010) 'Altered brain mitochondrial metabolism in healthy aging as assessed by in vivo magnetic resonance spectroscopy', *J Cereb Blood Flow Metab*, 30(1), pp. 211-21.
- Broughton, B. R., Reutens, D. C. and Sobey, C. G. (2009) 'Apoptotic mechanisms after cerebral ischemia', *Stroke*, 40(5), pp. e331-9.
- Brouns, R., Sheorajpanday, R., Wauters, A., De Surgeloose, D., Mariën, P. and De Deyn, P. P. (2008) 'Evaluation of lactate as a marker of metabolic stress and cause of secondary damage in acute ischemic stroke or TIA', *Clin Chim Acta*, 397(1-2), pp. 27-31.
- Brown, W. R., Moody, D. M., Challa, V. R., Thore, C. R. and Anstrom, J. A. (2002) 'Venous collagenosis and arteriolar tortuosity in leukoaraiosis', *J Neurol Sci*, 203-204, pp. 159-63.
- Buchweitz-Milton, E. and Weiss, H. R. (1987) 'Perfused capillary morphometry in the senescent brain', *Neurobiol Aging*, 8(3), pp. 271-6.

- Burke, M. and Bührle, C. (2006) 'BOLD response during uncoupling of neuronal activity and CBF', *Neuroimage*, 32(1), pp. 1-8.
- Cabeza, R. (2002) 'Hemispheric asymmetry reduction in older adults: the HAROLD model', *Psychol Aging*, 17(1), pp. 85-100.
- Calcinaghi, N., Wyss, M. T., Jolivet, R., Singh, A., Keller, A. L., Winnik, S., Fritschy, J. M., Buck, A., Matter, C. M. and Weber, B. (2013) 'Multimodal imaging in rats reveals impaired neurovascular coupling in sustained hypertension', *Stroke*, 44(7), pp. 1957-64.
- Carey, L. M., Abbott, D. F., Egan, G. F., O'Keefe, G. J., Jackson, G. D., Bernhardt, J. and Donnan, G. A. (2006) 'Evolution of brain activation with good and poor motor recovery after stroke', *Neurorehabil Neural Repair*, 20(1), pp. 24-41.
- Carmignoto, G. and Gómez-Gonzalo, M. (2010) 'The contribution of astrocyte signalling to neurovascular coupling', *Brain Res Rev*, 63(1-2), pp. 138-48.
- Casey, M. A. and Feldman, M. L. (1985) 'Aging in the rat medial nucleus of the trapezoid body. III. Alterations in capillaries', *Neurobiol Aging*, 6(1), pp. 39-46.
- Cenic, A., Craen, R. A., Howard-Lech, V. L., Lee, T. Y. and Gelb, A. W. (2000) 'Cerebral blood volume and blood flow at varying arterial carbon dioxide tension levels in rabbits during propofol anesthesia', *Anesth Analg*, 90(6), pp. 1376-83.
- Chan-Ling, T., Hughes, S., Baxter, L., Rosinova, E., McGregor, I., Morcos, Y., van Nieuwenhuyzen, P. and Hu, P. (2007) 'Inflammation and breakdown of the blood-retinal barrier during "physiological aging" in the rat retina: a model for CNS aging', *Microcirculation*, 14(1), pp. 63-76.
- Chavhan, G. B., Babyn, P. S., Thomas, B., Shroff, M. M. and Haacke, E. M. (2009) 'Principles, techniques, and applications of T₂*-based MR imaging and its special applications', *Radiographics*, 29(5), pp. 1433-49.
- Chen, B. R., Bouchard, M. B., McCaslin, A. F., Burgess, S. A. and Hillman, E. M. (2011) 'High-speed vascular dynamics of the hemodynamic response', *Neuroimage*, 54(2), pp. 1021-30.

Chen, V. C., Hsu, T. C., Chen, L. J., Chou, H. C., Weng, J. C. and Tzang, B. S. (2017) 'Effects of taurine on resting-state fMRI activity in spontaneously hypertensive rats', *PLoS One*, 12(7), pp. e0181122.

Cheng, L. L., Newell, K., Mallory, A. E., Hyman, B. T. and Gonzalez, R. G. (2002) 'Quantification of neurons in Alzheimer and control brains with ex vivo high resolution magic angle spinning proton magnetic resonance spectroscopy and stereology', *Magn Reson Imaging*, 20(7), pp. 527-33.

Cherry, S. R. (2001) 'Fundamentals of positron emission tomography and applications in preclinical drug development', *J Clin Pharmacol*, 41(5), pp. 482-91.

Chi, O. Z., Chang, Q. and Weiss, H. R. (1997) 'Effects of topical N-methyl-D-aspartate on blood-brain barrier permeability in the cerebral cortex of normotensive and hypertensive rats', *Neurol Res*, 19(5), pp. 539-44.

Chillon, J. M. and Baumbach, G. L. (1999) 'Effects of an angiotensin-converting enzyme inhibitor and a beta-blocker on cerebral arterioles in rats', *Hypertension*, 33(3), pp. 856-61.

Chollet, F., DiPiero, V., Wise, R. J., Brooks, D. J., Dolan, R. J. and Frackowiak, R. S. (1991) 'The functional anatomy of motor recovery after stroke in humans: a study with positron emission tomography', *Ann Neurol*, 29(1), pp. 63-71.

Christensen, H. (2001) 'What cognitive changes can be expected with normal ageing?', *Aust N Z J Psychiatry*, 35(6), pp. 768-75.

Cichocka, M. and Bereś, A. (2018) 'From fetus to older age: A review of brain metabolic changes across the lifespan', *Ageing Res Rev*, 46, pp. 60-73.

Cohen, Z., Bonvento, G., Lacombe, P. and Hamel, E. (1996) 'Serotonin in the regulation of brain microcirculation', *Prog Neurobiol*, 50(4), pp. 335-62.

Colcombe, S. J., Kramer, A. F., Erickson, K. I. and Scalf, P. (2005) 'The implications of cortical recruitment and brain morphology for individual differences in inhibitory function in aging humans', *Psychol Aging*, 20(3), pp. 363-75.

Cooper, L. L., Woodard, T., Sigurdsson, S., van Buchem, M. A., Torjesen, A. A., Inker, L. A., Aspelund, T., Eiriksdottir, G., Harris, T. B., Gudnason, V., Launer, L. J. and Mitchell, G. F.

(2016) 'Cerebrovascular Damage Mediates Relations Between Aortic Stiffness and Memory', *Hypertension*, 67(1), pp. 176-82.

Cordes, D., Haughton, V. M., Arfanakis, K., Wendt, G. J., Turski, P. A., Moritz, C. H., Quigley, M. A. and Meyerand, M. E. (2000) 'Mapping functionally related regions of brain with functional connectivity MR imaging', *AJNR Am J Neuroradiol*, 21(9), pp. 1636-44.

Coulson, J. M., Murphy, K., Harris, A. D., Fjodorova, M., Cockcroft, J. R. and Wise, R. G. (2015) 'Correlation between baseline blood pressure and the brainstem fMRI response to isometric forearm contraction in human volunteers: a pilot study', *J Hum Hypertens*, 29(7), pp. 449-55.

Coyle, P. and Jokelainen, P. T. (1982) 'Dorsal cerebral arterial collaterals of the rat', *Anat Rec*, 203(3), pp. 397-404.

Cuccione, E., Versace, A., Cho, T. H., Carone, D., Berner, L. P., Ong, E., Rousseau, D., Cai, R., Monza, L., Ferrarese, C., Sganzerla, E. P., Berthezène, Y., Nighoghossian, N., Wiart, M., Beretta, S. and Chauveau, F. (2017) 'Multi-site laser Doppler flowmetry for assessing collateral flow in experimental ischemic stroke: Validation of outcome prediction with acute MRI', *J Cereb Blood Flow Metab*, 37(6), pp. 2159-2170.

D'Esposito, M., Zarahn, E., Aguirre, G. K. and Rypma, B. (1999) 'The effect of normal aging on the coupling of neural activity to the bold hemodynamic response', *Neuroimage*, 10(1), pp. 6-14.

Dahlöf, B. (2007) 'Prevention of stroke in patients with hypertension', *Am J Cardiol*, 100(3A), pp. 17J-24J.

Dai, W., Lopez, O. L., Carmichael, O. T., Becker, J. T., Kuller, L. H. and Gach, H. M. (2008) 'Abnormal regional cerebral blood flow in cognitively normal elderly subjects with hypertension', *Stroke*, 39(2), pp. 349-54.

Dauphin, F., Richard, J. W., Seylaz, J., Quirion, R. and Hamel, E. (1991) 'Acetylcholine levels and choline acetyltransferase activity in rat cerebrovascular bed after uni- or bilateral sphenopalatine ganglionectomy', *J Cereb Blood Flow Metab*, 11(2), pp. 253-60.

- Davidson, A. O., Schork, N., Jaques, B. C., Kelman, A. W., Sutcliffe, R. G., Reid, J. L. and Dominiczak, A. F. (1995) 'Blood pressure in genetically hypertensive rats. Influence of the Y chromosome', *Hypertension*, 26(3), pp. 452-9.
- De Caterina, R., Libby, P., Peng, H. B., Thannickal, V. J., Rajavashisth, T. B., Gimbrone, M. A., Shin, W. S. and Liao, J. K. (1995) 'Nitric oxide decreases cytokine-induced endothelial activation. Nitric oxide selectively reduces endothelial expression of adhesion molecules and proinflammatory cytokines', *J Clin Invest*, 96(1), pp. 60-8.
- de Leeuw, F. E., de Groot, J. C., Oudkerk, M., Witteman, J. C., Hofman, A., van Gijn, J. and Breteler, M. M. (2002) 'Hypertension and cerebral white matter lesions in a prospective cohort study', *Brain*, 125(Pt 4), pp. 765-72.
- De Luca, M., Beckmann, C. F., De Stefano, N., Matthews, P. M. and Smith, S. M. (2006) 'fMRI resting state networks define distinct modes of long-distance interactions in the human brain', *Neuroimage*, 29(4), pp. 1359-67.
- Deiber, M. P., Wise, S. P., Honda, M., Catalan, M. J., Grafman, J. and Hallett, M. (1997) 'Frontal and parietal networks for conditional motor learning: a positron emission tomography study', *J Neurophysiol*, 78(2), pp. 977-91.
- Deitmer, J. W., Theparambil, S. M., Ruminot, I., Noor, S. I. and Becker, H. M. (2019) 'Energy Dynamics in the Brain: Contributions of Astrocytes to Metabolism and pH Homeostasis', *Front Neurosci*, 13, pp. 1301.
- Desilles, J. P., Loyau, S., Syvannarath, V., Gonzalez-Valcarcel, J., Cantier, M., Louedec, L., Lapergue, B., Amarenco, P., Ajzenberg, N., Jandrot-Perrus, M., Michel, J. B., Ho-Tin-Noe, B. and Mazighi, M. (2015) 'Alteplase Reduces Downstream Microvascular Thrombosis and Improves the Benefit of Large Artery Recanalization in Stroke', *Stroke*, 46(11), pp. 3241-8.
- Detre, J. A. and Wang, J. (2002) 'Technical aspects and utility of fMRI using BOLD and ASL', *Clin Neurophysiol*, 113(5), pp. 621-34.
- Dickey, P. S., Kailasnath, P., Bloomgarden, G., Goodrich, I. and Chaloupka, J. (1996) 'Computer modeling of cerebral blood flow following internal carotid artery occlusion', *Neurol Res*, 18(3), pp. 259-66.

- Didion, S. P. and Faraci, F. M. (2003) 'Angiotensin II produces superoxide-mediated impairment of endothelial function in cerebral arterioles', *Stroke*, 34(8), pp. 2038-42.
- Dijkhuizen, R. M., Ren, J., Mandeville, J. B., Wu, O., Ozdag, F. M., Moskowitz, M. A., Rosen, B. R. and Finklestein, S. P. (2001) 'Functional magnetic resonance imaging of reorganization in rat brain after stroke', *Proc Natl Acad Sci U S A*, 98(22), pp. 12766-71.
- Dijkhuizen, R. M., Singhal, A. B., Mandeville, J. B., Wu, O., Halpern, E. F., Finklestein, S. P., Rosen, B. R. and Lo, E. H. (2003) 'Correlation between brain reorganization, ischemic damage, and neurologic status after transient focal cerebral ischemia in rats: a functional magnetic resonance imaging study', *J Neurosci*, 23(2), pp. 510-7.
- Doggrell, S. A. and Brown, L. (1998) 'Rat models of hypertension, cardiac hypertrophy and failure', *Cardiovasc Res*, 39(1), pp. 89-105.
- Dormanns, K., Brown, R. G. and David, T. (2016) 'The role of nitric oxide in neurovascular coupling', *J Theor Biol*, 394, pp. 1-17.
- Dreier, J. P. (2011) 'The role of spreading depression, spreading depolarization and spreading ischemia in neurological disease', *Nat Med*, 17(4), pp. 439-47.
- Dringen, R. (2005) 'Oxidative and antioxidative potential of brain microglial cells', *Antioxid Redox Signal*, 7(9-10), pp. 1223-33.
- Driscoll, I., Resnick, S. M., Troncoso, J. C., An, Y., O'Brien, R. and Zonderman, A. B. (2006) 'Impact of Alzheimer's pathology on cognitive trajectories in nondemented elderly', *Ann Neurol*, 60(6), pp. 688-95.
- Dubeau, S., Ferland, G., Gaudreau, P., Beaumont, E. and Lesage, F. (2011) 'Cerebrovascular hemodynamic correlates of aging in the Lou/c rat: a model of healthy aging', *Neuroimage*, 56(4), pp. 1892-901.
- Duncan, N. W., Wiebking, C., Tiret, B., Marjańska, M., Hayes, D. J., Lyttleton, O., Doyon, J. and Northoff, G. (2013) 'Glutamate concentration in the medial prefrontal cortex predicts resting-state cortical-subcortical functional connectivity in humans', *PLoS One*, 8(4), pp. e60312.

Duncombe, J., Lennen, R. J., Jansen, M. A., Marshall, I., Wardlaw, J. M. and Horsburgh, K. (2017) 'Ageing causes prominent neurovascular dysfunction associated with loss of astrocytic contacts and gliosis', *Neuropathol Appl Neurobiol*, 43(6), pp. 477-491.

Elhousseiny, A. and Hamel, E. (2000) 'Muscarinic--but not nicotinic--acetylcholine receptors mediate a nitric oxide-dependent dilation in brain cortical arterioles: a possible role for the M5 receptor subtype', *J Cereb Blood Flow Metab*, 20(2), pp. 298-305.

Eltzschig, H. K. and Eckle, T. (2011) 'Ischemia and reperfusion--from mechanism to translation', *Nat Med*, 17(11), pp. 1391-401.

Endres, M., Laufs, U., Huang, Z., Nakamura, T., Huang, P., Moskowitz, M. A. and Liao, J. K. (1998) 'Stroke protection by 3-hydroxy-3-methylglutaryl (HMG)-CoA reductase inhibitors mediated by endothelial nitric oxide synthase', *Proc Natl Acad Sci U S A*, 95(15), pp. 8880-5.

Ernst, T., Chang, L., Melchor, R. and Mehringer, C. M. (1997) 'Frontotemporal dementia and early Alzheimer disease: differentiation with frontal lobe H-1 MR spectroscopy', *Radiology*, 203(3), pp. 829-36.

Eylers, V. V., Maudsley, A. A., Bronzlik, P., Dellani, P. R., Lanfermann, H. and Ding, X. Q. (2016) 'Detection of Normal Aging Effects on Human Brain Metabolite Concentrations and Microstructure with Whole-Brain MR Spectroscopic Imaging and Quantitative MR Imaging', *AJNR Am J Neuroradiol*, 37(3), pp. 447-54.

Fabiani, M., Gordon, B. A., Maclin, E. L., Pearson, M. A., Brumback-Peltz, C. R., Low, K. A., McAuley, E., Sutton, B. P., Kramer, A. F. and Gratton, G. (2014) 'Neurovascular coupling in normal aging: a combined optical, ERP and fMRI study', *Neuroimage*, 85 Pt 1, pp. 592-607.

Farkas, E., De Jong, G. I., Apró, E., De Vos, R. A., Steur, E. N. and Luiten, P. G. (2000) 'Similar ultrastructural breakdown of cerebrocortical capillaries in Alzheimer's disease, Parkinson's disease, and experimental hypertension. What is the functional link?', *Ann N Y Acad Sci*, 903, pp. 72-82.

Farkas, E. and Luiten, P. G. (2001) 'Cerebral microvascular pathology in aging and Alzheimer's disease', *Prog Neurobiol*, 64(6), pp. 575-611.

Feydy, A., Carlier, R., Roby-Brami, A., Bussel, B., Cazalis, F., Pierot, L., Burnod, Y. and Maier, M. A. (2002) 'Longitudinal study of motor recovery after stroke: recruitment and focusing of brain activation', *Stroke*, 33(6), pp. 1610-7.

Ficzere, A., Valikovics, A., Fülesdi, B., Juhász, A., Czuriga, I. and Csiba, L. (1997) 'Cerebrovascular reactivity in hypertensive patients: a transcranial Doppler study', *J Clin Ultrasound*, 25(7), pp. 383-9.

Filosa, J. A., Bonev, A. D., Straub, S. V., Meredith, A. L., Wilkerson, M. K., Aldrich, R. W. and Nelson, M. T. (2006) 'Local potassium signaling couples neuronal activity to vasodilation in the brain', *Nat Neurosci*, 9(11), pp. 1397-1403.

Flamant, M., Placier, S., Dubroca, C., Esposito, B., Lopes, I., Chatziantoniou, C., Tedgui, A., Dussaule, J. C. and Lehoux, S. (2007) 'Role of matrix metalloproteinases in early hypertensive vascular remodeling', *Hypertension*, 50(1), pp. 212-8.

Fox, M. D. and Raichle, M. E. (2007) 'Spontaneous fluctuations in brain activity observed with functional magnetic resonance imaging', *Nat Rev Neurosci*, 8(9), pp. 700-11.

Fox, P. T. and Raichle, M. E. (1986) 'Focal physiological uncoupling of cerebral blood flow and oxidative metabolism during somatosensory stimulation in human subjects', *Proc Natl Acad Sci U S A*, 83(4), pp. 1140-4.

Fridez, P., Makino, A., Miyazaki, H., Meister, J. J., Hayashi, K. and Stergiopoulos, N. (2001) 'Short-Term biomechanical adaptation of the rat carotid to acute hypertension: contribution of smooth muscle', *Ann Biomed Eng*, 29(1), pp. 26-34.

Fujishima, M., Ibayashi, S., Fujii, K. and Mori, S. (1995) 'Cerebral blood flow and brain function in hypertension', *Hypertens Res*, 18(2), pp. 111-7.

Ge, Y., Zhang, Z., Lu, H., Tang, L., Jaggi, H., Herbert, J., Babb, J. S., Rusinek, H. and Grossman, R. I. (2012) 'Characterizing brain oxygen metabolism in patients with multiple sclerosis with T₂-relaxation-under-spin-tagging MRI', *J Cereb Blood Flow Metab*, 32(3), pp. 403-12.

Girouard, H. and Iadecola, C. (2006) 'Neurovascular coupling in the normal brain and in hypertension, stroke, and Alzheimer disease', *J Appl Physiol (1985)*, 100(1), pp. 328-35.

- Godlewska, B. R., Clare, S., Cowen, P. J. and Emir, U. E. (2017) 'Ultra-High-Field Magnetic Resonance Spectroscopy in Psychiatry', *Front Psychiatry*, 8, pp. 123.
- Gordon, E. M., Lynch, C. J., Gratton, C., Laumann, T. O., Gilmore, A. W., Greene, D. J., Ortega, M., Nguyen, A. L., Schlaggar, B. L., Petersen, S. E., Dosenbach, N. U. F. and Nelson, S. M. (2018) 'Three Distinct Sets of Connector Hubs Integrate Human Brain Function', *Cell Rep*, 24(7), pp. 1687-1695.e4.
- Graham, G. D., Blamire, A. M., Howseman, A. M., Rothman, D. L., Fayad, P. B., Brass, L. M., Petroff, O. A., Shulman, R. G. and Prichard, J. W. (1992) 'Proton magnetic resonance spectroscopy of cerebral lactate and other metabolites in stroke patients', *Stroke*, 23(3), pp. 333-40.
- Griffin, K. M., Blau, C. W., Kelly, M. E., O'Herlihy, C., O'Connell, P. R., Jones, J. F. and Kerskens, C. M. (2010) 'Propofol allows precise quantitative arterial spin labelling functional magnetic resonance imaging in the rat', *Neuroimage*, 51(4), pp. 1395-404.
- Gussew, A., Rzanny, R., Erdtel, M., Scholle, H. C., Kaiser, W. A., Mentzel, H. J. and Reichenbach, J. R. (2010) 'Time-resolved functional 1H MR spectroscopic detection of glutamate concentration changes in the brain during acute heat pain stimulation', *Neuroimage*, 49(2), pp. 1895-902.
- Hajdu, M. A., Heistad, D. D., Siems, J. E. and Baumbach, G. L. (1990) 'Effects of aging on mechanics and composition of cerebral arterioles in rats', *Circ Res*, 66(6), pp. 1747-54.
- Hajdu, M. A., McElmurry, R. T., Heistad, D. D. and Baumbach, G. L. (1993) 'Effects of aging on cerebral vascular responses to serotonin in rats', *Am J Physiol*, 264(6 Pt 2), pp. H2136-40.
- Halani, S., Kwinta, J. B., Golestani, A. M., Khatamian, Y. B. and Chen, J. J. (2015) 'Comparing cerebrovascular reactivity measured using BOLD and cerebral blood flow MRI: The effect of basal vascular tension on vasodilatory and vasoconstrictive reactivity', *Neuroimage*, 110, pp. 110-23.
- Hamilton, C., Ma, Y. and Zhang, N. (2017) 'Global reduction of information exchange during anesthetic-induced unconsciousness', *Brain Struct Funct*, 222(7), pp. 3205-3216.

- Harrington, F., Saxby, B. K., McKeith, I. G., Wesnes, K. and Ford, G. A. (2000) 'Cognitive performance in hypertensive and normotensive older subjects', *Hypertension*, 36(6), pp. 1079-82.
- Hartkamp, M. J., van Der Grond, J., van Everdingen, K. J., Hillen, B. and Mali, W. P. (1999) 'Circle of Willis collateral flow investigated by magnetic resonance angiography', *Stroke*, 30(12), pp. 2671-8.
- Hayward, N. M., Yanev, P., Haapasalo, A., Miettinen, R., Hiltunen, M., Gröhn, O. and Jolkkonen, J. (2011) 'Chronic hyperperfusion and angiogenesis follow subacute hypoperfusion in the thalamus of rats with focal cerebral ischemia', *J Cereb Blood Flow Metab*, 31(4), pp. 1119-32.
- Heagerty, A. M., Aalkjaer, C., Bund, S. J., Korsgaard, N. and Mulvany, M. J. (1993) 'Small artery structure in hypertension. Dual processes of remodeling and growth', *Hypertension*, 21(4), pp. 391-7.
- Heffernan, K. S., Augustine, J. A., Lefferts, W. K., Spartano, N. L., Hughes, W. E., Jorgensen, R. S. and Gump, B. B. (2018) 'Arterial stiffness and cerebral hemodynamic pulsatility during cognitive engagement in younger and older adults', *Exp Gerontol*, 101, pp. 54-62.
- Hinds, J. W. and McNelly, N. A. (1982) 'Capillaries in aging rat olfactory bulb: a quantitative light and electron microscopic analysis', *Neurobiol Aging*, 3(3), pp. 197-207.
- Hoksbergen, A. W., Legemate, D. A., Csiba, L., Csáti, G., Síró, P. and Fülesdi, B. (2003) 'Absent collateral function of the circle of Willis as risk factor for ischemic stroke', *Cerebrovasc Dis*, 16(3), pp. 191-8.
- Hosp, J. A., Molina-Luna, K., Hertler, B., Atiemo, C. O., Stett, A. and Luft, A. R. (2008) 'Thin-film epidural microelectrode arrays for somatosensory and motor cortex mapping in rat', *J Neurosci Methods*, 172(2), pp. 255-62.
- Hu, Z. H., Wang, X. C., Li, L. Y., Liu, M. L., Liu, R., Ling, Z., Tian, Q., Tang, X. W., Wu, Y. G. and Wang, J. Z. (2004) 'Correlation of behavior changes and BOLD signal in Alzheimer-like rat model', *Acta Biochim Biophys Sin (Shanghai)*, 36(12), pp. 803-10.

- Hudetz, A. G. (1997) 'Blood flow in the cerebral capillary network: a review emphasizing observations with intravital microscopy', *Microcirculation*, 4(2), pp. 233-52.
- Huettel, S. A., Singerman, J. D. and McCarthy, G. (2001) 'The effects of aging upon the hemodynamic response measured by functional MRI', *Neuroimage*, 13(1), pp. 161-75.
- Hunter, A. J., Hatcher, J., Virley, D., Nelson, P., Irving, E., Hadingham, S. J. and Parsons, A. A. (2000) 'Functional assessments in mice and rats after focal stroke', *Neuropharmacology*, 39(5), pp. 806-16.
- Hutchinson, E., Avery, A. and Vandewoude, S. (2005) 'Environmental enrichment for laboratory rodents', *ILAR J*, 46(2), pp. 148-61.
- Hyder, F., Behar, K. L., Martin, M. A., Blamire, A. M. and Shulman, R. G. (1994) 'Dynamic magnetic resonance imaging of the rat brain during forepaw stimulation', *J Cereb Blood Flow Metab*, 14(4), pp. 649-55.
- Iadecola, C. and Gottesman, R. F. (2019) 'Neurovascular and Cognitive Dysfunction in Hypertension', *Circ Res*, 124(7), pp. 1025-1044.
- Janssen, B., Vugts, D. J., Funke, U., Molenaar, G. T., Kruijer, P. S., van Berckel, B. N., Lammertsma, A. A. and Windhorst, A. D. (2016) 'Imaging of neuroinflammation in Alzheimer's disease, multiple sclerosis and stroke: Recent developments in positron emission tomography', *Biochim Biophys Acta*, 1862(3), pp. 425-41.
- Jefferson, A. L., Cambroner, F. E., Liu, D., Moore, E. E., Neal, J. E., Terry, J. G., Nair, S., Pechman, K. R., Rane, S., Davis, L. T., Gifford, K. A., Hohman, T. J., Bell, S. P., Wang, T. J., Beckman, J. A. and Carr, J. J. (2018) 'Higher Aortic Stiffness Is Related to Lower Cerebral Blood Flow and Preserved Cerebrovascular Reactivity in Older Adults', *Circulation*, 138(18), pp. 1951-1962.
- Jenkinson, M., Bannister, P., Brady, M. and Smith, S. (2002) 'Improved optimization for the robust and accurate linear registration and motion correction of brain images', *Neuroimage*, 17(2), pp. 825-41.

Jennings, J. R., Heim, A. F., Sheu, L. K., Muldoon, M. F., Ryan, C., Gach, H. M., Schirda, C. and Gianaros, P. J. (2017) 'Brain Regional Blood Flow and Working Memory Performance Predict Change in Blood Pressure Over 2 Years', *Hypertension*, 70(6), pp. 1132-1141.

Jennings, J. R., Muldoon, M. F., Ryan, C. M., Mintun, M. A., Meltzer, C. C., Townsend, D. W., Sutton-Tyrrell, K., Shapiro, A. P. and Manuck, S. B. (1998) 'Cerebral blood flow in hypertensive patients: an initial report of reduced and compensatory blood flow responses during performance of two cognitive tasks', *Hypertension*, 31(6), pp. 1216-22.

Jennings, J. R., Muldoon, M. F., Whyte, E. M., Scanlon, J., Price, J. and Meltzer, C. C. (2008) 'Brain imaging findings predict blood pressure response to pharmacological treatment', *Hypertension*, 52(6), pp. 1113-9.

Jiang, H. X., Chen, P. C., Sobin, S. S. and Giannotta, S. L. (1992) 'Age related alterations in the response of the pial arterioles to adenosine in the rat', *Mech Ageing Dev*, 65(2-3), pp. 257-76.

Jin, T. and Kim, S. G. (2008) 'Functional changes of apparent diffusion coefficient during visual stimulation investigated by diffusion-weighted gradient-echo fMRI', *Neuroimage*, 41(3), pp. 801-12.

Joffres, M., Falaschetti, E., Gillespie, C., Robitaille, C., Loustalot, F., Poulter, N., McAlister, F. A., Johansen, H., Baclic, O. and Campbell, N. (2013) 'Hypertension prevalence, awareness, treatment and control in national surveys from England, the USA and Canada, and correlation with stroke and ischaemic heart disease mortality: a cross-sectional study', *BMJ Open*, 3(8), pp. e003423.

Jokinen, H., Schmidt, R., Ropele, S., Fazekas, F., Gouw, A. A., Barkhof, F., Scheltens, P., Madureira, S., Verdelho, A., Ferro, J. M., Wallin, A., Poggesi, A., Inzitari, D., Pantoni, L., Erkinjuntti, T. and Group, L. S. (2013) 'Diffusion changes predict cognitive and functional outcome: the LADIS study', *Ann Neurol*, 73(5), pp. 576-83.

Jonckers, E., Van Audekerke, J., De Visscher, G., Van der Linden, A. and Verhoye, M. (2011) 'Functional connectivity fMRI of the rodent brain: comparison of functional connectivity networks in rat and mouse', *PLoS One*, 6(4), pp. e18876.

Jucker, M., Bättig, K. and Meier-Ruge, W. (1990) 'Effects of aging and vincamine derivatives on pericapillary microenvironment: stereological characterization of the cerebral capillary network', *Neurobiol Aging*, 11(1), pp. 39-46.

Kannurpatti, S. S., Motes, M. A., Rypma, B. and Biswal, B. B. (2010) 'Neural and vascular variability and the fMRI-BOLD response in normal aging', *Magn Reson Imaging*, 28(4), pp. 466-76.

Katsura, K., Kristián, T., Smith, M. L. and Siesjö, B. K. (1994) 'Acidosis induced by hypercapnia exaggerates ischemic brain damage', *J Cereb Blood Flow Metab*, 14(2), pp. 243-50.

Kazama, K., Anrather, J., Zhou, P., Girouard, H., Frys, K., Milner, T. A. and Iadecola, C. (2004) 'Angiotensin II impairs neurovascular coupling in neocortex through NADPH oxidase-derived radicals', *Circ Res*, 95(10), pp. 1019-26.

Kelly, M. E., Blau, C. W., Griffin, K. M., Gobbo, O. L., Jones, J. F. and Kerskens, C. M. (2010) 'Quantitative functional magnetic resonance imaging of brain activity using bolus-tracking arterial spin labeling', *J Cereb Blood Flow Metab*, 30(5), pp. 913-22.

Kennerley, A. J., Berwick, J., Martindale, J., Johnston, D., Papadakis, N. and Mayhew, J. E. (2005) 'Concurrent fMRI and optical measures for the investigation of the hemodynamic response function', *Magn Reson Med*, 54(2), pp. 354-65.

Khalil, M. M., Tremoleda, J. L., Bayomy, T. B. and Gsell, W. (2011) 'Molecular SPECT Imaging: An Overview', *Int J Mol Imaging*, 2011, pp. 796025.

Kilkenny, C., Browne, W. J., Cuthill, I. C., Emerson, M. and Altman, D. G. (2010) 'Improving bioscience research reporting: The ARRIVE guidelines for reporting animal research', *J Pharmacol Pharmacother*, 1(2), pp. 94-9.

Kim, S. G. and Ogawa, S. (2012) 'Biophysical and physiological origins of blood oxygenation level-dependent fMRI signals', *J Cereb Blood Flow Metab*, 32(7), pp. 1188-206.

Kim, Y. R., Huang, I. J., Lee, S. R., Tejima, E., Mandeville, J. B., van Meer, M. P., Dai, G., Choi, Y. W., Dijkhuizen, R. M., Lo, E. H. and Rosen, B. R. (2005) 'Measurements of BOLD/CBV ratio show altered fMRI hemodynamics during stroke recovery in rats', *J Cereb Blood Flow Metab*, 25(7), pp. 820-9.

- Kim, Y. R., van Meer, M. P., Mandeville, J. B., Tejima, E., Dai, G., Topalkara, K., Qui, J., Dijkhuizen, R. M., Moskowitz, M. A., Lo, E. H. and Rosen, B. R. (2007) 'fMRI of delayed albumin treatment during stroke recovery in rats: implication for fast neuronal habituation in recovering brains', *J Cereb Blood Flow Metab*, 27(1), pp. 142-53.
- Kitagawa, K., Oku, N., Kimura, Y., Yagita, Y., Sakaguchi, M., Hatazawa, J. and Sakoda, S. (2009) 'Relationship between cerebral blood flow and later cognitive decline in hypertensive patients with cerebral small vessel disease', *Hypertens Res*, 32(9), pp. 816-20.
- Klijn, C. J. and Kappelle, L. J. (2010) 'Haemodynamic stroke: clinical features, prognosis, and management', *Lancet Neurol*, 9(10), pp. 1008-17.
- Kloska, S. P., Wintermark, M., Engelhorn, T. and Fiebach, J. B. (2010) 'Acute stroke magnetic resonance imaging: current status and future perspective', *Neuroradiology*, 52(3), pp. 189-201.
- Kramer, D. R., Fujii, T., Ohiorhenuan, I. and Liu, C. Y. (2016) 'Cortical spreading depolarization: Pathophysiology, implications, and future directions', *J Clin Neurosci*, 24, pp. 22-7.
- Krejza, J., Mariak, Z., Walecki, J., Szydlik, P., Lewko, J. and Ustymowicz, A. (1999) 'Transcranial color Doppler sonography of basal cerebral arteries in 182 healthy subjects: age and sex variability and normal reference values for blood flow parameters', *AJR Am J Roentgenol*, 172(1), pp. 213-8.
- Kuge, Y., Minematsu, K., Hasegawa, Y., Yamaguchi, T., Mori, H., Matsuura, H., Hashimoto, N. and Miyake, Y. (1997) 'Positron emission tomography for quantitative determination of glucose metabolism in normal and ischemic brains in rats: an insoluble problem by the Harderian glands', *J Cereb Blood Flow Metab*, 17(1), pp. 116-20.
- L, L., X, W. and Z, Y. (2016) 'Ischemia-reperfusion Injury in the Brain: Mechanisms and Potential Therapeutic Strategies', *Biochem Pharmacol (Los Angel)*, 5(4).
- Lacoste, B., Tong, X. K., Lahjouji, K., Couture, R. and Hamel, E. (2013) 'Cognitive and cerebrovascular improvements following kinin B1 receptor blockade in Alzheimer's disease mice', *J Neuroinflammation*, 10, pp. 57.

- Lahti, K. M., Ferris, C. F., Li, F., Sotak, C. H. and King, J. A. (1999) 'Comparison of evoked cortical activity in conscious and propofol-anesthetized rats using functional MRI', *Magn Reson Med*, 41(2), pp. 412-6.
- Lake, E. M. R., Bazzigaluppi, P., Mester, J., Thomason, L. A. M., Janik, R., Brown, M., McLaurin, J., Carlen, P. L., Corbett, D., Stanisiz, G. J. and Stefanovic, B. (2017a) 'Neurovascular unit remodelling in the subacute stage of stroke recovery', *Neuroimage*, 146, pp. 869-882.
- Lake, E. M. R., Mester, J., Thomason, L. A., Adams, C., Bazzigaluppi, P., Koletar, M., Janik, R., Carlen, P., McLaurin, J., Stanisiz, G. J. and Stefanovic, B. (2017b) 'Modulation of the peri-infarct neurogliovascular function by delayed COX-1 inhibition', *J Magn Reson Imaging*, 46(2), pp. 505-517.
- Lammie, G. A. (2002) 'Hypertensive cerebral small vessel disease and stroke', *Brain Pathol*, 12(3), pp. 358-70.
- Lauritzen, M. and Hansen, A. J. (1992) 'The effect of glutamate receptor blockade on anoxic depolarization and cortical spreading depression', *J Cereb Blood Flow Metab*, 12(2), pp. 223-9.
- Le Bihan, D., Urayama, S., Aso, T., Hanakawa, T. and Fukuyama, H. (2006a) 'Direct and fast detection of neuronal activation in the human brain with diffusion MRI', *Proc Natl Acad Sci U S A*, 103(21), pp. 8263-8.
- Le Bihan, D., Urayama, S., Aso, T., Hanakawa, T. and Fukuyama, H. (2006b) 'Direct and fast detection of neuronal activation in the human brain with diffusion MRI', *Proc Natl Acad Sci U S A*, 103(21), pp. 8263-8.
- Ledo, A., Lourenço, C. F., Caetano, M., Barbosa, R. M. and Laranjinha, J. (2015) 'Age-associated changes of nitric oxide concentration dynamics in the central nervous system of Fisher 344 rats', *Cell Mol Neurobiol*, 35(1), pp. 33-44.
- Lee, R. M. (1995) 'Morphology of cerebral arteries', *Pharmacol Ther*, 66(1), pp. 149-73.
- Lenz, C., Rebel, A., van Ackern, K., Kuschinsky, W. and Waschke, K. F. (1998) 'Local cerebral blood flow, local cerebral glucose utilization, and flow-metabolism coupling during sevoflurane versus isoflurane anesthesia in rats', *Anesthesiology*, 89(6), pp. 1480-8.

- Li, X., Liang, Y., Chen, Y., Zhang, J., Wei, D., Chen, K., Shu, N., Reiman, E. M. and Zhang, Z. (2015) 'Disrupted Frontoparietal Network Mediates White Matter Structure Dysfunction Associated with Cognitive Decline in Hypertension Patients', *J Neurosci*, 35(27), pp. 10015-24.
- Libby, P. (2012) 'Inflammation in atherosclerosis', *Arterioscler Thromb Vasc Biol*, 32(9), pp. 2045-51.
- Lim, K. O. and Spielman, D. M. (1997) 'Estimating NAA in cortical gray matter with applications for measuring changes due to aging', *Magn Reson Med*, 37(3), pp. 372-7.
- Lin, T. N., Sun, S. W., Cheung, W. M., Li, F. and Chang, C. (2002) 'Dynamic changes in cerebral blood flow and angiogenesis after transient focal cerebral ischemia in rats. Evaluation with serial magnetic resonance imaging', *Stroke*, 33(12), pp. 2985-91.
- Liu, W., Yamashita, T., Kurata, T., Kono, S., Hishikawa, N., Deguchi, K., Zhai, Y. and Abe, K. (2015) 'Protective effect of telmisartan on neurovascular unit and inflammasome in stroke-resistant spontaneously hypertensive rats', *Neurol Res*, 37(6), pp. 491-501.
- Liu, X., Zhu, X. H., Zhang, Y. and Chen, W. (2013) 'The change of functional connectivity specificity in rats under various anesthesia levels and its neural origin', *Brain Topogr*, 26(3), pp. 363-77.
- Lloyd-Jones, D., Adams, R., Carnethon, M., De Simone, G., Ferguson, T. B., Flegal, K., Ford, E., Furie, K., Go, A., Greenlund, K., Haase, N., Hailpern, S., Ho, M., Howard, V., Kissela, B., Kittner, S., Lackland, D., Lisabeth, L., Marelli, A., McDermott, M., Meigs, J., Mozaffarian, D., Nichol, G., O'Donnell, C., Roger, V., Rosamond, W., Sacco, R., Sorlie, P., Stafford, R., Steinberger, J., Thom, T., Wasserthiel-Smoller, S., Wong, N., Wylie-Rosett, J., Hong, Y. and Subcommittee, A. H. A. S. C. a. S. S. (2009) 'Heart disease and stroke statistics--2009 update: a report from the American Heart Association Statistics Committee and Stroke Statistics Subcommittee', *Circulation*, 119(3), pp. 480-6.
- Longa, E. Z., Weinstein, P. R., Carlson, S. and Cummins, R. (1989) 'Reversible middle cerebral artery occlusion without craniectomy in rats', *Stroke*, 20(1), pp. 84-91.

- Lourenço, C. F., Ledo, A., Caetano, M., Barbosa, R. M. and Laranjinha, J. (2018) 'Age-Dependent Impairment of Neurovascular and Neurometabolic Coupling in the Hippocampus', *Front Physiol*, 9, pp. 913.
- Love, S. (1999) 'Oxidative stress in brain ischemia', *Brain Pathol*, 9(1), pp. 119-31.
- Lowe, M. J., Dzemidzic, M., Lurito, J. T., Mathews, V. P. and Phillips, M. D. (2000) 'Correlations in low-frequency BOLD fluctuations reflect cortico-cortical connections', *Neuroimage*, 12(5), pp. 582-7.
- Machulda, M. M., Ward, H. A., Borowski, B., Gunter, J. L., Cha, R. H., O'Brien, P. C., Petersen, R. C., Boeve, B. F., Knopman, D., Tang-Wai, D. F., Ivnik, R. J., Smith, G. E., Tangalos, E. G. and Jack, C. R. (2003) 'Comparison of memory fMRI response among normal, MCI, and Alzheimer's patients', *Neurology*, 61(4), pp. 500-6.
- MacIntosh, B. J., Filippini, N., Chappell, M. A., Woolrich, M. W., Mackay, C. E. and Jezzard, P. (2010) 'Assessment of arterial arrival times derived from multiple inversion time pulsed arterial spin labeling MRI', *Magn Reson Med*, 63(3), pp. 641-7.
- MacVicar, B. A. and Newman, E. A. (2015) 'Astrocyte regulation of blood flow in the brain', *Cold Spring Harb Perspect Biol*, 7(5).
- Major, S., Petzold, G. C., Reiffurth, C., Windmüller, O., Foddiss, M., Lindauer, U., Kang, E. J. and Dreier, J. P. (2017) 'A role of the sodium pump in spreading ischemia in rats', *J Cereb Blood Flow Metab*, 37(5), pp. 1687-1705.
- Makowska, I. J. and Weary, D. M. (2016) 'The importance of burrowing, climbing and standing upright for laboratory rats', *R Soc Open Sci*, 3(6), pp. 160136.
- Malonek, D. and Grinvald, A. (1996) 'Interactions between electrical activity and cortical microcirculation revealed by imaging spectroscopy: implications for functional brain mapping', *Science*, 272(5261), pp. 551-4.
- Manganotti, P., Patuzzo, S., Cortese, F., Palermo, A., Smania, N. and Fiaschi, A. (2002) 'Motor disinhibition in affected and unaffected hemisphere in the early period of recovery after stroke', *Clin Neurophysiol*, 113(6), pp. 936-43.

Mansfield, P. and Maudsley, A. A. (1977) 'Medical imaging by NMR', *Br J Radiol*, 50(591), pp. 188-94.

Marjańska, M., McCarten, J. R., Hodges, J., Hemmy, L. S., Grant, A., Deelchand, D. K. and Terpstra, M. (2017) 'Region-specific aging of the human brain as evidenced by neurochemical profiles measured noninvasively in the posterior cingulate cortex and the occipital lobe using', *Neuroscience*, 354, pp. 168-177.

Markus, T. M., Tsai, S. Y., Bollnow, M. R., Farrer, R. G., O'Brien, T. E., Kindler-Baumann, D. R., Rausch, M., Rudin, M., Wiessner, C., Mir, A. K., Schwab, M. E. and Kartje, G. L. (2005) 'Recovery and brain reorganization after stroke in adult and aged rats', *Ann Neurol*, 58(6), pp. 950-3.

Marshall, O., Lu, H., Brisset, J. C., Xu, F., Liu, P., Herbert, J., Grossman, R. I. and Ge, Y. (2014) 'Impaired cerebrovascular reactivity in multiple sclerosis', *JAMA Neurol*, 71(10), pp. 1275-81.

Martin, C., Berwick, J., Johnston, D., Zheng, Y., Martindale, J., Port, M., Redgrave, P. and Mayhew, J. (2002) 'Optical imaging spectroscopy in the unanaesthetised rat', *J Neurosci Methods*, 120(1), pp. 25-34.

Martin, C. J., Kennerley, A. J., Berwick, J., Port, M. and Mayhew, J. E. (2013) 'Functional MRI in conscious rats using a chronically implanted surface coil', *J Magn Reson Imaging*, 38(3), pp. 739-44.

Martin, W. R. (2007) 'MR spectroscopy in neurodegenerative disease', *Mol Imaging Biol*, 9(4), pp. 196-203.

Masamoto, K., Fukuda, M., Vazquez, A. and Kim, S. G. (2009a) 'Dose-dependent effect of isoflurane on neurovascular coupling in rat cerebral cortex', *Eur J Neurosci*, 30(2), pp. 242-50.

Masamoto, K., Fukuda, M., Vazquez, A. and Kim, S. G. (2009b) 'Dose-dependent effect of isoflurane on neurovascular coupling in rat cerebral cortex', *Eur J Neurosci*, 30(2), pp. 242-50.

- Mentis, M. J., Salerno, J., Horwitz, B., Grady, C., Schapiro, M. B., Murphy, D. G. and Rapoport, S. I. (1994) 'Reduction of functional neuronal connectivity in long-term treated hypertension', *Stroke*, 25(3), pp. 601-7.
- Mescher, M., Merkle, H., Kirsch, J., Garwood, M. and Gruetter, R. (1998) 'Simultaneous in vivo spectral editing and water suppression', *NMR Biomed*, 11(6), pp. 266-72.
- Messerli, F. H., Williams, B. and Ritz, E. (2007) 'Essential hypertension', *Lancet*, 370(9587), pp. 591-603.
- Metea, M. R. and Newman, E. A. (2006) 'Glial cells dilate and constrict blood vessels: a mechanism of neurovascular coupling', *J Neurosci*, 26(11), pp. 2862-70.
- Mitschelen, M., Garteiser, P., Carnes, B. A., Farley, J. A., Doblas, S., Demoe, J. H., Warrington, J. P., Yan, H., Nicolle, M. M., Towner, R. and Sonntag, W. E. (2009) 'Basal and hypercapnia-altered cerebrovascular perfusion predict mild cognitive impairment in aging rodents', *Neuroscience*, 164(3), pp. 918-28.
- Mooradian, A. D., Morin, A. M., Cipp, L. J. and Haspel, H. C. (1991) 'Glucose transport is reduced in the blood-brain barrier of aged rats', *Brain Res*, 551(1-2), pp. 145-9.
- Mori, S., Kato, M. and Fujishima, M. (1995) 'Impaired maze learning and cerebral glucose utilization in aged hypertensive rats', *Hypertension*, 25(4 Pt 1), pp. 545-53.
- Moseley, M. (2002) 'Diffusion tensor imaging and aging - a review', *NMR Biomed*, 15(7-8), pp. 553-60.
- Mullins, P. G., McGonigle, D. J., O'Gorman, R. L., Puts, N. A., Vidyasagar, R., Evans, C. J., Edden, R. A. and GABA, C. S. o. M. o. (2014) 'Current practice in the use of MEGA-PRESS spectroscopy for the detection of GABA', *Neuroimage*, 86, pp. 43-52.
- Nagahama, H., Nakazaki, M., Sasaki, M., Kataoka-Sasaki, Y., Namioka, T., Namioka, A., Oka, S., Onodera, R., Suzuki, J., Sasaki, Y., Kocsis, J. D. and Honmou, O. (2018) 'Preservation of interhemispheric cortical connections through corpus callosum following intravenous infusion of mesenchymal stem cells in a rat model of cerebral infarction', *Brain Res*, 1695, pp. 37-44.
- Nair, D. G. (2005) 'About being BOLD', *Brain Res Brain Res Rev*, 50(2), pp. 229-43.

Naumczyk, P., Sabisz, A., Witkowska, M., Graff, B., Jodzio, K., Gąsecki, D., Szurowska, E. and Narkiewicz, K. (2017) 'Compensatory functional reorganization may precede hypertension-related brain damage and cognitive decline: a functional magnetic resonance imaging study', *J Hypertens*, 35(6), pp. 1252-1262.

Nordberg, A. (1994) 'Human nicotinic receptors--their role in aging and dementia', *Neurochem Int*, 25(1), pp. 93-7.

Nour, M., Scalzo, F. and Liebeskind, D. S. (2013) 'Ischemia-reperfusion injury in stroke', *Interv Neurol*, 1(3-4), pp. 185-99.

Nunes, D., Ianus, A. and Shemesh, N. (2019) 'Layer-specific connectivity revealed by diffusion-weighted functional MRI in the rat thalamocortical pathway', *Neuroimage*, 184, pp. 646-657.

Ogawa, S., Tank, D. W., Menon, R., Ellermann, J. M., Kim, S. G., Merkle, H. and Ugurbil, K. (1992) 'Intrinsic signal changes accompanying sensory stimulation: functional brain mapping with magnetic resonance imaging', *Proc Natl Acad Sci U S A*, 89(13), pp. 5951-5.

Oler, J. A. and Markus, E. J. (1998) 'Age-related deficits on the radial maze and in fear conditioning: hippocampal processing and consolidation', *Hippocampus*, 8(4), pp. 402-15

Olsen, T. S., Skriver, E. B. and Herning, M. (1985) 'Cause of cerebral infarction in the carotid territory. Its relation to the size and the location of the infarct and to the underlying vascular lesion', *Stroke*, 16(3), pp. 459-66.

Paasonen, J., Stenroos, P., Salo, R. A., Kiviniemi, V. and Gröhn, O. (2018) 'Functional connectivity under six anesthesia protocols and the awake condition in rat brain', *Neuroimage*, 172, pp. 9-20.

Palmer, A. J., Bulpitt, C. J., Fletcher, A. E., Beevers, D. G., Coles, E. C., Ledingham, J. G., O'Riordan, P. W., Petrie, J. C., Rajagopalan, B. E. and Webster, J. (1992) 'Relation between blood pressure and stroke mortality', *Hypertension*, 20(5), pp. 601-5.

Park, L., Koizumi, K., El Jamal, S., Zhou, P., Previti, M. L., Van Nostrand, W. E., Carlson, G. and Iadecola, C. (2014) 'Age-dependent neurovascular dysfunction and damage in a mouse model of cerebral amyloid angiopathy', *Stroke*, 45(6), pp. 1815-21.

- Patil, A. V., Safaie, J., Moghaddam, H. A., Wallois, F. and Grebe, R. (2011) 'Experimental investigation of NIRS spatial sensitivity', *Biomed Opt Express*, 2(6), pp. 1478-93.
- Pawela, C. P., Biswal, B. B., Hudetz, A. G., Schulte, M. L., Li, R., Jones, S. R., Cho, Y. R., Matloub, H. S. and Hyde, J. S. (2009) 'A protocol for use of medetomidine anesthesia in rats for extended studies using task-induced BOLD contrast and resting-state functional connectivity', *Neuroimage*, 46(4), pp. 1137-47.
- Paxinos, G. and Watson, C. (2014) *The rat brain in stereotaxic coordinates*. Seventh edition. edn. Amsterdam: Elsevier, Academic Press.
- Peeters, R. R., Tindemans, I., De Schutter, E. and Van der Linden, A. (2001) 'Comparing BOLD fMRI signal changes in the awake and anesthetized rat during electrical forepaw stimulation', *Magn Reson Imaging*, 19(6), pp. 821-6.
- Pelegrí, C., Canudas, A. M., del Valle, J., Casadesus, G., Smith, M. A., Camins, A., Pallàs, M. and Vilaplana, J. (2007) 'Increased permeability of blood-brain barrier on the hippocampus of a murine model of senescence', *Mech Ageing Dev*, 128(9), pp. 522-8.
- Penhune, V. B. and Doyon, J. (2005) 'Cerebellum and M1 interaction during early learning of timed motor sequences', *Neuroimage*, 26(3), pp. 801-12.
- Petcharunpaisan, S., Ramalho, J. and Castillo, M. (2010) 'Arterial spin labeling in neuroimaging', *World J Radiol*, 2(10), pp. 384-98.
- Pfefferbaum, A., Adalsteinsson, E., Spielman, D., Sullivan, E. V. and Lim, K. O. (1999) 'In vivo spectroscopic quantification of the N-acetyl moiety, creatine, and choline from large volumes of brain gray and white matter: effects of normal aging', *Magn Reson Med*, 41(2), pp. 276-84.
- Prichard, J., Rothman, D., Novotny, E., Petroff, O., Kuwabara, T., Avison, M., Howseman, A., Hanstock, C. and Shulman, R. (1991a) 'Lactate rise detected by ¹H NMR in human visual cortex during physiologic stimulation', *Proc Natl Acad Sci U S A*, 88(13), pp. 5829-31.
- Prichard, J., Rothman, D., Novotny, E., Petroff, O., Kuwabara, T., Avison, M., Howseman, A., Hanstock, C. and Shulman, R. (1991b) 'Lactate rise detected by ¹H NMR in human visual cortex during physiologic stimulation', *Proc Natl Acad Sci U S A*, 88(13), pp. 5829-31.

- Rahmim, A. and Zaidi, H. (2008) 'PET versus SPECT: strengths, limitations and challenges', *Nucl Med Commun*, 29(3), pp. 193-207.
- Raichle, M. E. (1998) 'Behind the scenes of functional brain imaging: a historical and physiological perspective', *Proc Natl Acad Sci U S A*, 95(3), pp. 765-72.
- Raizada, M. K., Kimura, B. and Phillips, M. I. (1990) 'Immunoreactive atrial natriuretic peptide in neuronal and glial cells of spontaneously hypertensive rat brain', *Am J Physiol*, 258(1 Pt 1), pp. C109-14.
- Ramadan, S., Lin, A. and Stanwell, P. (2013) 'Glutamate and glutamine: a review of in vivo MRS in the human brain', *NMR Biomed*, 26(12), pp. 1630-46.
- Rapp, P. R., Rosenberg, R. A. and Gallagher, M. (1987) 'An evaluation of spatial information processing in aged rats', *Behav Neurosci*, 101(1), pp. 3-12.
- Raz, N., Rodrigue, K. M. and Acker, J. D. (2003) 'Hypertension and the brain: vulnerability of the prefrontal regions and executive functions', *Behav Neurosci*, 117(6), pp. 1169-80.
- Reimann, H. M., Todiras, M., Hodge, R., Huelnhagen, T., Millward, J. M., Turner, R., Seeliger, E., Bader, M., Pohlmann, A. and Niendorf, T. (2018) 'Somatosensory BOLD fMRI reveals close link between salient blood pressure changes and the murine neuromatrix', *Neuroimage*, 172, pp. 562-574.
- Reuter-Lorenz, P. A., Jonides, J., Smith, E. E., Hartley, A., Miller, A., Marshuetz, C. and Koeppel, R. A. (2000) 'Age differences in the frontal lateralization of verbal and spatial working memory revealed by PET', *J Cogn Neurosci*, 12(1), pp. 174-87.
- Richardson, J. D., Baker, J. M., Morgan, P. S., Rorden, C., Bonilha, L. and Fridriksson, J. (2011) 'Cerebral perfusion in chronic stroke: implications for lesion-symptom mapping and functional MRI', *Behav Neurol*, 24(2), pp. 117-22.
- Riva, M., Pappadà, G. B., Papadakis, M., Cuccione, E., Carone, D., Menendez, V. R., Sganzerla, E. P. and Beretta, S. (2012) 'Hemodynamic monitoring of intracranial collateral flow predicts tissue and functional outcome in experimental ischemic stroke', *Exp Neurol*, 233(2), pp. 815-20.

Rivard, A., Fabre, J. E., Silver, M., Chen, D., Murohara, T., Kearney, M., Magner, M., Asahara, T. and Isner, J. M. (1999) 'Age-dependent impairment of angiogenesis', *Circulation*, 99(1), pp. 111-20.

Rosen, Y. and Lenkinski, R. E. (2007) 'Recent advances in magnetic resonance neurospectroscopy', *Neurotherapeutics*, 4(3), pp. 330-45.

Rosenblum, W. I. (2008) 'Fibrinoid necrosis of small brain arteries and arterioles and miliary aneurysms as causes of hypertensive hemorrhage: a critical reappraisal', *Acta Neuropathol*, 116(4), pp. 361-9.

Ross, M. H., Yurgelun-Todd, D. A., Renshaw, P. F., Maas, L. C., Mendelson, J. H., Mello, N. K., Cohen, B. M. and Levin, J. M. (1997) 'Age-related reduction in functional MRI response to photic stimulation', *Neurology*, 48(1), pp. 173-6.

Samuels, S., Fish, I., Schwartz, S. A. and Hochgeschwender, U. (1983) 'Age related changes in blood-to-brain amino acid transport and incorporation into brain protein', *Neurochem Res*, 8(2), pp. 167-77.

Sander, C. Y., Hooker, J. M., Catana, C., Rosen, B. R. and Mandeville, J. B. (2016) 'Imaging Agonist-Induced D2/D3 Receptor Desensitization and Internalization In Vivo with PET/fMRI', *Neuropsychopharmacology*, 41(5), pp. 1427-36.

Sanganahalli, B. G., Herman, P., Behar, K. L., Blumenfeld, H., Rothman, D. L. and Hyder, F. (2013) 'Functional MRI and neural responses in a rat model of Alzheimer's disease', *Neuroimage*, 79, pp. 404-11.

Sauter, A., Reese, T., Pórszász, R., Baumann, D., Rausch, M. and Rudin, M. (2002) 'Recovery of function in cytoprotected cerebral cortex in rat stroke model assessed by functional MRI', *Magn Reson Med*, 47(4), pp. 759-65.

Schlegel, F., Schroeter, A. and Rudin, M. (2015) 'The hemodynamic response to somatosensory stimulation in mice depends on the anesthetic used: Implications on analysis of mouse fMRI data', *Neuroimage*, 116, pp. 40-9.

Schmitz, B., Wang, X., Barker, P. B., Pilatus, U., Bronzlik, P., Dadak, M., Kahl, K. G., Lanfermann, H. and Ding, X. Q. (2018) 'Effects of Aging on the Human Brain: A Proton and Phosphorus MR Spectroscopy Study at 3T', *J Neuroimaging*, 28(4), pp. 416-421.

Schroeter, A., Schlegel, F., Seuwen, A., Grandjean, J. and Rudin, M. (2014) 'Specificity of stimulus-evoked fMRI responses in the mouse: the influence of systemic physiological changes associated with innocuous stimulation under four different anesthetics', *Neuroimage*, 94, pp. 372-384.

Schuff, N., Amend, D. L., Meyerhoff, D. J., Tanabe, J. L., Norman, D., Fein, G. and Weiner, M. W. (1998) 'Alzheimer disease: quantitative H-1 MR spectroscopic imaging of frontoparietal brain', *Radiology*, 207(1), pp. 91-102.

Selman, W. R., Lust, W. D., Pundik, S., Zhou, Y. and Ratcheson, R. A. (2004) 'Compromised metabolic recovery following spontaneous spreading depression in the penumbra', *Brain Res*, 999(2), pp. 167-74.

Seminog, O. O., Scarborough, P., Wright, F. L., Rayner, M. and Goldacre, M. J. (2019) 'Determinants of the decline in mortality from acute stroke in England: linked national database study of 795 869 adults', *BMJ*, 365, pp. l1778.

Shao, W. H., Li, C., Chen, L., Qiu, X., Zhang, W., Huang, C. X., Xia, L., Kong, J. M. and Tang, Y. (2010) 'Stereological investigation of age-related changes of the capillaries in white matter', *Anat Rec (Hoboken)*, 293(8), pp. 1400-7.

Sharp, P. S., Ameen-Ali, K. E., Boorman, L., Harris, S., Wharton, S., Howarth, C., Shabir, O., Redgrave, P. and Berwick, J. (2019) 'Neurovascular coupling preserved in a chronic mouse model of Alzheimer's disease: Methodology is critical', *J Cereb Blood Flow Metab*, pp. 271678X19890830.

Sheth, S. A., Nemoto, M., Guiou, M. W., Walker, M. A. and Toga, A. W. (2005) 'Spatiotemporal evolution of functional hemodynamic changes and their relationship to neuronal activity', *J Cereb Blood Flow Metab*, 25(7), pp. 830-41.

Shih, Y. Y., Huang, S., Chen, Y. Y., Lai, H. Y., Kao, Y. C., Du, F., Hui, E. S. and Duong, T. Q. (2014) 'Imaging neurovascular function and functional recovery after stroke in the rat striatum using forepaw stimulation', *J Cereb Blood Flow Metab*, 34(9), pp. 1483-92.

- Shim, W. H., Suh, J. Y., Kim, J. K., Jeong, J. and Kim, Y. R. (2016a) 'Enhanced Thalamic Functional Connectivity with No fMRI Responses to Affected Forelimb Stimulation in Stroke-Recovered Rats', *Front Neural Circuits*, 10, pp. 113.
- Shim, W. H., Suh, J. Y., Kim, J. K., Jeong, J. and Kim, Y. R. (2016b) 'Enhanced Thalamic Functional Connectivity with No fMRI Responses to Affected Forelimb Stimulation in Stroke-Recovered Rats', *Front Neural Circuits*, 10, pp. 113.
- Shin, H. K., Dunn, A. K., Jones, P. B., Boas, D. A., Moskowitz, M. A. and Ayata, C. (2006) 'Vasoconstrictive neurovascular coupling during focal ischemic depolarizations', *J Cereb Blood Flow Metab*, 26(8), pp. 1018-30.
- Sicard, K. M., Henninger, N., Fisher, M., Duong, T. Q. and Ferris, C. F. (2006) 'Long-term changes of functional MRI-based brain function, behavioral status, and histopathology after transient focal cerebral ischemia in rats', *Stroke*, 37(10), pp. 2593-600.
- Simpson, R., Devenyi, G. A., Jezzard, P., Hennessy, T. J. and Near, J. (2017) 'Advanced processing and simulation of MRS data using the FID appliance (FID-A)-An open source, MATLAB-based toolkit', *Magn Reson Med*, 77(1), pp. 23-33.
- Slotboom, J., Creyghton, J. H., Korbee, D., Mehlkopf, A. F. and Bovée, W. M. (1993) 'Spatially selective RF pulses and the effects of digitization on their performance', *Magn Reson Med*, 30(6), pp. 732-40.
- Stanimirovic, D. B. and Friedman, A. (2012) 'Pathophysiology of the neurovascular unit: disease cause or consequence?', *J Cereb Blood Flow Metab*, 32(7), pp. 1207-21.
- Stanley, J. A. and Raz, N. (2018) 'Functional Magnetic Resonance Spectroscopy: The "New" MRS for Cognitive Neuroscience and Psychiatry Research', *Front Psychiatry*, 9, pp. 76.
- Stenroos, P., Paasonen, J., Salo, R. A., Jokivarsi, K., Shatillo, A., Tanila, H. and Gröhn, O. (2018) 'Awake Rat Brain Functional Magnetic Resonance Imaging Using Standard Radio Frequency Coils and a 3D Printed Restraint Kit', *Front Neurosci*, 12, pp. 548.
- Strebel, S., Lam, A. M., Matta, B., Mayberg, T. S., Aaslid, R. and Newell, D. W. (1995) 'Dynamic and static cerebral autoregulation during isoflurane, desflurane, and propofol anesthesia', *Anesthesiology*, 83(1), pp. 66-76.

- Strong, A. J., Smith, S. E., Whittington, D. J., Meldrum, B. S., Parsons, A. A., Krupinski, J., Hunter, A. J., Patel, S. and Robertson, C. (2000) 'Factors influencing the frequency of fluorescence transients as markers of peri-infarct depolarizations in focal cerebral ischemia', *Stroke*, 31(1), pp. 214-22.
- Swisher, J. D., Sexton, J. A., Gatenby, J. C., Gore, J. C. and Tong, F. (2012) 'Multishot versus single-shot pulse sequences in very high field fMRI: a comparison using retinotopic mapping', *PLoS One*, 7(4), pp. e34626.
- Takeda, Y., Zhao, L., Jacewicz, M., Pulsinelli, W. A. and Nowak, T. S. (2011) 'Metabolic and perfusion responses to recurrent peri-infarct depolarization during focal ischemia in the Spontaneously Hypertensive Rat: dominant contribution of sporadic CBF decrements to infarct expansion', *J Cereb Blood Flow Metab*, 31(9), pp. 1863-73.
- Tang, W., Paulding, W. R. and Sumners, C. (1993) 'ANP receptors in neurons and astrocytes from spontaneously hypertensive rat brain', *Am J Physiol*, 265(1 Pt 1), pp. C106-12.
- Tarumi, T., Ayaz Khan, M., Liu, J., Tseng, B. Y., Tseng, B. M., Parker, R., Riley, J., Tinajero, C. and Zhang, R. (2014) 'Cerebral hemodynamics in normal aging: central artery stiffness, wave reflection, and pressure pulsatility', *J Cereb Blood Flow Metab*, 34(6), pp. 971-8.
- Tarumi, T. and Zhang, R. (2018) 'Cerebral blood flow in normal aging adults: cardiovascular determinants, clinical implications, and aerobic fitness', *J Neurochem*, 144(5), pp. 595-608.
- Tecchio, F., Zappasodi, F., Tombini, M., Oliviero, A., Pasqualetti, P., Vernieri, F., Ercolani, M., Pizzella, V. and Rossini, P. M. (2006) 'Brain plasticity in recovery from stroke: an MEG assessment', *Neuroimage*, 32(3), pp. 1326-34.
- Thomas, D. L., Lythgoe, M. F., van der Weerd, L., Ordidge, R. J. and Gadian, D. G. (2006a) 'Regional variation of cerebral blood flow and arterial transit time in the normal and hypoperfused rat brain measured using continuous arterial spin labeling MRI', *J Cereb Blood Flow Metab*, 26(2), pp. 274-82.
- Thomas, D. L., Lythgoe, M. F., van der Weerd, L., Ordidge, R. J. and Gadian, D. G. (2006b) 'Regional variation of cerebral blood flow and arterial transit time in the normal and hypoperfused rat brain measured using continuous arterial spin labeling MRI', *J Cereb Blood Flow Metab*, 26(2), pp. 274-82.

- Thompson, J. K., Peterson, M. R. and Freeman, R. D. (2003) 'Single-neuron activity and tissue oxygenation in the cerebral cortex', *Science*, 299(5609), pp. 1070-2.
- Thorin-Trescases, N., de Montgolfier, O., Pinçon, A., Raignault, A., Caland, L., Labbé, P. and Thorin, E. (2018) 'Impact of pulse pressure on cerebrovascular events leading to age-related cognitive decline', *Am J Physiol Heart Circ Physiol*, 314(6), pp. H1214-H1224.
- Tomassoni, D., Avola, R., Di Tullio, M. A., Sabbatini, M., Vitaioli, L. and Amenta, F. (2004a) 'Increased expression of glial fibrillary acidic protein in the brain of spontaneously hypertensive rats', *Clin Exp Hypertens*, 26(4), pp. 335-50.
- Tomassoni, D., Bellagamba, G., Postacchini, D., Venarucci, D. and Amenta, F. (2004b) 'Cerebrovascular and brain microanatomy in spontaneously hypertensive rats with streptozotocin-induced diabetes', *Clin Exp Hypertens*, 26(4), pp. 305-21.
- Tombari, D., Loubinoux, I., Pariente, J., Gerdelat, A., Albuher, J. F., Tardy, J., Cassol, E. and Chollet, F. (2004) 'A longitudinal fMRI study: in recovering and then in clinically stable sub-cortical stroke patients', *Neuroimage*, 23(3), pp. 827-39.
- Toornvliet, R., van Berckel, B. N., Luurtsema, G., Lubberink, M., Geldof, A. A., Bosch, T. M., Oerlemans, R., Lammertsma, A. A. and Franssen, E. J. (2006) 'Effect of age on functional P-glycoprotein in the blood-brain barrier measured by use of (R)-[(11)C]verapamil and positron emission tomography', *Clin Pharmacol Ther*, 79(6), pp. 540-8.
- Tremoleda, J. L., Kerton, A. and Gsell, W. (2012) 'Anaesthesia and physiological monitoring during in vivo imaging of laboratory rodents: considerations on experimental outcomes and animal welfare', *EJNMMI Res*, 2(1), pp. 44.
- Trotman-Lucas, M., Kelly, M. E., Janus, J., Fern, R. and Gibson, C. L. (2017) 'An alternative surgical approach reduces variability following filament induction of experimental stroke in mice', *Dis Model Mech*, 10(7), pp. 931-938.
- Tsurugizawa, T., Ciobanu, L. and Le Bihan, D. (2013) 'Water diffusion in brain cortex closely tracks underlying neuronal activity', *Proc Natl Acad Sci U S A*, 110(28), pp. 11636-41.
- Tsurugizawa, T., Takahashi, Y. and Kato, F. (2016) 'Distinct effects of isoflurane on basal BOLD signals in tissue/vascular microstructures in rats', *Sci Rep*, 6, pp. 38977.

- Tuor, U. I., Kelly, P. A., Edvinsson, L. and McCulloch, J. (1990) 'Neuropeptide Y and the cerebral circulation', *J Cereb Blood Flow Metab*, 10(5), pp. 591-601.
- Uchida, S., Suzuki, A., Kagitani, F. and Hotta, H. (2000) 'Effects of age on cholinergic vasodilation of cortical cerebral blood vessels in rats', *Neurosci Lett*, 294(2), pp. 109-12.
- Van Lieshout, J. J., Wieling, W., Karemaker, J. M. and Secher, N. H. (2003) 'Syncope, cerebral perfusion, and oxygenation', *J Appl Physiol (1985)*, 94(3), pp. 833-48.
- van Meer, M. P., Otte, W. M., van der Marel, K., Nijboer, C. H., Kavelaars, A., van der Sprenkel, J. W., Viergever, M. A. and Dijkhuizen, R. M. (2012) 'Extent of bilateral neuronal network reorganization and functional recovery in relation to stroke severity', *J Neurosci*, 32(13), pp. 4495-507.
- van Meer, M. P., van der Marel, K., Otte, W. M., Berkelbach van der Sprenkel, J. W. and Dijkhuizen, R. M. (2010a) 'Correspondence between altered functional and structural connectivity in the contralesional sensorimotor cortex after unilateral stroke in rats: a combined resting-state functional MRI and manganese-enhanced MRI study', *J Cereb Blood Flow Metab*, 30(10), pp. 1707-11.
- van Meer, M. P., van der Marel, K., Wang, K., Otte, W. M., El Bouazati, S., Roeling, T. A., Viergever, M. A., Berkelbach van der Sprenkel, J. W. and Dijkhuizen, R. M. (2010b) 'Recovery of sensorimotor function after experimental stroke correlates with restoration of resting-state interhemispheric functional connectivity', *J Neurosci*, 30(11), pp. 3964-72.
- Vanzetta, I., Hildesheim, R. and Grinvald, A. (2005) 'Compartment-resolved imaging of activity-dependent dynamics of cortical blood volume and oximetry', *J Neurosci*, 25(9), pp. 2233-44.
- Vorbrodt, A. W., Dobrogowska, D. H., Meeker, H. C. and Carp, R. I. (1999) 'Immunogold study of regional differences in the distribution of glucose transporter (GLUT-1) in mouse brain associated with physiological and accelerated aging and scrapie infection', *J Neurocytol*, 28(9), pp. 711-9.
- Vorbrodt, A. W., Dobrogowska, D. H., Ueno, M. and Lossinsky, A. S. (1995) 'Immunocytochemical studies of protamine-induced blood-brain barrier opening to endogenous albumin', *Acta Neuropathol*, 89(6), pp. 491-9.

- Vriens, E. M., Kraaier, V., Musbach, M., Wieneke, G. H. and van Huffelen, A. C. (1989) 'Transcranial pulsed Doppler measurements of blood velocity in the middle cerebral artery: reference values at rest and during hyperventilation in healthy volunteers in relation to age and sex', *Ultrasound Med Biol*, 15(1), pp. 1-8.
- Vrselja, Z., Brkic, H., Mrdenovic, S., Radic, R. and Curic, G. (2014) 'Function of circle of Willis', *J Cereb Blood Flow Metab*, 34(4), pp. 578-84.
- Waldstein, S. R., Ryan, C. M., Polefrone, J. M. and Manuck, S. B. (1994) 'Neuropsychological performance of young men who vary in familial risk for hypertension', *Psychosom Med*, 56(5), pp. 449-56.
- Walls, A. B., Waagepetersen, H. S., Bak, L. K., Schousboe, A. and Sonnewald, U. (2015) 'The glutamine-glutamate/GABA cycle: function, regional differences in glutamate and GABA production and effects of interference with GABA metabolism', *Neurochem Res*, 40(2), pp. 402-9.
- Wang, R., Foniok, T., Wamsteeker, J. I., Qiao, M., Tomanek, B., Vivanco, R. A. and Tuor, U. I. (2006) 'Transient blood pressure changes affect the functional magnetic resonance imaging detection of cerebral activation', *Neuroimage*, 31(1), pp. 1-11.
- Wang, S. H., Zhang, Z. J., Guo, Y. J., Zhou, H., Teng, G. J. and Chen, B. A. (2009) 'Anhedonia and activity deficits in rats: impact of post-stroke depression', *J Psychopharmacol*, 23(3), pp. 295-304.
- Ward, N. S., Brown, M. M., Thompson, A. J. and Frackowiak, R. S. (2003a) 'Neural correlates of motor recovery after stroke: a longitudinal fMRI study', *Brain*, 126(Pt 11), pp. 2476-96.
- Ward, N. S., Brown, M. M., Thompson, A. J. and Frackowiak, R. S. (2003b) 'Neural correlates of outcome after stroke: a cross-sectional fMRI study', *Brain*, 126(Pt 6), pp. 1430-48.
- Weber, R., Ramos-Cabrera, P., Justicia, C., Wiedermann, D., Strecker, C., Sprenger, C. and Hoehn, M. (2008) 'Early prediction of functional recovery after experimental stroke: functional magnetic resonance imaging, electrophysiology, and behavioral testing in rats', *J Neurosci*, 28(5), pp. 1022-9.

Weber, R., Ramos-Cabrer, P., Wiedermann, D., van Camp, N. and Hoehn, M. (2006) 'A fully noninvasive and robust experimental protocol for longitudinal fMRI studies in the rat', *Neuroimage*, 29(4), pp. 1303-10.

Wegener, S., Wu, W. C., Perthen, J. E. and Wong, E. C. (2007) 'Quantification of rodent cerebral blood flow (CBF) in normal and high flow states using pulsed arterial spin labeling magnetic resonance imaging', *J Magn Reson Imaging*, 26(4), pp. 855-62.

Weiller, C., Chollet, F., Friston, K. J., Wise, R. J. and Frackowiak, R. S. (1992) 'Functional reorganization of the brain in recovery from striatocapsular infarction in man', *Ann Neurol*, 31(5), pp. 463-72.

West, K. L., Zuppichini, M. D., Turner, M. P., Sivakolundu, D. K., Zhao, Y., Abdelkarim, D., Spence, J. S. and Rypma, B. (2019) 'BOLD hemodynamic response function changes significantly with healthy aging', *Neuroimage*, 188, pp. 198-207.

Wey, H. Y., Catana, C., Hooker, J. M., Dougherty, D. D., Knudsen, G. M., Wang, D. J., Chonde, D. B., Rosen, B. R., Gollub, R. L. and Kong, J. (2014) 'Simultaneous fMRI-PET of the opioidergic pain system in human brain', *Neuroimage*, 102 Pt 2, pp. 275-82.

Wierenga, C. E., Benjamin, M., Gopinath, K., Perlstein, W. M., Leonard, C. M., Rothi, L. J., Conway, T., Cato, M. A., Briggs, R. and Crosson, B. (2008) 'Age-related changes in word retrieval: role of bilateral frontal and subcortical networks', *Neurobiol Aging*, 29(3), pp. 436-51.

Williams, D. S., Detre, J. A., Leigh, J. S. and Koretsky, A. P. (1992) 'Magnetic resonance imaging of perfusion using spin inversion of arterial water', *Proc Natl Acad Sci U S A*, 89(1), pp. 212-6.

Woitzik, J., Hecht, N., Pinczolits, A., Sandow, N., Major, S., Winkler, M. K., Weber-Carstens, S., Dohmen, C., Graf, R., Strong, A. J., Dreier, J. P., Vajkoczy, P. and group, C. s. (2013) 'Propagation of cortical spreading depolarization in the human cortex after malignant stroke', *Neurology*, 80(12), pp. 1095-102.

Woolrich, M. W., Ripley, B. D., Brady, M. and Smith, S. M. (2001a) 'Temporal autocorrelation in univariate linear modeling of FMRI data', *Neuroimage*, 14(6), pp. 1370-86.

- Woolrich, M. W., Ripley, B. D., Brady, M. and Smith, S. M. (2001b) 'Temporal autocorrelation in univariate linear modeling of fMRI data', *Neuroimage*, 14(6), pp. 1370-86.
- Xin, L. and Tkáč, I. (2017) 'A practical guide to in vivo proton magnetic resonance spectroscopy at high magnetic fields', *Anal Biochem*, 529, pp. 30-39.
- Zahr, N. M., Mayer, D., Rohlfing, T., Chanraud, S., Gu, M., Sullivan, E. V. and Pfefferbaum, A. (2013) 'In vivo glutamate measured with magnetic resonance spectroscopy: behavioral correlates in aging', *Neurobiol Aging*, 34(4), pp. 1265-76.
- Zarow, G. J., Karibe, H., States, B. A., Graham, S. H. and Weinstein, P. R. (1997) 'Endovascular suture occlusion of the middle cerebral artery in rats: effect of suture insertion distance on cerebral blood flow, infarct distribution and infarct volume', *Neurol Res*, 19(4), pp. 409-16.
- Zarrinkoob, L., Ambarki, K., Wåhlin, A., Birgander, R., Carlberg, B., Eklund, A. and Malm, J. (2016) 'Aging alters the dampening of pulsatile blood flow in cerebral arteries', *J Cereb Blood Flow Metab*, 36(9), pp. 1519-27.
- Zhang, Y., Brady, M. and Smith, S. (2001) 'Segmentation of brain MR images through a hidden Markov random field model and the expectation-maximization algorithm', *IEEE Trans Med Imaging*, 20(1), pp. 45-57.
- Zhou, H., Sun, J., Ji, X., Lin, J., Tang, S., Zeng, J. and Fan, Y. H. (2016) 'Correlation Between the Integrity of the Circle of Willis and the Severity of Initial Noncardiac Cerebral Infarction and Clinical Prognosis', *Medicine (Baltimore)*, 95(10), pp. e2892.
- Zhu, H. and Barker, P. B. (2011) 'MR spectroscopy and spectroscopic imaging of the brain', *Methods Mol Biol*, 711, pp. 203-26.
- Zivin, J. A. (1998) 'Factors determining the therapeutic window for stroke', *Neurology*, 50(3), pp. 599-603.